General Disclaimer

One or more of the Following Statements may affect this Document

- This document has been reproduced from the best copy furnished by the organizational source. It is being released in the interest of making available as much information as possible.

- This document may contain data, which exceeds the sheet parameters. It was furnished in this condition by the organizational source and is the best copy available.

- This document may contain tone-on-tone or color graphs, charts and/or pictures, which have been reproduced in black and white.

- This document is paginated as submitted by the original source.

- Portions of this document are not fully legible due to the historical nature of some of the material. However, it is the best reproduction available from the original submission.

DOE/NASA/4936-3
NASA CR-168286
CTR 0748-84003

POSITIVE DISPLACEMENT COMPOUNDING OF A HEAVY DUTY DIESEL ENGINE

Raj Sekar
Roy Kamo
Cummins Engine Company, Inc.

November 1983

Prepared for
NATIONAL AERONAUTICS AND SPACE ADMINISTRATION
Lewis Research Center

Under DOE Contract DE-AC02-78CS54936

for
U.S. DEPARTMENT OF ENERGY
Conservation and Solar Energy
Office of Transportation Programs

1. Report No.	2. Government Accession No.	3. Recipient's Catalog No.
NASA CR168286		

4. Title and Subtitle	5. Report Date
Positive Displacement Compounding of a Heavy Duty Diesel Engine	December, 1983
	6. Performing Organization Code

7. Author(s)	8. Performing Organization Report No.
Raj Sekar Roy Kamo	
	10. Work Unit No.

9. Performing Organization Name and Address	11. Contract or Grant No.
Cummins Engine Company, Inc. Box 3005 Columbus, IN 47202	DE-AC02-78CS54936
	13. Type of Report and Period Covered
12. Sponsoring Agency Name and Address	Contractor's Final Report
U.S. Department of Energy Office of Vehicle and Engine R&D Washington, D.C. 20585	14. Sponsoring Agency Code
	DOE/NASA/4936-3

15. Supplementary Notes

Interagency Agreement #DE-A101-80CS50194
James C. Wood, Project Manager
NASA-Lewis Research Center
Cleveland, OH 44135

16. Abstract

A helical screw type positive displacement (PD) compressor and expander was considered in this study as an alternative to the turbocharger and the power turbine in the Cummins Advanced Turbocompound engine. The Institute of Gas Technology (IGT) completed the design, layout, and performance prediction of the PD machines under a subcontract from Cummins. The results of the study indicate that a screw compressor-expander system is feasible up to at least 750 HP, dry operation of the rotors is feasible, cost and producibility are uncertain, and the system will yield about 4% improvement in brake specific fuel consumption (BSFC) over the Advanced Turbocompound engine.

17. Key Words (Suggested by Author(s))	18. Distribution Statement
Positive Displacement Compressor, Expander - Diesel Engine - Turbocompound	Unclassified - unlimited

19. Security Classif. (of this report)	20. Security Classif. (of this page)	21. No. of pages	22. Price*
Unclassified	Unclassified		

*For sale by the National Technical Information Service, Springfield, Virginia 22161

DOE/NASA/4936-3

NASA CR No. 168286

FINAL REPORT

Positive Displacement Compounding of a Heavy Duty Diesel Engine

Raj Sekar
Roy Kamo

Cummins Engine Company, Inc.
Columbus, Indiana

NASA/DOE Contract No. DE-AC02-78CS54936

D.O.E. Program Manager - E. W. Gregory II

NASA Program Manager - J. C. Wood

November, 1983

(Reference: DOE/NASA/4936-2 Report)

FOREWORD

This is the last technical report to fulfill the scope of work of Contract DE-AC02-78CS54936 between the Department of Energy and Cummins Engine Company. The previous two reports, DOE/NASA/4936-1 and DOE/NASA/4936-2, cover all the experimental work done on the Cummins NH turbocompound engine. This report contains all the analyses that were made to study the feasibility of a helical screw compressor and expander being used to replace the turbocharger and the power turbine of the Cummins turbocompound engine.

This program was conducted by the office of vehicle and engine R&D. Program officers from DOE were Mr. E. W. Gregory II and Mr. A. A. Chesnes. The technical monitor was NASA-Lewis Research Center in Cleveland, Ohio. The NASA Program Manager was Mr. J. C. Wood.

The bulk of this work was performed by Mr. J. Wurm from the Institute of Gas Technology under a subcontract from Cummins. The performance analysis was made by Mr. M. M. Kamel of Cummins. The Technical Director at Cummins was Mr. Roy Kamo.

SUMMARY

When the Cummins Advanced Turbocompound Diesel Engine Program was nearing completion, a task was added to study the effects of using a helical screw type positive displacement (PD) compressor and expander on the turbocompound engine. The PD machines were to replace the Cummins/Komatsu turbocharger and the power turbine used in the advanced turbocompound engine. The Institute of Gas Technology (IGT) completed the design, layout, and performance analysis of the PD machines under a subcontract from Cummins. The results of this study indicate that: (1) a screw compressor expander system can be used on engines up to at least 750 bhp, (2) dry operation of the rotors is feasible, (3) the physical layout is acceptable in a Cummins turbocompound engine, (4) cost and producibility of ceramic expanders are uncertain, and (5) an additional brake specific fuel consumption (BSFC) improvement of about 4% is possible if PD machinery is used on the turbocompound engine. Based on this study, Cummins has concluded that an experimental screw compressor and expander should be developed and tested to verify the predicted component efficiency and system BSFC gains.

INTRODUCTION

The fuel economy improvements in turbocompounding a heavy duty diesel engine have been demonstrated [1,2,3]*. The turbocompound system consists of a power turbine downstream of the turbocharger turbine and a gear train to feed the power recovered to the engine crankshaft. It has also been well established that the efficiencies of the compressor and the turbines are very critical parameters in the overall engine brake specific fuel consumption (BSFC). In a previous study by the Institute of Gas Technology (IGT) of Chicago for Cummins Engine Company, it was found that the helical screw type compressors and expanders have significantly higher efficiencies compared to the turbomachinery used in diesel engines. Based on this information, it was decided to study the feasibility of using a positive displacement (PD) helical screw type compressor and expander in place of the Komatsu/Cummins turbocharger and the power turbine used in the turbocompound system tests. This report contains the analysis of PD compounding of the Cummins NTC engine.

OBJECTIVES

The study of PD compounding included the following activities:

1. Preliminary design of a PD expander-compressor system to replace the present Cummins-Komatsu turbocharger and the power turbine in the NH turbocompound engine. Included in this activity are (a) system layout drawings, (b) details of the rotary components of the expander, and (c) component efficiency predictions.

2. An engine performance analysis based on the performance maps of the PD compressor and expander and a comparison of the results to the advanced turbocompound engine. This comparison will be made at 1300, 1600,, and 1900 rpm full load points only.

3. A brief cost analysis and manufacturing plan.

---

*Numbers in brackets designate references at the end of the report.

4. Normally most of the current production applications of screw compressors use oil lubrication as well as "oil flooding" techniques for sealing. Since oil mist in the air stream is not acceptable in the diesel engine application, a brief assessment of operation without oil, or "dry" operation, is necessary.
5. Establishment of any limitation for the PD system in terms of engine horsepower.

DISCUSSION

The Institute of Gas Technology (IGT) was subcontracted to complete four of the activities mentioned above. When the efficiency maps of the PD equipment were received, Cummins conducted the engine performance analysis. The complete subcontract report from IGT is included as Appendix 1. The following discussion briefly highlights the results of the five subtasks.

1. Design of the PD expander-compressor System to replace the present Cummins-Komatsu turbocharger and the power turbine

IGT designed the helical screw expander in detail. Their subcontract work emphasized expander design, since the application of helical screw machines as expanders is new. Sufficient information is available on screw compressors, and it was felt that a state-of-the-art compressor could be selected for this application. The design procedure for the expander was developed by IGT. The IGT subcontractor report, including the performance analysis, layout drawings, and the design procedure, is presented in Appendix 1. The results are summarized below.

Basic Design Specifications for Expander:

Rotor Outer Diameter	161 mm
Rotor Length	241 mm
Male Rotor Tip Speed at Engine Rated Operating Conditions	170 m/s
Male Rotor rpm at Engine Rated Operating Conditions	20,100 rpm

Basic Design Specifications for Compressor:

Rotor Outer Diameter	130 mm
Rotor Length	230 mm
Male Rotor Tip Speed at Engine Rated Conditions	137 m/s
Male Rotor rpm at Engine Rated Conditions	20,100 rpm

It should be noted that a comparable turbocompound system operates at 60,000 to 100,000 rpm.

2. Engine Performance Analysis

Cummins conducted a performance analysis of the compounded engine system using a cycle analysis program called "TRANSENG". This is an improved version of the Cummins Diesel Cycle Simulation (DCS) program. Cummins analysis was carried out in a generalized manner to study the effects of varying all the component efficiencies (i.e. compressor, turbine or expander, and power turbine for the baseline case) from 70 to 90%. This was done for 1900, 1600, and 1300 rpm engine speeds. Depending upon the component efficiency improvements of the screw machines, the curves presented in Appendix 2 could be utilized to obtain the engine performance improvements. As an example, if the component efficiencies of the compressor, turbine, and power turbine of the turbocompound engine are 80% each; and if these are replaced by a PD compressor and expander with efficiencies of 87.5% each, then engine efficiency gains are 3.3% and 4.7% at 1900 and 1300 rpm, respectively. For the specific comparison of the Cummins Advanced Turbocompound Engine (DOE/NASA/4936-2) with the PD machines designed here, the 3.3% and 4.7% gains at 1900 and 1300 rpm represent the best available data. As experimental data on component efficiencies become available in the future, the same set of curves presented here could be utilized to quantify engine system efficiencies.

3. Cost Analysis and Manufacturing Plan

The manufacturing cost of the screw machines is rather difficult to assess since many new and untested features are present in the design. Currently compressors are produced at relatively low volumes compared to the potential volumes for screw compressor-expanders in turbocompound engines for the heavy-duty truck market. The cost estimate generated by IGT is shown in Appendix 1. Our visit to Gardner-Denver produced a more optimistic estimate from that manufacturer. Without taking into account mass production factors, we estimate that screw compressor-expander sets could be manufactured for turbocompound engines for $900. This is broken down as follows:

Compressor Helical Rotors Fully Machined $100/piece	= $200
Expander Ceramic Rotors Fully Machined $200/piece	= $400
Housing, Timing Gears, Miscellaneous	= $300
Total	= $900

The cost of turbocompounding hardware is $840/engine. If the design could be simplified by coating or spraying the expander with ceramic or eliminate timing gears, this cost could be significantly reduced. A considerable amount of producibility research, especially for the expander, is needed. In addition, the use of screw machines offers the possibility of replacing the turbocompound gear train and fluid coupling with inexpensive belt drives. The cost analysis presented here is preliminary and brief. As hardware is developed, the cost estimate should be revised and improved.

The manufacturing plan for compressors assumes the introduction of mass production techniques and emphasizes cost reduction. For the expander, manufacturing depends on ceramic rotor production technology. Some research in this area has already been done at Lawrence Livermore Laboratory and is underway at Cummins on different programs. A producibility evaluation program for expanders should include a variety of methods of making composite rotors such as reaction bonding, coatings, etc. with emphasis on low cost mass production.

4. Assessment of Dry Contact Operation of PD Machines

Helical screw compressors are in production and commonly used in several applications now. Most of these machines are oil lubricated and oil mist "flooded" to provide good sealing characteristics. The application for supercharging a diesel engine is new and the engine cannot tolerate oil mist in the intake air. Therefore, "dry" operation of the rotors is necessary. There are screw machines in production now which operate dry. This was observed during a visit to the Gardner-Denver plant in Quincy, Illinois. It is believed that such operation is feasible if rotor surfaces have compatible solid lubricant properties. Making rotors out of ceramics is likely to result in close clearances and good sealing. According to screw machine manufacturers, such as Gardner-Denver, Sullair, and SRM, the problems of dry contacts can be substantially alleviated if:

(a) New rotor profiles are developed for which sealing properties would not be worsened, but the relative sliding velocities would be reduced, and machinability improved. According to Sullair and SRM, this is possible.

(b) Power transmission is directed through the male rotor. In such a case, only nominal forces act on the timing gears or the interacting lobes (in applications where timing gears are not used). IGT has conducted a separate study for Cummins under a different contract to analyze in detail the dry operation of screw machines (IGT Project No. 65904, Final Report by J. Wurm, dated February, 1983).

However, a conclusive judgement on the effective, dry operation of screw machines will require experimental evaluation.

5. Establishment of Upper Power Limit of the Engine for the Application of PD Machinery

This criterion is necessary primarily for packaging considerations. IGT determined the rotor dimensions for a 750 HP diesel engine. The 750 HP level was chosen primarily because that is the highest HP level of interest to Cummins as far as turbocompounding is concerned. It was also felt that, within the packaging constraints for the 750 HP engine, the recommended rotor tip speeds might be marginal. For the screw compressor, IGT determined the rotor dimensions by following generally acceptable geometrical rules and other design practices. However, the operating conditions for the expander are much more severe and the design constraints differ from those of the compressor. This necessitated a different optimization of the rotor tip speeds. The basis for this optimization was an estimate of local inlet Mach number governing the level of hydraulic loss. This justifies the use of higher speeds (compared to compressors) and, therefore, matches the large engines with expander dimensions that are well within the practical sizes of commonly manufactured screw compressor components. Specifically, the expander size corresponding to rotors of around 200 mm does not impose any extra dimensional problems for engines in the 750 HP category. Therefore, it is concluded that screw machines can be successfully used on engines of at least 750 HP output. The layout of the expander designed by IGT is shown in Figure 1.

Based on these discussions, it is clear that the helical screw type compressor and expander does offer advantages for the turbocompound engine. The following is a summary of the advantages.

1. Lower operating speed range of the screw expander, with a simpler reduction of expander power output shaft speed to the reciprocator power shaft (15,000 to 20,000 rpm for a screw expander instead of 60,000 to 100,000 rpm for the turbo-expander).

2. No interstage thermal losses. This is due to the fact that available after-cylinder heat energy is converted into useful mechanical work within one stage (unlike in the case of a turbocharged/ turbocompound system where part of the heat energy is extracted with a high pressure, turbocharger stage and the rest is extracted with a low pressure, power turbine stage).

FIGURE 1

SCREW EXPANDER DESIGN

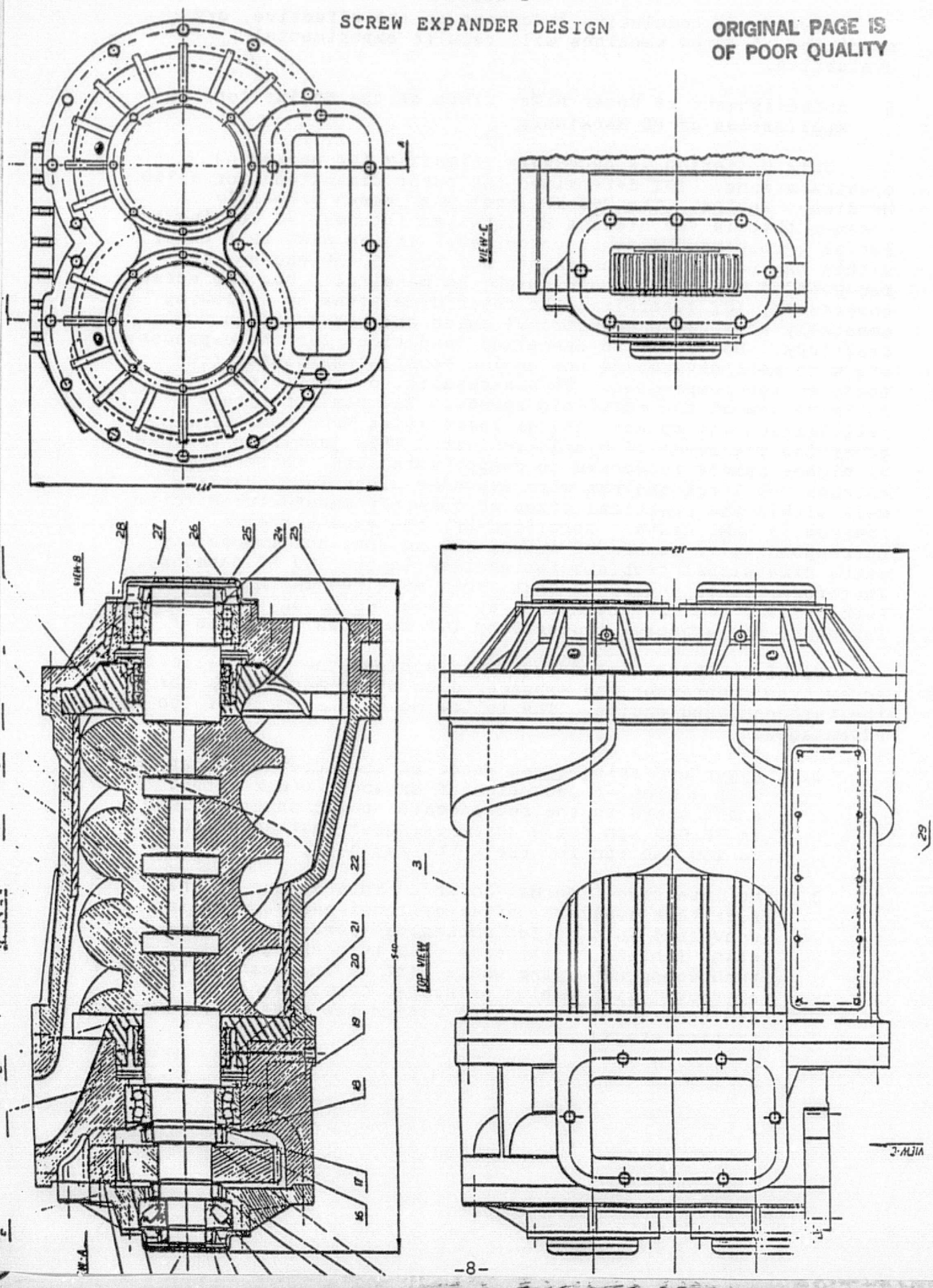

3. Potentially high overall efficiencies for the expander and compressor. The specific PD machines designed for the Cummins NTC-400 engine have 87-89% efficiency compared to turbomachinery efficiencies of 79-80%. In addition, PD equipment has better part load efficiencies than turbomachinery.

4. The screw expander, unlike a turbo-expander, will have inherent features protecting it against overspeeding if it is unexpectedly unloaded. This is accomplished through direct mechanical connections between the engine and the compound system.

5. Due to mechanical supercharging, a positive displacement screw supercharged/compound system could have better dynamic response characteristics, especially for small light-duty systems, due to the low inertia of the compressor and expander. For bigger sizes or heavy-duty systems with higher moments of inertia of both subcomponents, predicting the potential advantages in system response are more difficult. However, this problem might be overcome by adequate mass reduction of the reciprocator flywheel and/or other elements in which mass reduction would be possible.

CONCLUSIONS

1. PD compounding of heavy duty diesel engines shows good promise for continued investigation.

2. Based on the preliminary design presented here, additional analysis on noise, clearance control, and engine integration of the helical compressor and expander should be conducted.

3. Detailed component design should be conducted and prototypes should be produced.

4. PD prototype machines should be tested on a test stand and on an engine to verify the efficiency gains.

REFERENCES

1. J. L. Hoehne and J. R. Werner, "The Cummins Advanced Turbocompound Diesel Engine Evaluation", DOE/NASA/4936-2, April, 1983.

2. M. C. Brands, J. R. Werner, J. L. Hoehne, and S. Kramer, "Vehicle Testing of Cummins Turbocompound Diesel Engine", SAE Paper No. 810073.

3. R. Kamo and W. Bryzik, "Adiabatic Turbocompound Engine Performance", SAE Paper No. 810070.

INSTITUTE OF GAS TECHNOLOGY
IIT CENTER
CHICAGO, ILLINOIS 60616

DESIGN OF A HELICAL POSITIVE DISPLACEMENT EXPANDER FOR DIESEL POSITIVE DISPLACEMENT COMPOUNDING

Final Report

by

T. Bulicz
J. A. Kinast
H. Banasiuk
J. Wurm

Project 65904

for

CUMMINS ENGINE COMPANY

June 1983

TABLE OF CONTENTS

TABLE OF CONTENTS, Cont.

LIST OF FIGURES AND TABLES

LIST OF FIGURES AND TABLES, Cont.

EXECUTIVE SUMMARY

The objectives of this project were: 1) to prepare a preliminary design of a screw expander for diesel exhaust energy recovery for the Cummins NTC-400, 400 hp diesel engine, 2) to develop a method of matching a screw expander to an engine, 3) to evaluate the potential overall efficiency of the expander, and 4) to compare the system efficiencies of the screw expander compound system relative to the existing turbocompound system.

In this project, the screw expander was designed. The mounting arrangement of the expander with an equivalent compressor was defined. The size and placement of the machines would require installation similar to the turbocompound system, so that the changes required to incorporate the positive displacement subsystem may be kept to a minimum.

As part of the design work, the stresses on the expander were evaluated, showing that the design had a minimum safety factor of eight. In addition, a concept was designed to prevent overexpansion of the exhaust gases and the resulting drop in efficiency.

The sizing and efficiency estimates are based on current compressor design data, adjusted for the change from symmetric to asymmetric rotor profiles, improved bearings, and estimated improvements due to expander instead of compressor operation. A maximum efficiency of 95% was calculated. In comparison with the turbocompound system, the positive displacement compound system was estimated to have 7% higher brake mean effective pressure and 5% better brake specific fuel consumption at rated conditions. Due to higher part load efficiencies, engine performance would benefit even further from the application of the positive displacement subsystem.

This preliminary design was developed using a conservative approach. It is probable that further simplification, particularly in bearings and seals, can be made to make the expander, as well as the compressor, less complex and less costly.

As a result of this work, we concluded that there is a potential benefit in applying screw machines to this type of service. The projected performance of the positive displacement compound system is comparable to or better than the turbocompound system. The stress analysis and the design and installation

(on paper) have shown that the compound system is technically feasible. Experimental verification of materials, manufacturing technique, and performance is, of course, required. Therefore, we have concluded that the concept of screw positive displacement compound diesel systems represents a significant technology advancement that should be further pursued, primarily in terms of identifying manufacturing methods to produce machines at affordable costs.

INTRODUCTION

The primary objective of this project was to prepare a preliminary design of a screw expander for diesel exhaust energy recovery for the Cummins NTC-400, 400 hp diesel engine.

Secondary objectives were: to develop a method to match a positive displacement screw expander with a given engine; to evaluate the potential overall efficiency of the expander; and to compare overall system efficiencies of the existing turbocompound unit with those of the proposed screw expander compound alternative.

Our approach to this work consisted of two steps:

- Developing engineering methods for sizing and selecting a screw expander given a combustion engine.
- Generating an engineering design of an expander that is dimensionally compatible with the existing hardware.

Throughout the project, we emphasized consideration of the system performance and characteristics, with special attention paid to the high operating temperatures, mechanical loads, and unconventional, high variable operating conditions.

The conceptual design and analysis is based on the use of ceramics for the following reasons:

- The peak exhaust manifold temperature for the turbocompounded thermally insulated engine has been measured at 1070°F. Exhaust temperature predictions for the advanced adiabatic diesel are as high as 1500°F. The temperature is very close to the temperature range in which the structural properties of steel deteriorates. For example, M50 steel tensile strength decreases from 125×10^3 psi at 1100°F to 25×10^3 psi at 1500°F.
- The efficiency of a screw expander is extremely dependent on the clearances between its components. The coefficient of thermal expansion for ceramics is less than 1/4 that of steel. Thus, control of clearances is easier with ceramics than with steel.
- The density of ceramics is about 1/2 that of steel. Thus, ceramic rotors would have lower rotational inertial characteristics than steel. This is advantageous in terms of the total system dynamic response behavior.
- The use of ceramics for the housing of the expander would result in less heat loss than with steel because the thermal conductivity of ceramic materials is about 1/2 that of steel.

TECHNICAL ACHIEVEMENTS

The details of our design and analysis of a screw expander for compound diesel operation are described below.

System Analysis

Baseline System Data Analysis and Evaluation

The screw expander, acting as an exhaust energy recovery device, operates within the thermodynamic conditions defined by the design characteristics and operating conditions of an engine. In addition, the expander also has to physically fit into the engine's existing structural arrangement. A careful assessment of the conditions that the expander should match was the logical first step of this project.

The screw expander compound system was to be designed for the Cummins NTC-400 engine. This was also the baseline engine for the previously developed turbocompound hybrid system of Cummins Engine Co. Performance data for that system were provided to IGT by Cummins for comparison with the expander system. Since the screw expander is a positive displacement replacement for the low-pressure power turbine in addition to the supercharger turbine in the existing turbocompound diesel engine TCPD-450, almost all the available performance and operating data as well as some design features of this system can be used to establish the base for performance predictions and specifications of design requirements of the screw expander compound system.

The data received from Cummins consisted of values of performance and operating parameters of the hybrid system load characteristics measured at three engine speeds: 1300, 1600, and 1900 rpm. Performance data were determined for the hybrid system, the diesel engine, and low-pressure power turbine separately. The performance data of special interest for analysis of the expander were brake horsepower and brake specific fuel consumption. For the components of the hybrid system and for the system as a whole, measurements were made at the following points of the turbocompound system: compressor inlet, engine inlet manifold, compressor turbine inlet, power turbine inlet, and power turbine outlet. For our work, the important data were: air mass flow to the engine, air pressure and temperature at inlet manifold, and exhaust pressure and temperature in outlet manifold. These data as well as

other factors (such as turbocharger performance, pressure drop across the engine, etc.) were assessed. Design point conditions for sizing the expander were based on load distribution versus engine speed during average driving operation. (These data were provided by Cummins.) Since the baseline NTC-400 engine was designed as a heavy-duty, long-haul vehicle engine and the same application for the screw expander compound system was assumed, most of the operating time is in the vicinity of maximum load.

Mounting arrangements for the expander and the method of compounding it into the system were to be defined from several engineering drawings of the existing arrangement of the NTC-400 diesel, turbocompound drive train layout, and current exhaust manifolds.

These data and technical information were used for evaluating the requirements to be met by the screw expander and constituted the base level for our analysis and design specifications which are discussed below.

Overall Adiabatic Efficiency of the Screw Expander

One of the advantages of the positive displacement screw expander compounding over turbocompounding lies in its potentially higher overall adiabatic efficiency. The overall adiabatic efficiency of the screw expander has an important influence on the total efficiency of the compounded system. However, use of screw positive displacement expanders is at a very early stage, so the procedure for identifying design specifications for a screw expander from the desired adiabatic efficiency has not been previously established. The limited time schedule and funds have not allowed for a more detailed mathematical study of this problem. In an attempt to narrow the existing gap in knowledge, we studied the existing compressor data and the possible effects of various thermodynamic, operating, and design factors on the overall efficiency of a screw expander. This allowed us to estimate the performance and establish a sound basis for the design.

Our studies have led us to the following guidelines for deriving the efficiency characteristics of the expander:

- Expander characteristics are functionally similar to compressor characteristics and as such can be derived from existing performance specifications of commercial screw compressors.

- Recent achievements in improving efficiency could be taken into account in our prediction of the potential expander total adiabatic efficiency as well.
- Overall adiabatic efficiency of the expander can be derived by correcting the overall adiabatic efficiency of a compressor for the difference between the hydraulic losses associated with compression and those with expansion.

Using these guidelines, we have selected a compressor made by Gutehoffnungshütte, a West German compressor manufacturer. The compressor has overall adiabatic efficiency characteristics, $\eta_{oad,com}$, defined as a function of pressure ratio, operating speed, and delivered capacity (Chlumsky) as shown in Figure 1. This compressor represents the traditional dry machine with a symmetric rotor profile and plain bearings. The compressor was selected because it is the most recent design characterized in enough detail for our use. These characteristics were used to calculate overall adiabatic efficiency as a function of male rotor speed for values of pressure ratio. This function provides the basis for deriving the potential expander overall adiabatic efficiency lines.

The main contributions to improved expander efficiency are from replacing plain journal bearings with ball or roller bearings, and replacement of symmetrical rotor profiles with asymmetrical low internal leakage profile. According to Wichert, a mechanical journal bearing efficiency, η_{mJB}, of 0.93 can be increased to a rolling bearing efficiency, η_{mRB}, of 0.97; knowing η_{mJB}, the internal adiabatic efficiency, $\eta_{ad,com}$, of the compressor could be found.

$$\eta_{ad,com} = \frac{\eta_{oad,com}}{\eta_{mJB}} \tag{1}$$

The effect of changing from symmetric to asymmetric profiles (Schibbey) is shown in Figure 2 in the form of a ratio of internal adiabatic efficiencies for asymmetric and symmetric profiles as a function of tip speed of the male rotor. Making the simplifying assumption that the adiabatic efficiency ratio is not influenced by varying pressure ratio, the internal adiabatic efficiency, $\eta'_{ad,com}$, of the compressor corrected for an asymmetric profile can be defined as:

$$\eta'_{ad,com} = \eta_{ad,com}\ \lambda \tag{2}$$

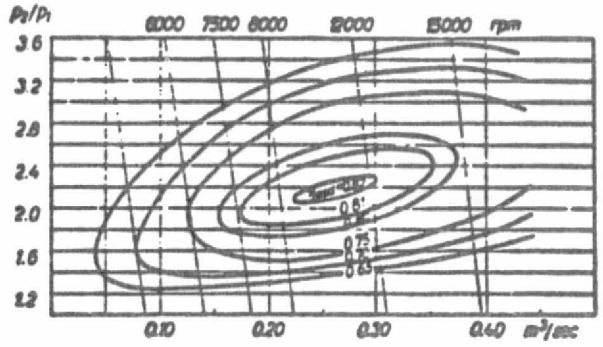

Figure 1. CURVES OF CONSTANT EFFICIENCY PLOTTED AGAINST DELIVERED GAS QUANTITY AND COMPRESSION RATIO FOR A SINGLE-STAGE SCREW COMPRESSOR MADE BY GUTEHOFFNUNGSHÜTTE, GFR

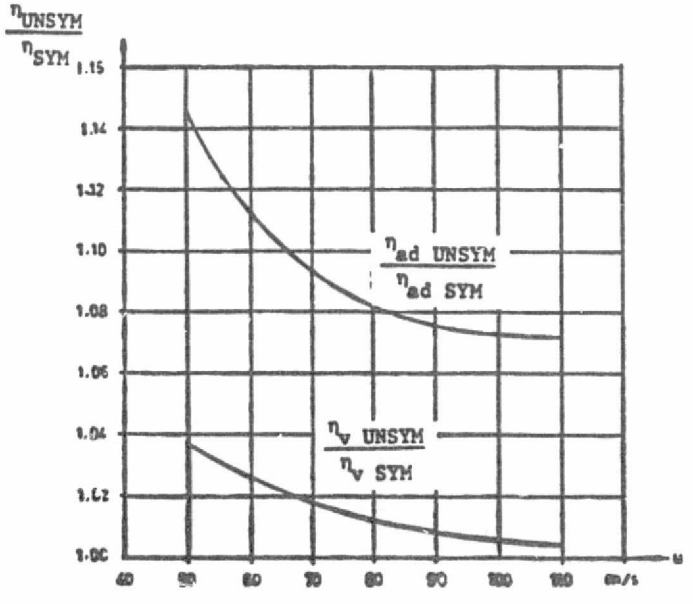

Figure 2. RATIO OF EFFICIENCIES BETWEEN ASYMMETRIC AND SYMMETRIC PROFILE MACHINES FOR VARYING TIP SPEEDS

Leakage between rotor volumes affects expander efficiency differently than a compressor. Leakage for an expander occurs in the direction of flow from high to low pressure areas rather than against the flow direction. Exhaust gases leaking around a rotor lobe decrease the pressure of the entrained volume and thus decrease the level of expansion that could otherwise be achieved. However, they also increase the temperature and pressure of the volume they are entering; because of this increase, partial recovery of the loss can be achieved by using a larger volume expansion ratio. A more detailed analytical evaluation of the potential gains in expander efficiency was beyond the scope of this work. However, we assumed that a 2% gain of expander internal adiabatic efficiency is conceivable throughout the operating range of pressure ratios and speed, resulting in:

$$\eta_{ad,exp} = 1.02\ \eta'_{ad,com} \tag{3}$$

The last step in determining the potential total expander adiabatic efficiency was to account for the rolling bearing mechanical efficiency, $\eta_{mRB} = 0.97$, resulting in:

$$\eta_{oad,exp} = \eta_{ad,exp}\ \eta_{mRB} \tag{4}$$

The corresponding lines for $\eta_{oad,exp}$ are plotted next to corresponding lines for $\eta_{oad,com}$ in Figure 3.

For further analysis, we needed to establish the expander's efficiency characteristics at operating speeds corresponding to the engine operating speeds at which the data used for this analysis have been measured. An upper limit was imposed on the operating speed since available compressor data only extends to 100 m/sec rotor tip speed (approximately 15,000 rpm in this case). Compressor speeds of 10,000; 12,000; and 14,000 rpm were selected. These speeds are below the upper limit and maintain an almost fixed ratio between compressor and engine speeds. At this point the deviations from a fixed gear ratio are insignificant. The compressor efficiency curves were then replotted as a function of pressure ratio in Figure 4. It can be seen that the baseline compressor efficiency drops as the operating pressure ratio deviates from the design pressure. An expander, however, is not expected to be as sensitive as the compressor to the difference between the operating and design pressure ratios.

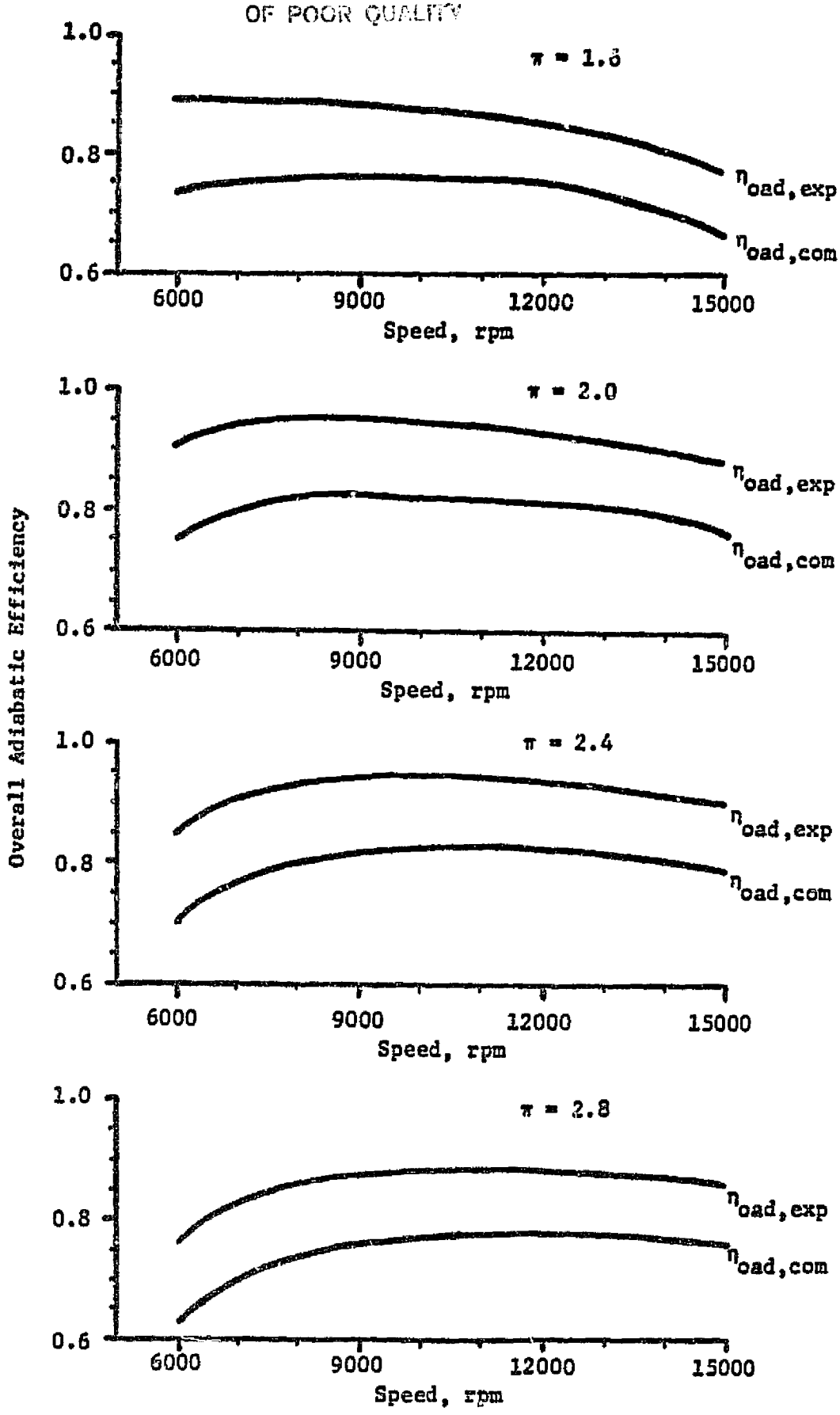

Figure 3. EFFICIENCY CURVES FOR COMPRESSOR AND ADVANCED EXPANDER

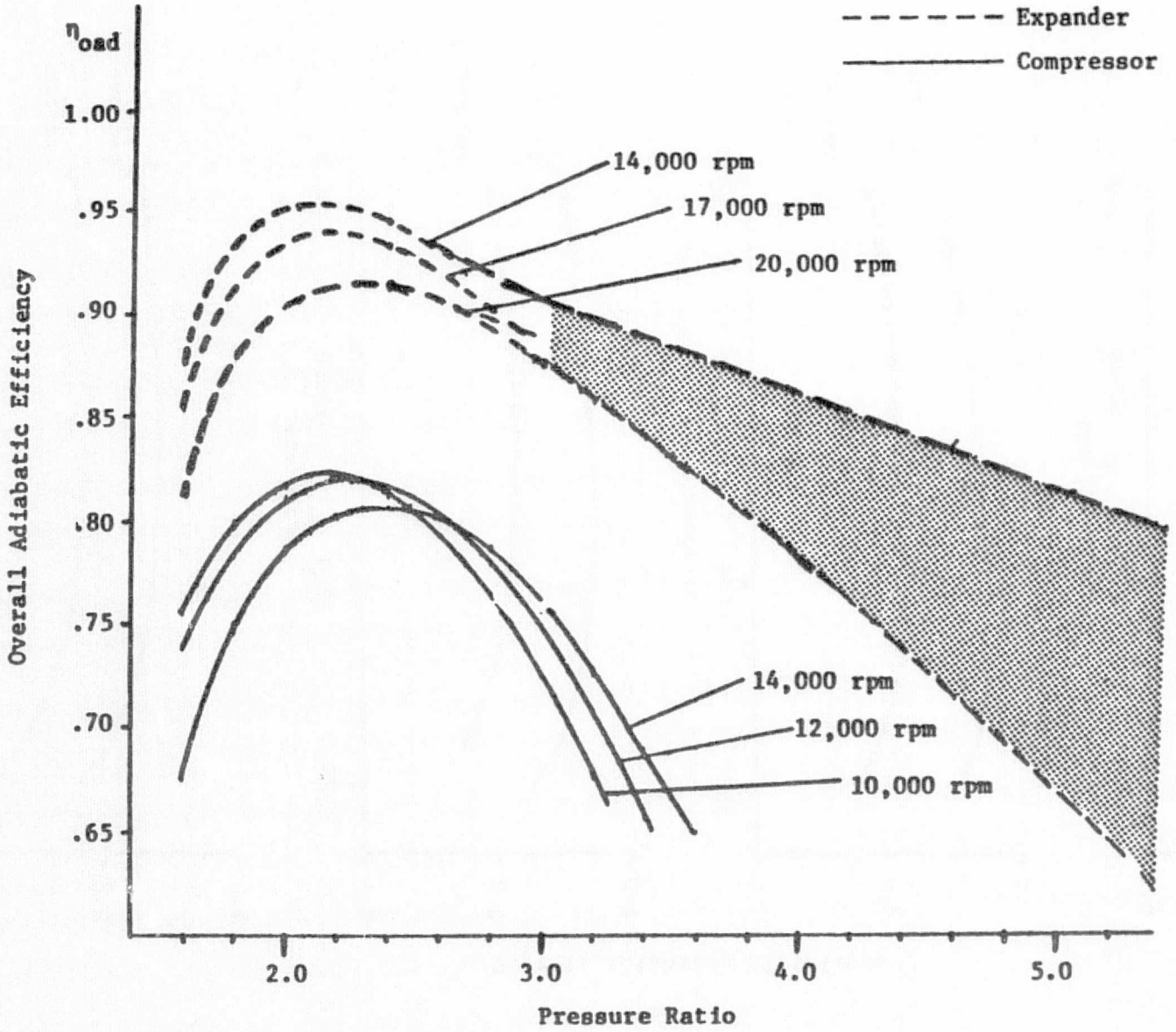

Figure 4. EFFICIENCY VERSUS PRESSURE RATIO FOR COMPRESSOR AND ADVANCED EXPANDER WITH ESTIMATES FOR HIGH PRESSURE RATIO

The last step in determining the adiabatic efficiency of the screw expander was to identify the influence of high speeds on expander efficiency. For a reasonably sized expander providing total expansion of exhaust gases defined by the engine rating point, our calculations showed that the expander will run at approximately 20,000 rpm. Following the ratio between engine and expander speed for the speeds where engine load characteristics were taken, corresponding expander speeds are 17,000 and 14,000 rpm, respectively. These values were beyond the range covered by both the screw compressor and expander characteristics as shown in Figure 3.

Considering the influence of expander speed on adiabatic efficiency, increased speeds would tend to decrease both internal and external leakages and to increase hydraulic losses generated at the inlet to the machine, during high velocity flow of the working medium along the rotors, and at the outlet from the unit.

Comparing the operating conditions of a screw machine acting as a compressor or as an expander, the expander will operate at much higher temperatures than those experienced by compressors. Therefore, the local Mach numbers (see "Expander-Compressor Design Study for Heavy Duty Compounded, Adiabatic Diesel Engines, Final Report," February 1983) are much higher, which allows higher operating tip speeds. The following differences will also affect their relative hydraulic loss characteristics:

- The compressor accelerates the working medium at its inlet from zero velocity to rotor tip velocity; an expander is fed with gas having some finite speed at its inlet caused by the blowdown and forced discharge of the engine. Because inlet hydraulic losses are proportional to inlet gas acceleration within the machine, total inlet hydraulic losses will increase with expander tip speed slower than for the compressor.

- The high velocity of gas inside the machine produces frictional losses which, in the charging and expansion phases of the expander cycle, can be partially recovered as generated heat. For a compressor, no friction-related loss is recoverable.

- Discharge in a compressor takes place after a compression phase through a discharge port which, due to design conditions, may be more restricted in size than an expander outlet. Outlet hydraulic losses of the expander may be kept at a lower level as a result.

- The high velocity of gases entering the expander in combination with the high frequency of pressure changes may improve the charging efficiency of the expander.

Our conclusion from the above considerations is that a screw machine will have better efficiency characteristics at higher speeds when it operates as an expander than as a compressor. An exact determination of the possible gains in efficiency at higher speeds for a screw expander is impossible without a more detailed analysis. Therefore, we assumed that the combined effect would make the overall adiabatic efficiencies derived for the expander at 10,000; 12,000; and 14,000 rpm equal to that expected at speeds of 14,000; 17,000; and 20,000 rpm, respectively. Based on this assumption, the lines for the final values of $\eta_{oad,exp}$ as a function of pressure ratio were drawn in Figure 4. With this approach, we estimated a maximum potential overall adiabatic efficiency of 95% for the expander. Further study is, of course, required to verify this number before proceeding with later experimental work. Several approaches to extrapolate these curves for higher pressure ratios were considered. These included: non-linear approximations in which the derivatives within the higher pressure ratio range follow the derivatives defined from existing data for lower pressure ratios; linear approximations in which straight lines containing points for pressure ratios of 2.4 and 2.8 represent potential expander efficiencies for higher pressure ratios; and linear approximations where numerical values of overall adiabatic efficiencies were assumed for a pressure ratio of 5. Different slopes for given speeds were established to account for the influence of gas dynamics as well as interactions between engine and expander.

This last extrapolation most closely resembled the trend shown by the theoretical compressor adiabatic efficiency. As a result, it was used for estimating values of expander overall adiabatic efficiency at operating points of the baseline system. These values were used to determine the screw expander compound system performance and efficiency characteristics.

Efficiency and Other Characteristics of the Screw Expander Compound System

The major objectives of this analysis were:

- Estimate the technological competitiveness of the screw expander compound system with special emphasis on evaluating its potential advantages over the existing turbocompound system.
- Define the economy and operational optimization of the system in terms of engine exhaust back-pressure.

These objectives were reached by using a simplified model describing the screw expander compound system, composed of a positive displacement supercharger,

positive displacement diesel engine, and positive displacement screw expander. All analyses carried out were based on the following assumptions:

- Boosting characteristics of the engine after conversion from turbo-compounding to positive displacement compounding remains unchanged, which implies that the positive displacement supercharger replacing the turbo-charger in the baseline system will be able to duplicate air flow, intake air pressure, and intake air temperature to the engine at the monitored points of engine load characteristics.

- Thermodynamics of the engine combustion process are not influenced by back-pressure buildup in the engine exhaust manifold caused by interaction between engine and expander. The effect of this assumption was that values of engine brake shaft power determined at measured characteristic points could be directly used in our analysis.

- The analysis was carried out for several cases in which the system design pressure ratios were greater than 3. This assumption was made to simplify the calculation procedure by limiting the scope of analysis only to the cases where the operating expansion ratios of the screw expander compound system exceeded those of the baseline turbocompound system.

- The system operates at steady-state conditions.

The schematic of the positive displacement compound system is shown in Figure 5. Exhaust gases partially expanded in the engine enter the positive displacement expander to complete thermodynamic expansion. Mechanical power generated during this post-cylinder expansion is transmitted through the drive train to the engine. The power, decreased by the amount required to drive the positive displacement compressor, adds to the total power output from the system shaft.

The thermodynamic working cycle of the system is identical to the turbo-compound system and the p-V diagram is shown in Figure 6. This figure also establishes the parameter notations used. Numbers indicating points on the p-V diagram are used as subscripts of thermodynamic state parameters at those points. The expander generates mechanical power from the potential thermal energy contained in exhaust gases at the end of the engine cylinder expansion (flow dynamics assumed to be negligible).

A block diagram of the interactions among individual parts of the system is shown in Figure 7. The block element representing the expander has been divided into two parts to show that there are two volumes incorporated into the total displacement of the screw expander, each of them performing

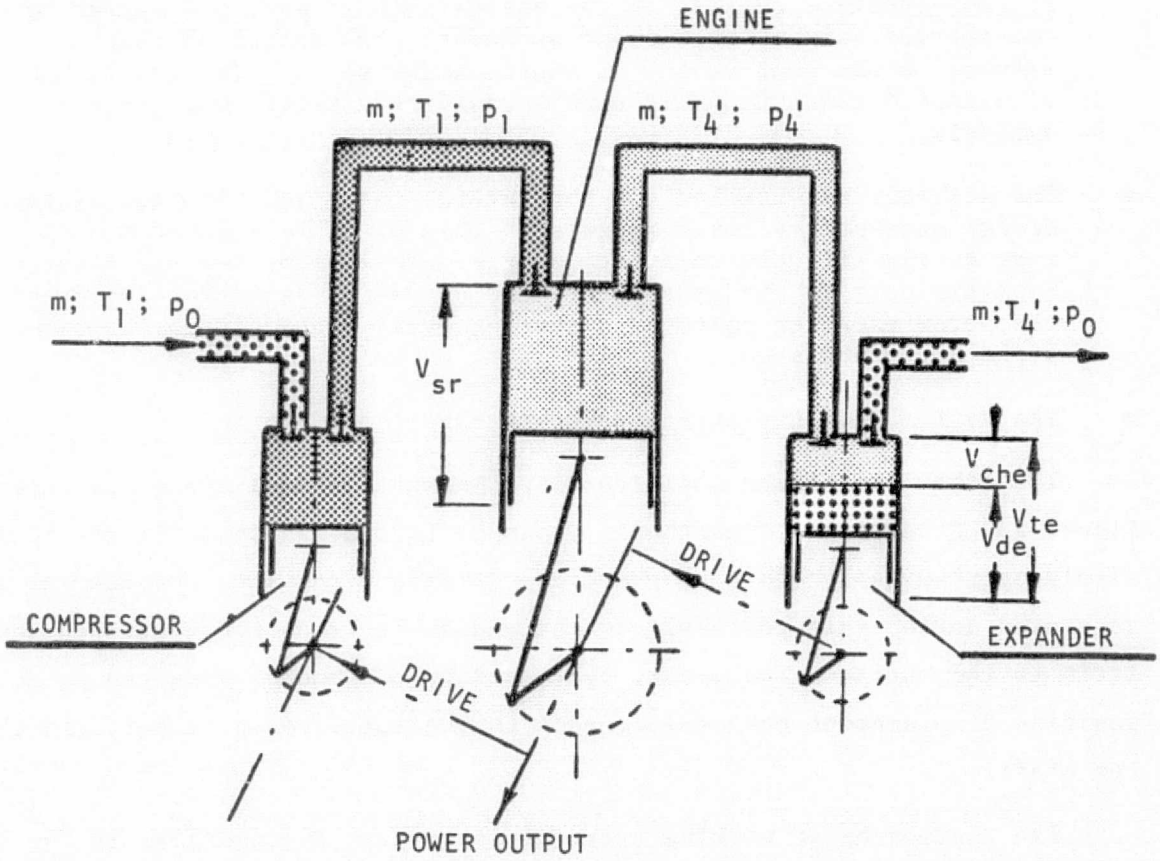

Figure 5. SCHEMATIC OF POSITIVE DISPLACEMENT COMPOUND SYSTEM

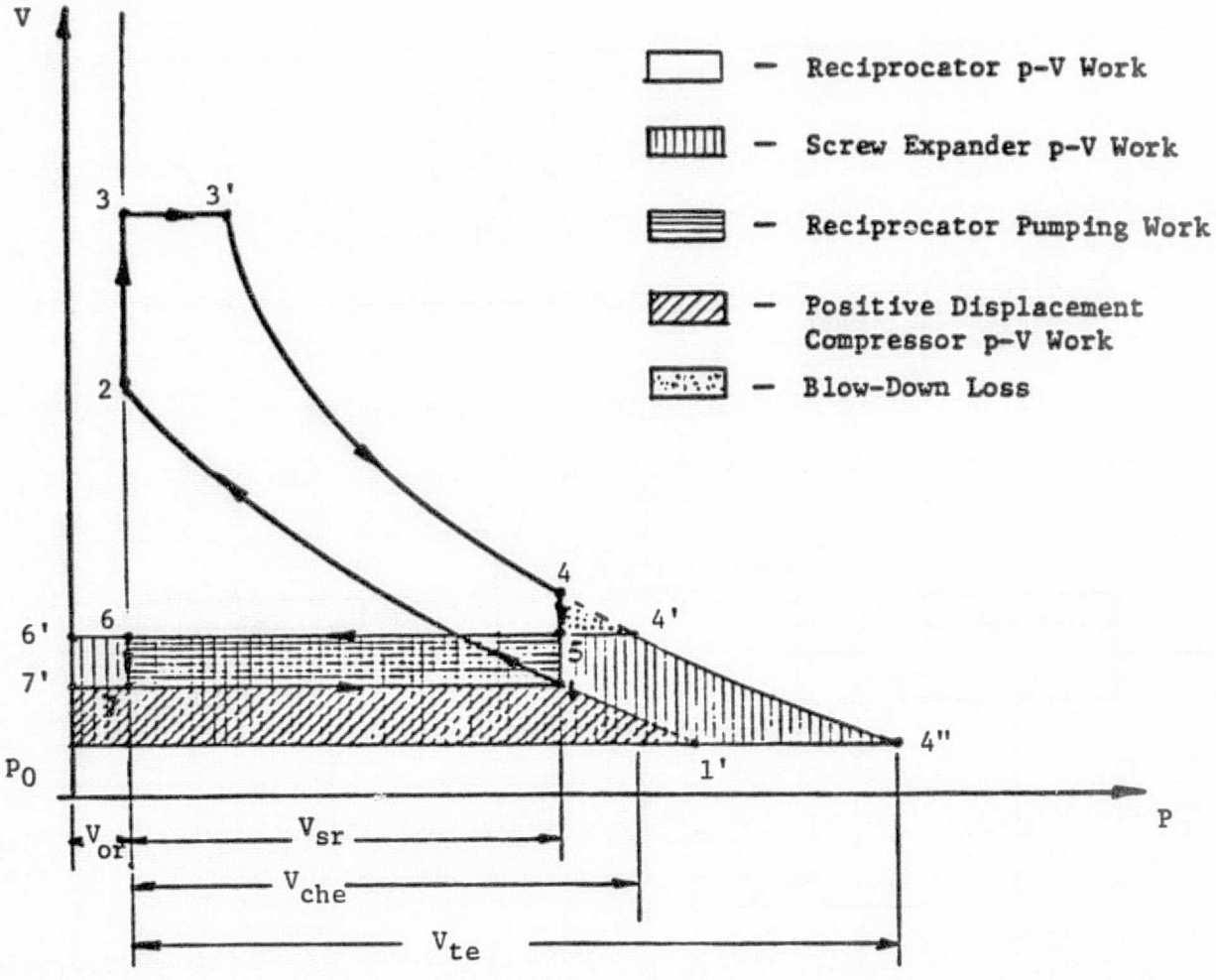

P_0 = Atmospheric pressure

P_{7-1} = Supercharging pressure

P_4 = Reciprocator expansion end pressure

P_{4-5} = Blow-down pressure drop

$P_{6'-4'}$ = Expander charging pressure (Approx. equal to reciprocator discharge pressure and exhaust manifold back-pressure)

V_{or} = Reciprocator clearance volume

V_{sr} = Reciprocator displacement volume

V_{che} = Expander charging volume

V_{te} = Expander total displacement volume

Figure 6. POSITIVE DISPLACEMENT COMPOUND SYSTEM p-V DIAGRAM

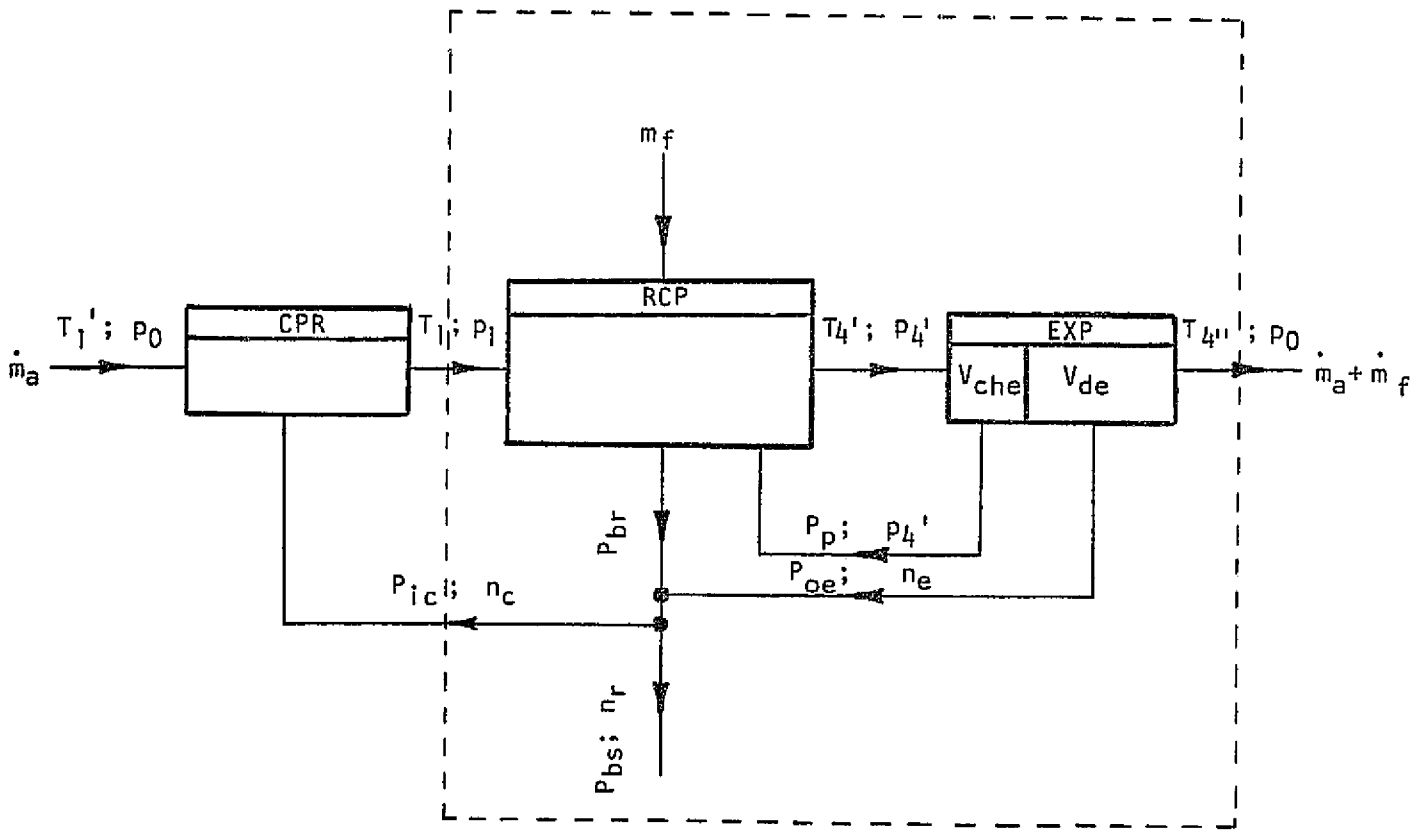

Figure 7. BLOCK DIAGRAM OF INTERACTIONS BETWEEN COMPRESSOR, RECIPROCATOR, AND EXPANDER

different functions; the charging volume, V_{che}, responsible for the flow rate of gases through the system, controls the back-pressure in the exhaust manifold; and the expansion volume, V_{de}, where the expansion process takes place. The charging volume, by controlling back-pressure p_4', contributes to cylinder pumping losses while V_{de} contributes to the expansion process, generating p-V work which is directed to the engine shaft at a rate determined by the expander power output shaft speed, n_e. This determines expander power output, P_{oe}. Because the charging volume of the expander is an important design parameter of the system, as it controls the cylinder back-pressure which is practically identical to the expander inlet pressure and influences the performance of the engine and the expander, we have examined its effect on the pressure at the expander inlet, p_4'.

From the mass conservation principle and the ideal gas equation applied to the points at the inlet and outlet of the reciprocator:

$$\frac{p_1 \dot{V}_{sr}}{RT_1} = \frac{p_4' \dot{V}_{che}}{R\, T_4'} \tag{5}$$

where:

T_1 = Reciprocator intake temperature

p_1 = Reciprocator intake pressure

T_4' = Expander inlet temperature

p_4' = Expander inlet pressure

$\dot{V}_{sr}$ = Volume flow capacity of reciprocator (engine)

$\dot{V}_{che}$ = Volume flow capacity of expander.

Considering that:

$$\dot{V}_{sr} = \frac{n_r}{2} V_{sr} \text{ (for four-stroke cycle)} \tag{6}$$

where:

n_r = Reciprocator shaft speed (engine)

V_{sr} = Reciprocator displacement

and:

$$\dot{V}_{che} = 4 n_e V_{ch} \text{ (for four lobe male rotor)} \quad (7)$$

where:

V_{ch} = Charging volume of individual interlobe cell

n_e = Expander male rotor speed.

Equation 7 after rearrangement is:

$$V_{ch} = \frac{1}{8} \frac{p_1}{p_4'} \frac{T_4'}{T_1} \frac{n_r}{n_e} V_{sr} \quad (8)$$

In Equation 8, p_1, T_1, T_4' and n_r are engine parameters depending only on the operating point. If these values are determined, then the charging volume becomes only a function of engine back-pressure and expander speed.

For given operating conditions of an engine (such as the rated conditions) and the desired back-pressure level and drive ratio between the engine and expander, the charging volume of an individual interlobe cell can be determined. Figure 8 shows curves of charging volume for values of engine outlet pressure within the range of n_e developed for the operating conditions of our baseline system (p_1 = 2.41 kg/cm^2, T_1 = 424°K, T_4' = 850°K, n_r = 1900 rpm, and V_{sr} = 14 dm^3).

After a description of the pressure levels at the expander inlet was developed, we formulated a model of the expander compound system to determine its performance. The measure of performance selected was brake specific fuel consumption, comparing that of the turbocompound system (determined experimentally) with that of the screw expander compound system.

Referring to the block diagram of the screw expander compound system in Figure 7, brake specific fuel consumption, $BSFC_D$, is:

$$BSFC_D = \frac{\dot{m}_f}{P_{bs}} \quad (9)$$

where:

$\dot{m}_f$ = Fuel rate to the system

P_{bs} = Brake power output from the system.

Note:

Values calculated for rated engine conditions:

Engine Inlet Pressure, p_1 = 2.41 kg/cm^2

Engine Inlet Temperature, T_1 = 424 °K

Engine Exhaust Temperature, T_4' = 850°K

Engine Ratio, rpm = 1900

Engine Displacement = 14 dm^3

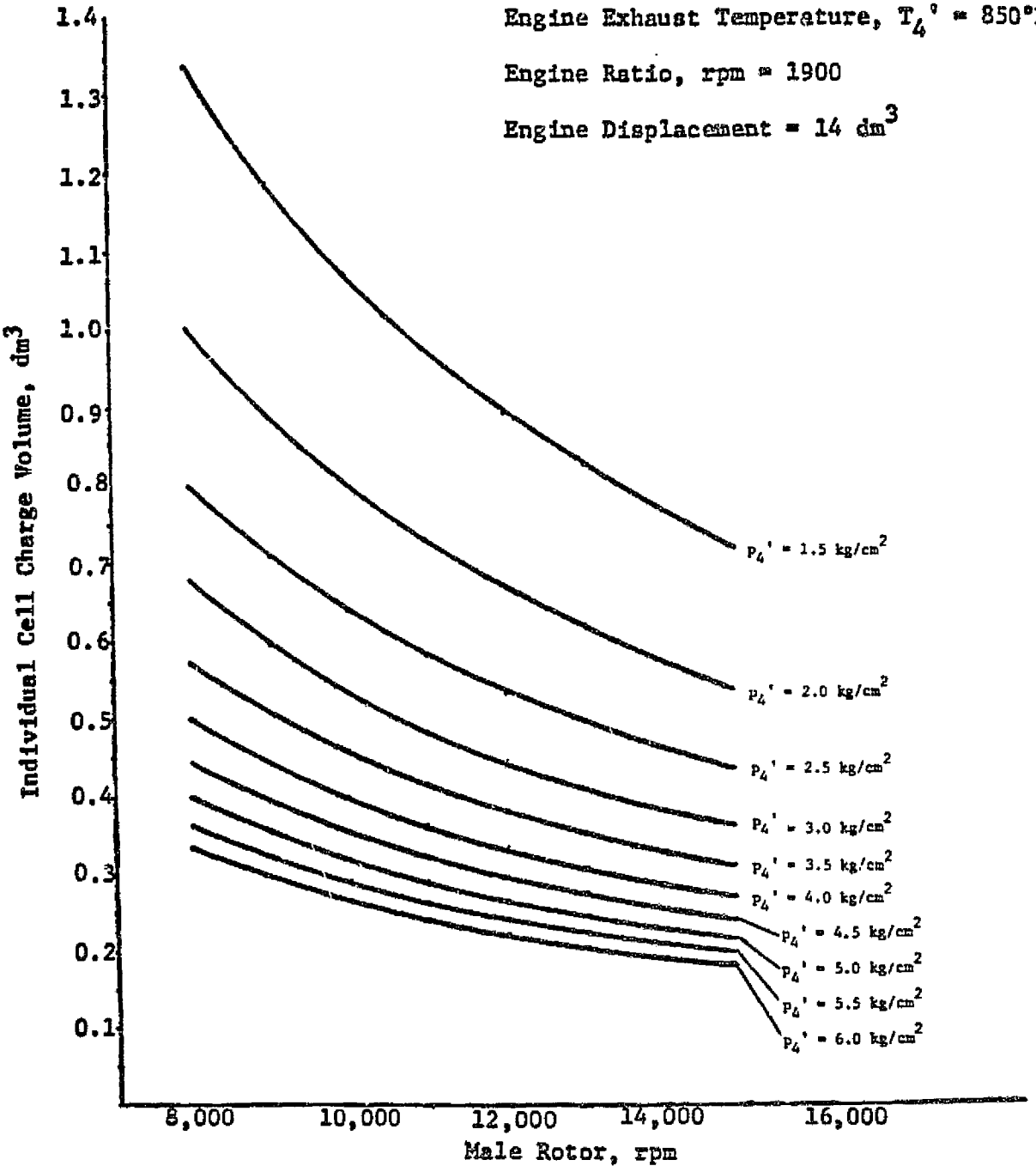

Figure 8. EXPANDER CHARGING VOLUME GIVEN EXPANDER INLET PRESSURE AND MALE ROTOR SPEED

Analysis of the power balance within the system leads to:

$$P_{bs} = P_{br} + P_{be} - P_p/\eta_{mr} - P_{ic} \tag{10}$$

where:

P_{br} = Brake power of reciprocator

P_{be} = Brake power output of expander

P_p = Indicated pumping power losses induced by manifold back-pressure

η_{mr} = Reciprocator mechanical efficiency (const = 0.90)

P_{ic} = Compressor power input.

The expander brake power is determined by:

$$P_{be} = P_{oe}\ \eta_{mdt} \tag{11}$$

where:

P_{oe} = Expander shaft power output

η_{mdt} = Power drive train mechanical efficiency (const = 0.97)

and the shaft power by:

$$P_{oe} = P_{a,e}\ \eta_{oad,exp} \tag{12}$$

where:

$P_{a,e}$ = Expander theoretical adiabatic power

$\eta_{oad,exp}$ = Overall adiabatic expander efficiency

The theoretical adiabatic power is found from:

$$P_{a,e} = 6.4103 * 10^{-3}\ \dot{m}\ T_4'\ (1 + R_f)\ \frac{\kappa}{\kappa - 1}\ \left(1 - \left[\frac{P_0}{P_4'}\right]^{\frac{\kappa - 1}{\kappa}}\right), \quad hp \tag{13}$$

where:

$\dot{m}$ = Mass flow rate of air through system, kg/min

T_4' = Temperature at expander inlet, °K

R_f = Fuel/air ratio of working engine

κ = Adiabatic exponent for air (1.4)

p_0 = Ambient Pressure, kg/cm^2

p_4' = Actual manifold back-pressure, kg/cm^2.

The compressor power is found by:

$$P_{ic} = \frac{P_{ac}}{\eta_{oc}} \tag{14}$$

where:

P_{ac} = Compressor theoretical adiabatic power

η_{oc} = Overall adiabatic efficiency of the positive displacement supercharger (assumed in calculations as constant = 0.75)

$$P_{ac} = 6.4103\ 10^{-3}\ \dot{m}\ T_1'\ \frac{\kappa}{\kappa - 1}\ ([\frac{p_1}{p_0}])^{\frac{\kappa - 1}{\kappa}} - 1), \quad hp \tag{15}$$

where:

T_1' = Temperature at reciprocator intake, °K

p_1 = Pressure at reciprocator intake, kg/cm^2.

Indicated pumping power loss P_p represents the work rate performed by the engine piston against the back-pressure in the exhaust manifold during its exhaust stroke. Under the assumption that back-pressure does not change the energy conversion process in the cylinder, the engine indicated power at two different back-pressures will differ by the difference between the respective pumping losses. As is schematically shown in Figure 9, this can be mathematically expressed as:

$$P_{ir}\ (p_{4'D}) = P_{ir}\ (p_{4'T}) \pm \Delta P_p \tag{16}$$

where:

$p_{4'T}$ = Back-pressure corresponding to the operating point of the turbocompound system

$p_{4'D}$ = Back-pressure corresponding to the same operating point for the screw expander compound system

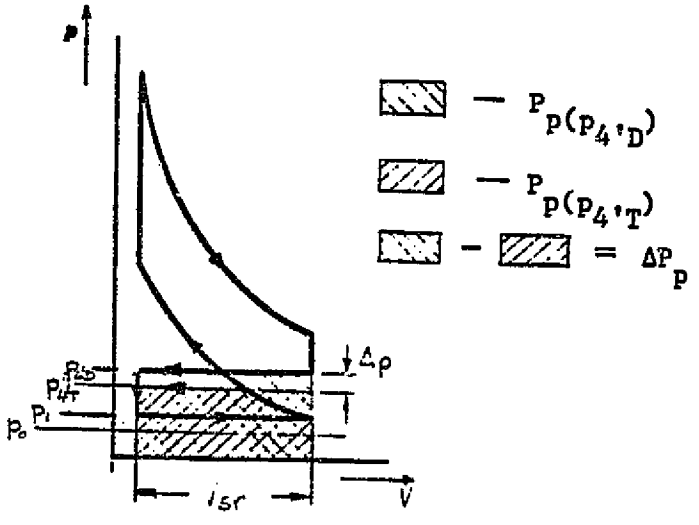

$P_{p(P_4'D)}$ = Indicated pumping power of reciprocator compounded with screw expander operating at back pressure $P_{4'D}$

$P_{p(P_4'T)}$ = Indicated pumping power of reciprocator compounded with turbo-expander operating at back-pressure $P_{4'T}$

ΔP_p = Pumping power difference caused by back-pressure difference

Δp = Pumping loss pressure head

Figure 9. p-V DIAGRAM OF TURBOCOMPOUND AND POSITIVE DISPLACEMENT COMPOUND SYSTEMS

$P_{ir(p_4'_D)}$ = Indicated (internal) power of reciprocator compounded with screw expander operating at back-pressure $p_4'_D$

$P_{ir(p_4'_T)}$ = Indicated power of reciprocator compounded with turbo-expander operating at back-pressure $p_4'_T$

ΔP_p = Pumping power difference caused by back-pressure difference.

For equal conditions at the engine inlet it can be shown that:

$$\Delta P_p = V_{ss}\, n_r\, (p_{4'D} - p_{4'T}) \tag{17}$$

where:

V_{sr} = Reciprocator swept volume

n_r = Reciprocator speed, rpm.

Finally, Equation 17 can be rearranged to:

$$\Delta P_p = 1.538\ 10^{-2}\ n_r\ \Delta p,\ hp \tag{17a}$$

where:

$$\Delta p = (p_{4'D} - p_{4'T}),\ kg/cm^2 \tag{18}$$

After developing the individual power consumption and generation terms for Equation 10, Equation 19 can be used for predicting the potential brake specific fuel consumption of our system.

Screw expander power output performance is shown in Figure 10. Screw expander shaft power curves were generated for an expander design pressure ratio of 3.5 with the engine load characteristics at an engine speed of 1900 rpm using Equations 12 and 13 and data from the baseline system. The curve representing screw expander brake power represents effective power generated by the expander and available on the system power output shaft, which accounts for parasitic losses of the compressor drive.

Figure 10.

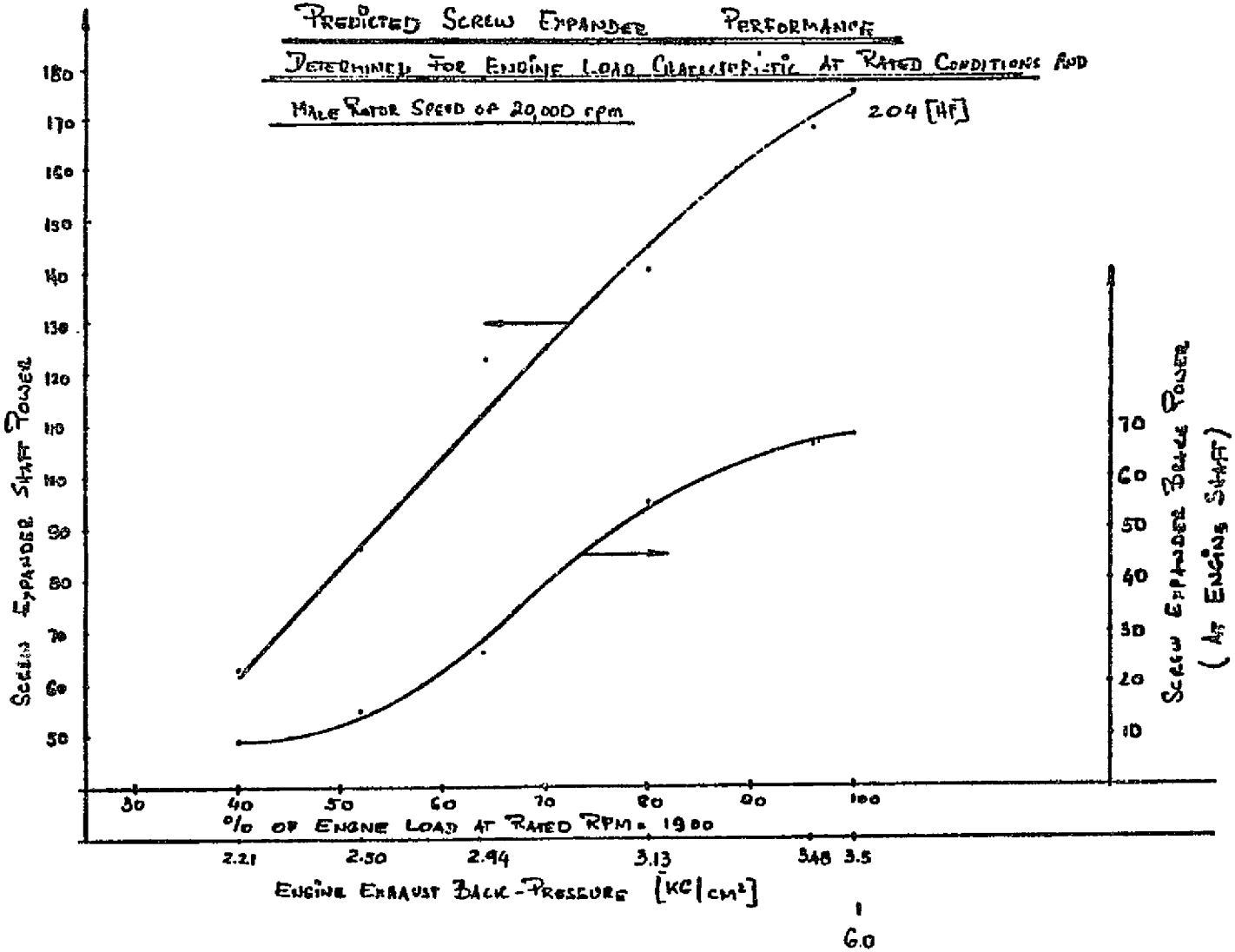

Design Procedures

Basic Design Parameters

Sizing of the screw expander began with specifying the design point of the system. Since the system is to be applied as a heavy-duty, long-haul-truck prime mover and to achieve maximum energy recovery ability through complete expansion, we took the rated operating point of the engine as the design point for the expander. Based on Cummins Diesel Co. data, at the outlet from the engine (which is approximately that at the expander inlet) the design point is defined by $\dot{m}$ = 32.6 kg/min and T_4' = 850°K, which can be used to calculate the volumetric flow rate $\dot{V}_4$. (All subscripts and superscripts defined in Figure 6). Based on the results of our performance analysis, the optimal value for the design expansion pressure ratio π_{ed} is 3.5, under the assumption of complete expansion to ambient pressure. The volume flow capacity of the expander $\dot{V}_{che}$, defined as the volume flow rate at the inlet to the expander $\dot{V}_4'$ at its rated operating point conditions is expressed by:

$$\dot{V}_4' = \frac{\dot{m} R T_4'}{p_4'} \tag{19}$$

where:

$\dot{m}$ = Rated air mass flow rate through system

T_4' = Temperature of exhaust gas at expander inlet for rated operating point

p_4' = Design value of back-pressure for rated operating point.

If the expansion is adiabatic and ends at ambient pressure, the volume flow rate of exhaust gases at outlet conditions to be handled by the expander is:

$$\dot{V}_4'' = \dot{V}_4' \left(\frac{p_4'}{p_0}\right)^{\frac{1}{\kappa}} \tag{20}$$

At design conditions, this flow rate is equal to the displacement flow rate of the expander, $\dot{V}_{te}$ = 56.6 m^3/min. The ideal relationship (volumetric efficiency = 100%) between design factors of the screw expander and its volume flow rate is given by:

$$\dot{V}_{te} = C\, C_{wa}\, D^3 \frac{L}{D} n_m \tag{21}$$

where:

C = Active area profile constant

C_{wa} = Wrap angle constant

D = Rotor outside diameter, m

L = Rotor length, m

n_m = Theoretical male rotor speed, rpm.

C and C_{wa} are related to the rotor profile and can be determined analytically for all existing designs. They are held proprietary by screw machinery manufacturers. For the first selection of rotor dimensions the Svenska Rotor Maskiner A.B. (SRM) values of $C = 0.501$ and $C_{wa} = 0.9688$, valid for an unspecified asymmetric profile, were used. The volumetric characterization for a profile actually used were corrected later but the rotor diameter was retained. The rotor diameter must be determined as a compromise between expander size and rotor tip speed found to assure good overall adiabatic efficiency and an expander box volume compatible with both the engine and the total compound system dimensions. These considerations led us to select a diameter of 161 mm (see Figure 1, of "Expander-Compressor Design Study for Heavy Duty Compounded Adiabatic, Diesel Engines"). Practicality and a desire for rigidness of the unit were the reasons for selecting $L/D = 1.5$.

Determination of Theoretical Expander Charging Volume

The expander charging volume, which affects the back-pressure level, is one of the expander design characteristics to be determined in relation to the design expansion pressure ratio and can be defined as:

$$V_{che} = \dot{V}_{4'}/n_e \tag{22}$$

Equation 22 defines the charging volume for one revolution of the male rotor. However, it is convenient to relate charging volume to the individual interlobe volume:

$$V'_{che} = \frac{\dot{V}_{4'}}{n_e i} \tag{22a}$$

where:

i = Number of interlobe cells involved in charging process per one revolution of male rotor.

For values of rated conditions, $\pi_{ed} = 3.5$ and $i = 4$, $V_{che} = 1245$ cm^3 and $V'_{che} = 311$ cm^3.

Determination of Theoretical Expander Displacement

The expander displacement can be defined as the total volume generated by the interlobe working volume during one revolution of the male rotor and can be expressed as:

$$V_{te} = \frac{\dot{V}_{te}}{n_e} \tag{23}$$

or, if related to an individual working volume

$$V'_{te} = \frac{\dot{V}_{te}}{n_e i} \tag{23a}$$

For the above values, $V_{te} = 3.048$ dm^3 and $V'_{te} = 0.762$ dm^3.

Rotor Profile Selection

The rotor profile has a strong influence on the overall performance of a screw compressor. Profile development has continued for over 40 years, primarily by SRM of Sweden. Most compressor manufacturers have built their capabilities as SRM licensees; there have been exceptions, such as Aerzahner Maschinenfabrik A.G. in West Germany. This arrangement will probably change, since the basic patent protection on the rotors and their profiles will end around 1985. After that, manufacturers will be free to apply advanced profiles possibly of their own design for better performance.

The intended use of the machine is important in determining the rotor geometry. An evaluation to consider the effects of profile will have to be performed eventually, including dynamic aspects and material and manufacturing problems. Most of this could be done analytically, including optimized profile generation. Experimental verification would then be needed for any profile.

For this project, we have used recent SRM asymmetric profiles for the rotors.

Characteristics of an Expander with Asymmetric Profile

After determining the detailed geometry for the female and male rotors, the expander volume characteristics (expander displacement, V_{te}, individual cell displacement, V'_{te}, charging volume, V_{che}, and individual cell charging volume, V'_{che}) can be identified. The following set of geometric equations describes basic meshing characteristics of lobed screw rotors, the arrangement of which is shown in Figure 11:

$$i_t = \frac{N_f}{N_m} \tag{24}$$

$$r_m = \frac{L_c}{i_t + 1} \tag{25}$$

$$r_f = \frac{i_t L_c}{i_t + 1} \tag{26}$$

$$R_I = L_c - R_o \tag{27}$$

$$a = r_m - R_I \tag{28}$$

where:

i_t = Screw machine timing gear ratio

N_f, N_m = Number of female and male rotor lobes, respectively

r_m = Pitch radius of male rotor

r_f = Pitch radius of female rotor

L_c = Distance between axes of rotors

R_o = Outside radius of both rotors

R_I = Male rotor root radius

a = Addendum of male rotor.

With $N_f = 6$, $N_m = 4$, $R_o = D/2 = 80.5$ mm, $L_c = 125$ mm, and assuming a practical value of the lobe radius, $r = 0.4\ R_o$, the additional basic characteristics of the profile are: $r = 30.5$ mm, $r_m = 50$ mm, $r_f = 75$ mm, $a = 5.5$ mm, and $R_I = 44.5$ mm. Other elements of the asymmetric profile are an arc

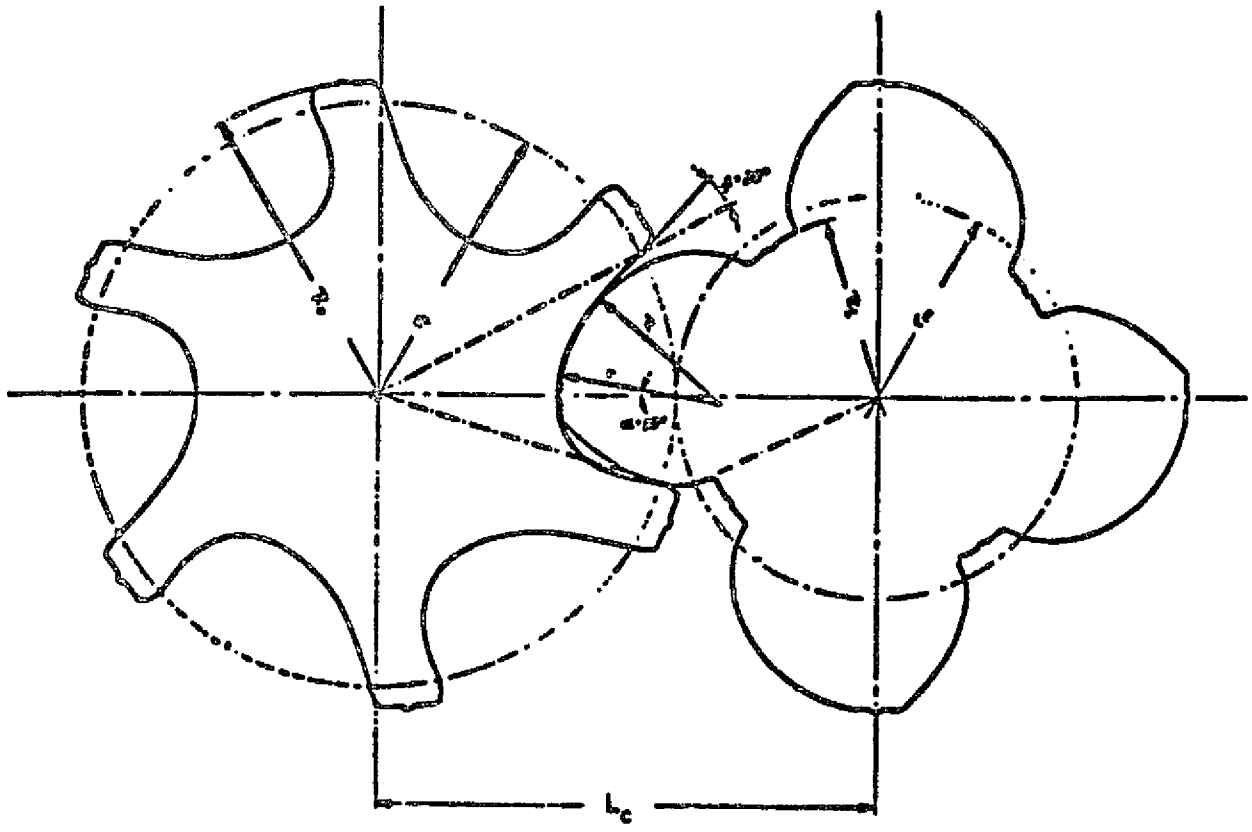

Figure 11. CHARACTERISTIC DIMENSIONS OF SCREW EXPANDER ROTORS WITH ASYMMETRIC PROFILES

angle, $\alpha = 10°$ of female flank base, circular portion radius R = 4/3, r = 40 mm and straight portion angle $\beta = 20°$. All other portions of flank profiles for both male and female lobes are generated curves and are subject to the proprietary position of SRM.

Determining the actual volume characteristics corresponding to the selected design profile, as a function of the male rotor's angular position was required to identify the actual displacement of the expander. Figure 12 shows several positions of the male and female rotors, and the volume formed between them and the housing. Using surface integration and an analytically determined engagement point where the male and female rotors completely mesh, the values of individual interlobe, V'^{*}_{te}, and overall volume displacement for one revolution, V^{*}_{te}, were calculated. For a wrap angle of 300°, a length of 241 mm, and 4 interlobe volumes for the expander, the overall volume displacement, V^{*}_{te} is 2.504 cm^3, with $V'^{*}_{te} = 0.626$ cm^3. The charging volume that would ensure the desired expansion pressure ratio of 3.5 was derived from:

$$V'^{*}_{che} = V'^{*}_{te} / \pi_{ed}^{\frac{1}{\kappa}} \qquad (29)$$

resulting in $V'^{*}_{che} = 0.256$ cm^3 or $V^{*}_{che} = 1.024$ cm^3.

Adjusted Design Parameters

Comparing the theoretical required displacement of the expander with the value determined for the selected rotor profiles shows that the latter values are lower than the theoretical by 18%. This discrepancy can be corrected through proper selection of the drive ratio. Assuming that the expander volumetric efficiency, η_{vol}, may be kept at 90%, using:

$$\dot{V}_4'' = i_{dt}\, n_r\, V^{*}_{te}\, \eta_{vol} \qquad (30)$$

Where:

$i_{dt} = n_m/n_r$ = Gear ratio between expander power shaft and reciprocator crankshaft.

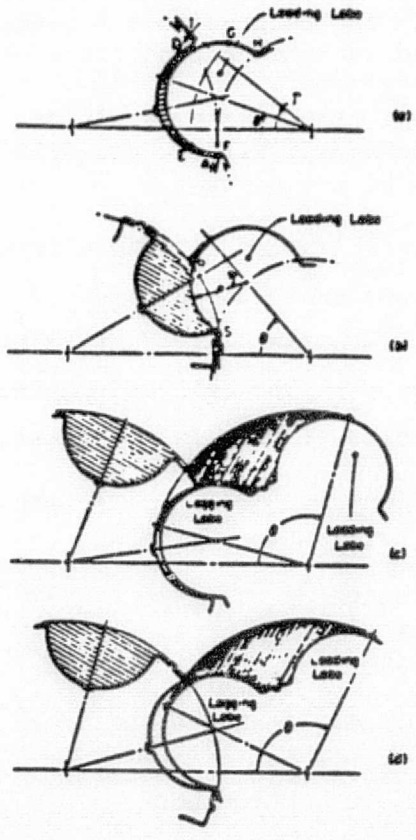

Figure 12. VARIOUS MESH POSITIONS DURING AREA CYCLE OF MALE AND FEMALE ROTORS

produces, for n_r = 1900 rpm, V^*_{te} = 2.504 dcm^3, $\dot{V}_4$" = 56.6 m^3/min, a power drive train ratio i_{at} of 10.594. The corrected expander rated speed is 20,130 rpm with a tip speed for the male rotor of 170 m/sec.

Timing and Porting

The inlet and outlet port design of the screw expander defines the operating points of both the charging and expansion process. Specifically, the design should achieve the following:

- Timing of inlet and outlet ports to meet the design value of the built-in volume expansion ratio and to provide the required pressure expansion ratio (total expansion to ambient conditions at the rating point)
- Minimization of hydraulic losses at the inlet and outlet, which strongly influence the total adiabatic efficiency, achieved by selection of the proper shape and size of the port.

The volume characteristic for an interlobe cell shown in Figure 13 was used to determine the opening and closing times of the ports. Theoretically, inlet closing should occur when the desired charging volume is built up. The outlet opening should occur when the cell volume has reached a maximum. Using these conditions, the following timing has been established:

Port Timing	Angle
Inlet Opening	0°
Inlet Closing	170°
Outlet Opening	380°
Outlet Closing	756°

Using this information in connection with the rotor profiles, the port contours can be established. It should be noted that optimization of the timing and porting would be continued empirically during the prototype phase when the effects of fluid dynamics can be evaluated.

Expansion Ratio Modulation System Concept

The desire for a high adiabatic efficiency of the screw expander requires some sort of modulation of the volume expansion ratio. If no modulation were possible, the fixed expansion ratio would significantly increase losses of the engine at part load operation. Regardless of the pressure ratio across the expander, the value of interlobe space pressure decreases along the rotor. Ideally, this pressure reaches ambient at the end of the rotor at design conditions. When the operating pressure ratio decreases, the point at which

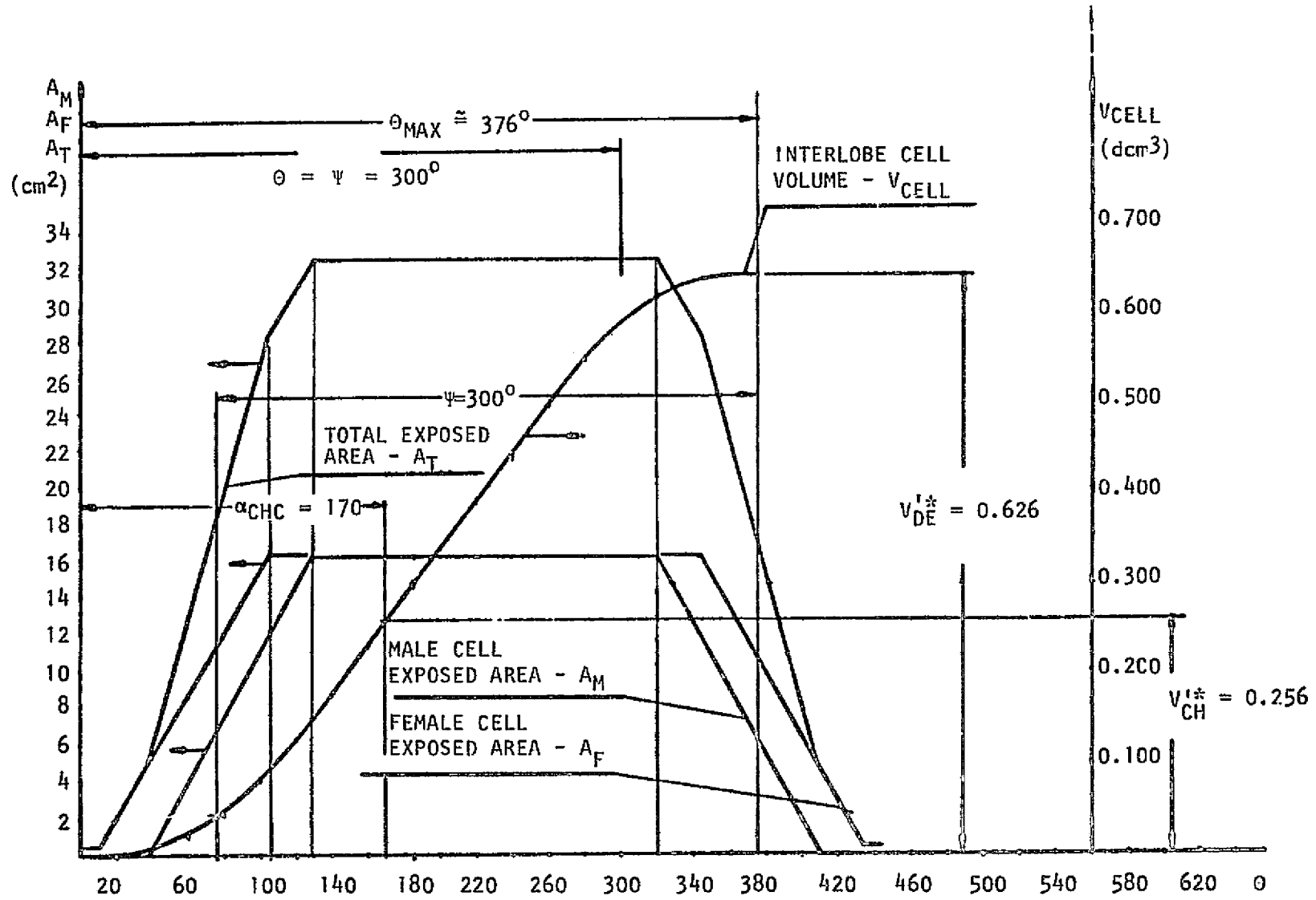

Figure 13. VOLUME CHARACTERISTICS FOR INDIVIDUAL INTERLOBE CELL

interlobe pressure reaches ambient moves nearer the inlet end of the rotor. With a built-in volume expansion ratio, a vacuum zone would be created between the ambient pressure point and the end of the rotor. This vacuum zone, which is a cause of inefficiency, can be eliminated by "venting" to the ambient through a set of communicating valves located in the rotor housing along the length of this zone. The engineering concept of the expansion ratio modulation system is shown on Figure 14. A set of valve guides (1) is machined in the housing. Each valve guide is connected through a passage (2) to the rotors and is closed by a valve seat plate (3) and connected through a vent port (4) to the low pressure (atmospheric) chamber (5). This chamber can be connected to the atmosphere or to the exhaust chamber (6) of the expander through the passage (7). Each of the valve guides accommodates a vent valve (8) of special design operated by the pressure difference between the inside and outside of the interlobe cell. Whenever the pressure in the interlobe cell is higher than that of the low pressure chamber, the valve is held by this difference against its seat and seals off both volumes. When overexpansion drops the interlobe pressure below that existing on the other side, the valve will open. Specially-shaped side grooves and bottom recesses inside the valve will form the venting passage of the interlobe cavity, preventing excessive overexpansion losses. Two rows of valves located along the housing on the male rotor side would provide for close spacing and effective expansion modulation as well as provide an adequate number of valves for effective flow through the venting area at low loads of the expander. Venting to the exhaust after the expander, instead of to the atmosphere, will reduce internal cooling of the interlobe cell because the exhaust gases have a higher temperature than ambient air. In this way, near adiabatic expansion within the working cell can still be achieved at low loads. The second potential advantage of this solution is that pressure build-up in the low pressure chamber over the valve might improve the valve's dynamic response.

Stress Analysis of the Screw Expander

Performing a comprehensive stress analysis on the screw expander is complex and beyond the scope of this study. The shape of the lobes and volumes, which form multiple spaces where pressures vary according to the working conditions and the position in the working cycle, form complex external loads on the expander rotors and other structural members. Internal

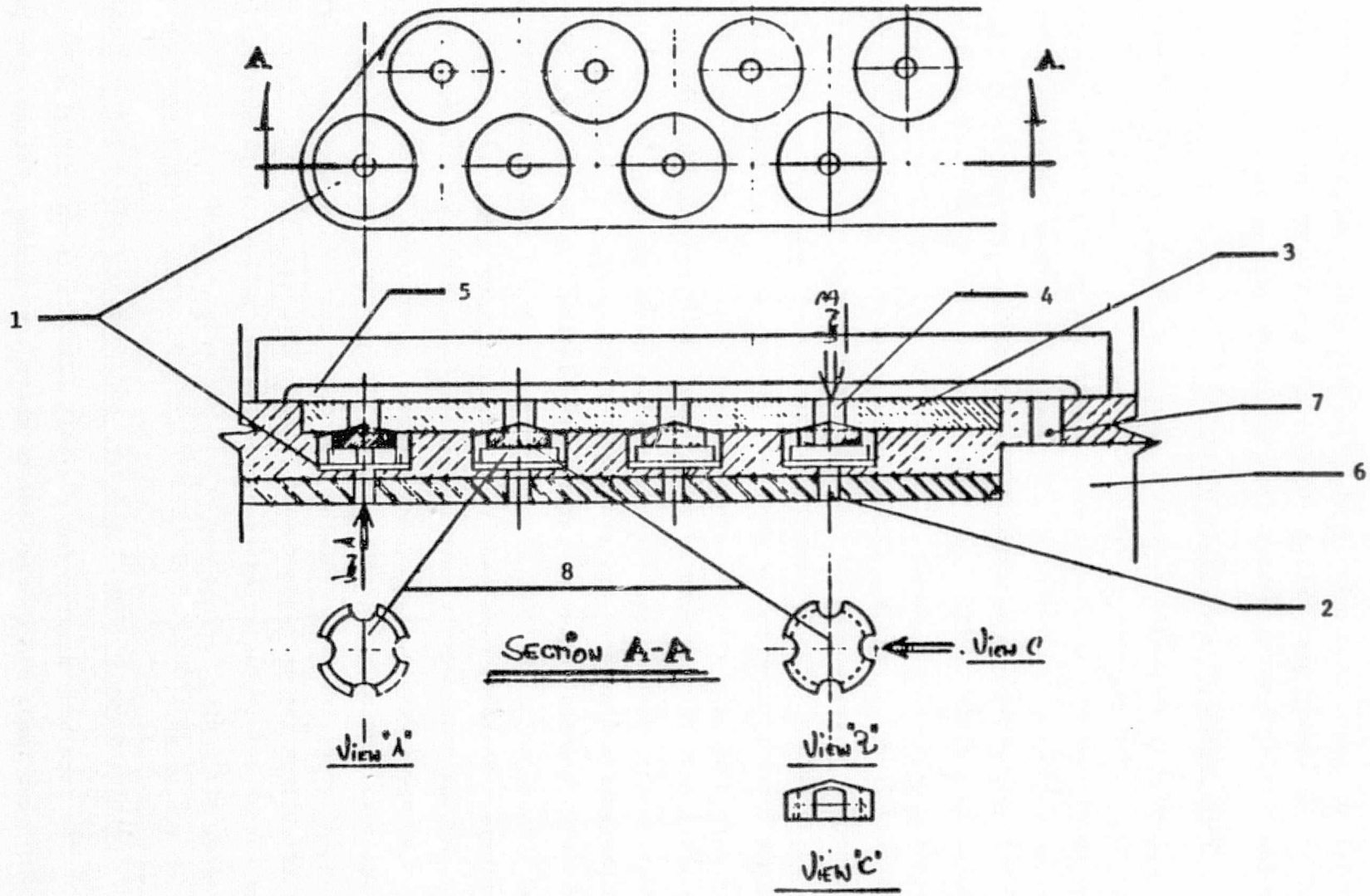

Figure 14. EXPANSION RATIO MODULATION SYSTEM

stresses and strains are complicated further by the high operating speeds and temperatures of the machine as well as the fact that two different materials (steel and ceramic) are involved. However, some knowledge about the stress and strain within the working elements is required for their successful design. Therefore, we analyzed a simplified model of the external loads.

Simplified Model of External Load

Figure 15 shows the schematic view of a simplified model of external load for the stress analysis of the screw expander. The main elements taking up the total mechanical and thermal loads are the male and female rotors, their bearings and bearing supports. The housing is exposed directly to the pressure loads, but it is a stationary member with no dynamic loads and lends itself to a rigid design. Our model assumed that pressure loading acts on both the male (1) and female (2) rotors in the form of two continuously distributed loads, w_1 and w_2; where w_1 has a constant value over the length of the rotors corresponding to the charging volume of the interlobe cells, while w_2 represents a linearly changing distributed load over the length of the rotors corresponding to the expansion process within interlobe cells. The pressure also acts axially, creating thrust force F_{ax}. The shaft is supported by three bearings represented in our model by force reactions R_1, R_2, and R_3. Additionally, both rotors are loaded with uneven torques, T_M and T_F, generated by pressure differences distributed over the rotor circumferences. The exact female/male rotor torque proportions is difficult to determine, however, it was assumed to be 10%/90%, respectively, which was accurate enough for this analysis. Corresponding gear forces resolve into a pair of tangential forces, F_{gt}, acting transversely upon the shafts, a pair of radial forces, F_{gr}, and a pair of axial forces, F_{gax}. The internal centrifugal forces which are distributed radially and act upon the external layers of the ceramic coating, also influence the stress of the expander rotors. Assuming that power output is taken from the male rotor shaft, this shaft transmits the major portion of the torque and is subjected to higher loads. Because it is more heavily loaded, all further stress and strain analysis was conducted for the male rotor subassembly.

Determination of Shearing Forces and Bending Moments for Male Shaft

The free body diagram for the male shaft is shown in Figure 16. The timing gear loads are omitted due to their low values. Because the problem is

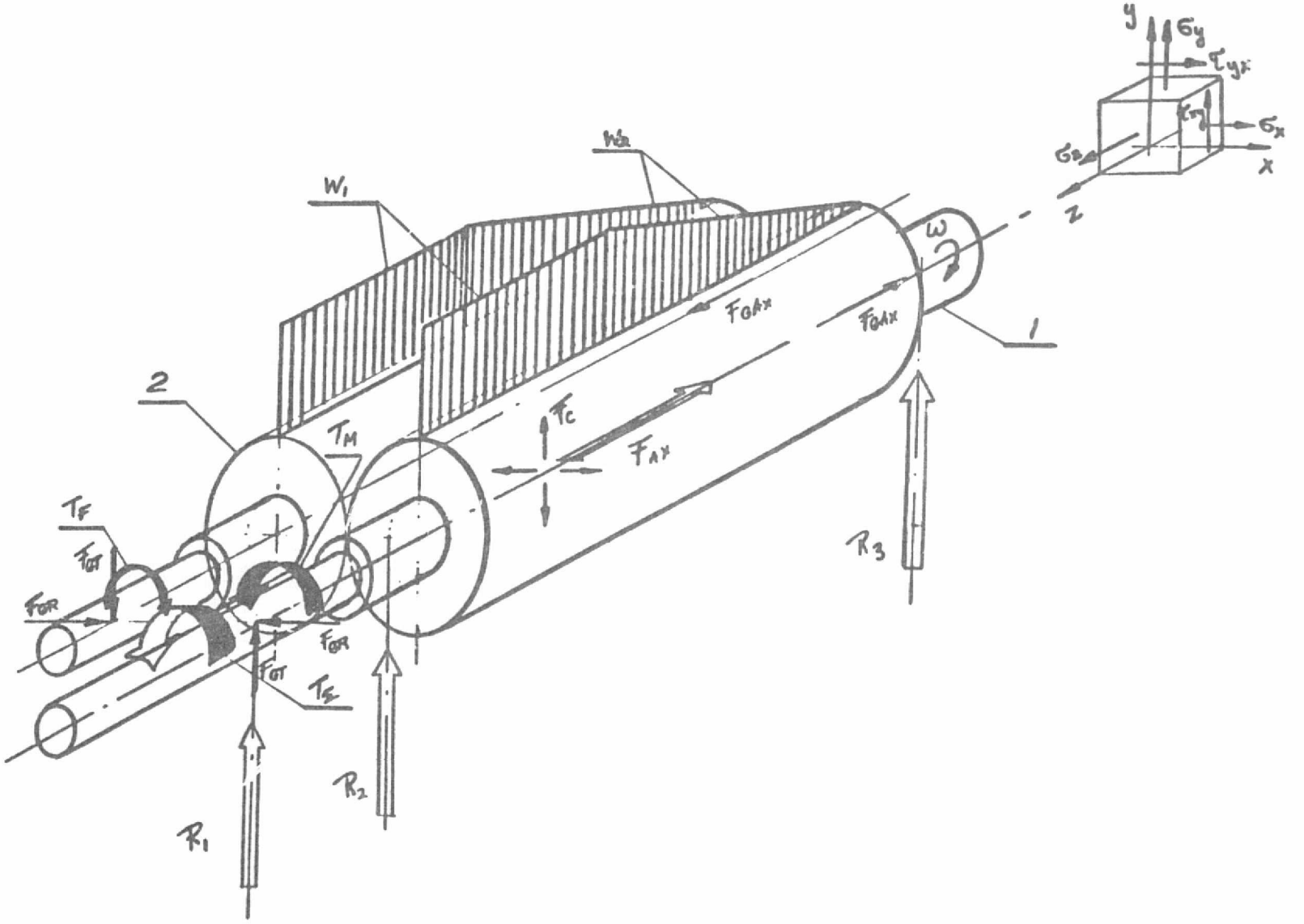

Figure 15. EXTERNAL LOADS ON ROTORS OF SCREW EXPANDER

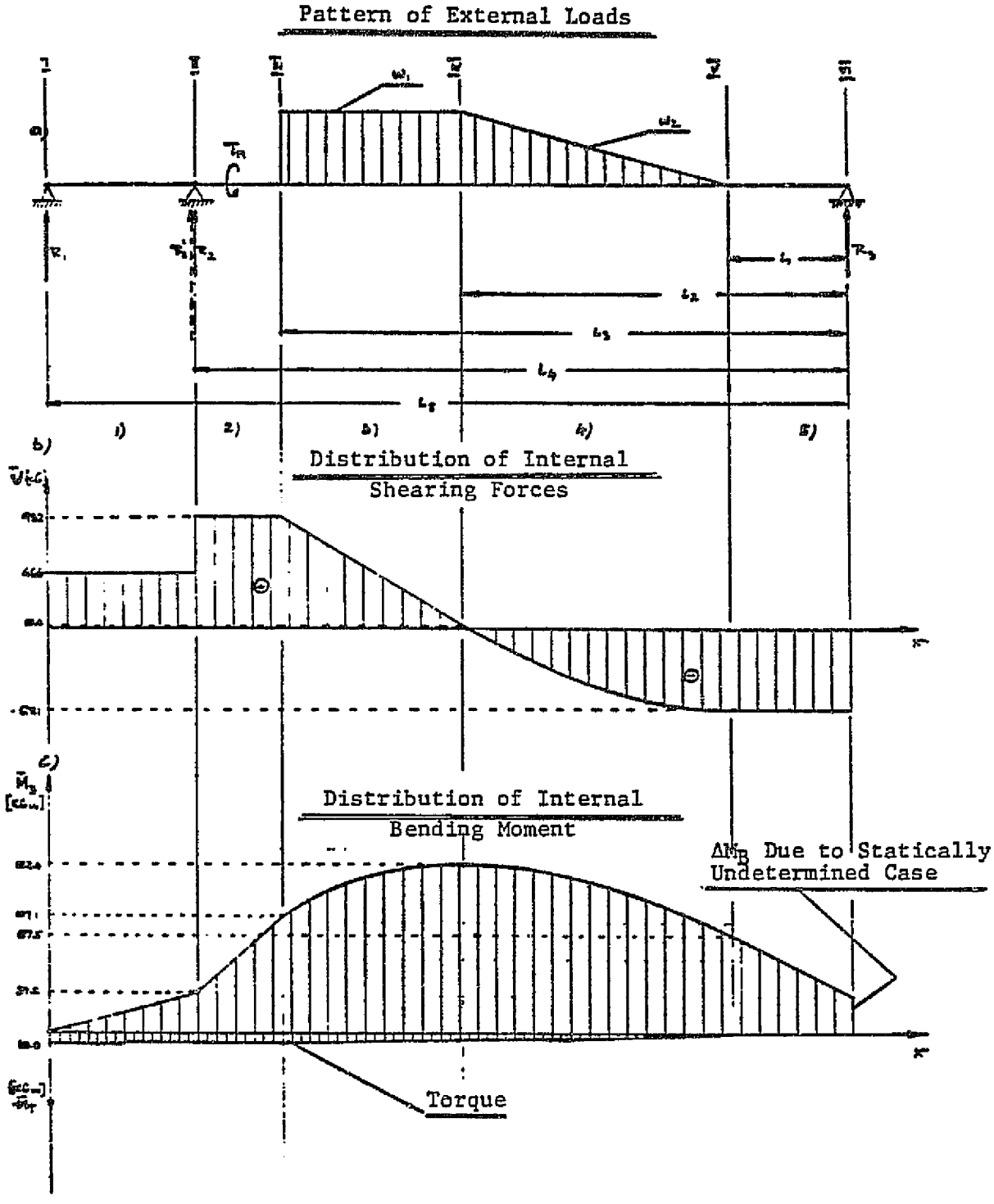

Figure 16. MODEL OF EXTERNAL LOAD DISTRIBUTION

statically indeterminate (three supporting bearings), the following set of simplified equilibrium equations have been written for R_2' and R_3 only:

$$\Sigma F_x = 0;\ R_2' - \int_o^{l_3 - l_2} w_1 dx^2 - \int_o^{l_2 - l_1} w_2 dx^1 + R_3 = 0 \tag{31}$$

$$\Sigma M_o = 0;\ R_2' l_4 - \left(\frac{l_3 - l_2}{2} + l_2\right) \int w_1 dx - \left(\frac{2(l_2 - l_1)}{3} + l_1\right) \int w_2 dx = 0 \tag{32}$$

Assuming that pressure is exerted on the upper side of the rotors only, then:

$$dw_1 = p_{max}\, D_o\, dx; \tag{33}$$

$$dw_2 = \left(p_{max}\, D_o - \frac{p_{max}\, D_o\, x}{l_2 - l_1}\right) dx \tag{34}$$

where:

P_{max} = Maximum pressure at expander inlet

D_o = Rotor outside diameter.

After substituting Equations 33 and 34 into 31 and 32, respectively, performing a stepwise integration and rearranging:

$$R_2' + p_{max}\, D_o(l_3 - l_2) + \frac{1}{2}\, p_{max}\, D_o(l_2 - l_1) + R_3 = 0 \tag{35}$$

$$R_2' l_4 - \left(\frac{1}{2}[l_3 - l_2]^2 + l_2[l_3 - l_2]\right) p_{max} D_o - \left(\frac{1}{3}[l_2 - l_1]^2 + \frac{l_1}{2}[l_2 - l_1]\right) p_{max} D_o = 0 \tag{36}$$

For: P_{max} = 6 atm, D_o = 16 cm, l_1 = 7.5 cm, l_2 = 21.9 cm, l_3 = 31.5 cm, and l_4 = 39.0 cm, values for R'_2 and R_3 are obtained: R'_2 = 937.5 kg and R_3 = 675.3 kg.

For determining the shearing and bending moments, it was assumed that reaction R_2' can be resolved in two equal components, R_1 and R_2 (Figure 15) acting on both bearing supports of the high pressure end of the rotor. This assumption, however, is not quite realistic as it will overestimate the stress conditions on the shaft. Once the external load system acting upon the shaft

is defined, the distribution of internal shearing forces and bending moments along the shaft can be determined.

Shearing forces are described by the following functions of shaft length, determined separately for each length interval shown in Figure 16b.

$$V^{1)} = R_1 \tag{37}$$

$$V^{2)} = R_1 + R_2 \tag{38}$$

$$V_{3)} = R_1 + R_2 - \int_{l_3}^{x} w_1 dx \tag{39}$$

$$V_{4)} = R_1 + R_2 - w_1 (l_3 - l_2) - \int_{l_2}^{x} (w_1 - \frac{w_1}{l_2 - l_1} x)\, dx \tag{40}$$

Numerical values for the shearing forces have been calculated and the shear diagram plotted in Figure 16b. Below are the numerical values of shear corresponding to the interval boundaries:

$V^{1)}(l_5) = V^{1)}(l_4) = 468$ kg

$V^{2)}(l_4) = V^{2)}(l_3) = 937$ kg

$V^{3)}(l_3) = V^{2)}(l_3) = 937$ kg

$V^{3)}(l_2) = 10.4$ kg

$V^{4)}(l_2) = V^{3)}(l_2) = 10.4$ kg

$V^{4)}(l_1) = -685$ kg

$V^{5)}(o) = V^{4)}$

The next step in our analysis was to determine the internal bending moment that is described by the following set of functions for the previously established shaft length intervals:

$$M^{1)} = R_1 x \tag{41}$$

$$M^{2)} = R_1 (l_5 - l_4 + x) + R_2 x \tag{42}$$

$$M^{3)} = R_1 (l_5 - l_3 + x) + R_2 (l_4 - l_3 + x) - \frac{w_1 x^2}{2} \tag{43}$$

$$M^{4)} = R_1 (l_5 - l_2 + x) + R_2 (l_4 - l_2 + x) - w_1 (l_3 - l_2) (\frac{l_3 - l_2}{2} + x) - \frac{w_1 x^2}{2} + \frac{1}{6} \frac{w_1}{(l_2 - l_1)} x^3 \tag{44}$$

Numerical values of bending moments have been calculated and the bending moment diagram plotted in Figure 16c. The numerical values of bending moment corresponding to boundaries of intervals are:

$$M^{1)}(l_4) = 37.28 \text{ kgm}$$

$$M^{2)}(l_3) = 107.18 \text{ kgm}$$

$$M^{3)}(l_3) = 107.18 \text{ kgm}$$

$$M^{3)}(l_2) = 152.41 \text{ kgm}$$

$$M^{4)}(l_2) = 152.41 \text{ kgm}$$

$$M^{4)}(l_1) = 87.54 \text{ kgm}$$

$$M^{5)}(0) = 36.51 \text{ kgm}$$

$$M^{(5)}(0) = 36.51 \text{ kgm}^*$$

* $M^{(5)}(0) \neq 0$ is the result of the assumption that $R_1 = R_2 = 1/2\ R_2'$. A more exact external load identification would be possible by using methods appropriate for a statically indeterminate case, which was beyond the scope of this analysis.

Determination of Torque

Pressure acting upon the rotor lobes generates the torque loading of the shafts. Exact determination of torques generated on the male and female rotors require three dimensional vector analysis which was beyond the scope of this work. For this study, it was sufficient to understand that due to the characteristics of the three dimensional load distribution, the tangential force for the male rotor is set significantly further off the rotor shaft axis than the tangential force acting on the female rotor. This is based on the fact that for rotors with symmetric profiles the female rotor force vector intersects the rotor axis, so no torque is produced. However, with asymmetric profiles some torque exists on the female rotor. As a result, the torque generated by the male rotor is also significantly larger and based on engineering practice, the male rotor torque/female rotor torque ratio can be assumed to be 9/1. Another aspect of torque generation for the screw expander is that the torque is a function of rotor length because of the variable pressure distribution. It was assumed that torque accumulates linearly along the length of the rotor.

The value of the total maximum torque can be determined from the equation:

$$\tau_{max} = 716.2 \frac{P_{max}}{n_m} \quad (46)$$

where:

τ_{max} = Maximum torque at the expander output shaft, kgm

P_{max} = Maximum expander power output considered, hp

n_m = Male rotor rpm at maximum power output

For P_{max} = 200 hp, and n_m = 19,000 rpm, τ_{max} = 7.53 kgm.

Determination of Axial Load

Axial loads exerteds on the rotors are generated by pressure differences existing between the high and low pressure ends. It was assumed that the distribution of axial pressure over high pressure rotor end would follow the pattern shown in Figure 17. Such a linear distribution can account for the decrease in pressure in the subsequent interlobe spaces where expansion occurs and for throttling of the working gas around the rotor in the small clearance between the rotor end and high pressure end plate.

The axial load can be expressed as:

$$F_{ax} = \frac{\pi D_o^2}{4} P_{MAX} K \quad (47)$$

where K = coefficient approximating load distribution.

For given values P_{max}, D_o and K = 0.75, F_{ax} = 904 kg.

Centrifugal Load and Corresponding State of Stress in Ceramic Shell of Rotor

High operating speeds of the male rotor will generate high centrifugal forces stressing the ceramic shell of the rotor. An approximate determination and evaluation of the stresses within the ceramic shell was performed to determine the possibility of overstressing the ceramic in the design, leading to failure. The complex form of the ceramic shell complicates the determination of the load generated by the centrifugal forces and the corresponding

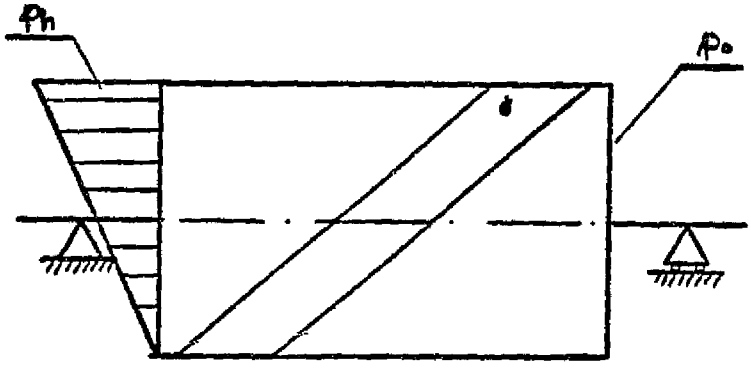

Figure 17. AXIAL LOADING OF
SCREW EXPANDER ROTOR

stresses. For the objectives of this project, a simplified approach was selected which reduces the problem to plane one-dimensional state of stress similar to that in walls of pressure vessels.

The basic assumptions of the load model are:

- Boundary surface between the core and ceramic shell is a free surface (no adhesive forces)
- Elementary centrifugal forces distributed in the body of the ceramic shell are substituted for by resultants acting at the centroids of portions of the cross-sectional area. The load model chosen for stress determination is shown in Figure 18, which represents static equilibrium for a quarter of the ceramic shell.

The total force exerted on one quarter of the ceramic shell is:

$$F_c = \Delta F_{c1} + \Delta F_{c2} \tag{48}$$

$$\Delta F_{c1} = \omega^2 r_1 \Delta m_1 = \omega^2 r_1 A_1 \Delta L' \rho \tag{49}$$

$$\Delta F_{c2} = \omega^2 r_2 \Delta m_2 = \omega^2 r_2 A_2 \Delta L' \rho \tag{50}$$

where:

ω = Angular velocity of rotor

r_1, r_2 = Radii of centroids of areas A_1 and A_2 from which the cross section of the quarter is composed

ΔL = Elementary lengths of screw axis of centroids of A_1 and A_2

ρ = Density of ceramics for fixed value of wrap angle.

Equations 48, 49, and 50, when combined, become:

$$F_c = w^2 \rho L (r_1 A_1 \Psi_1 + r_2) \tag{51}$$

Having determined the components of the centrifugal force loading the quarter of the ceramic shell and taking into account the axisymmetry of centrifugal load, the problem of determining the stress distribution within the ceramic shell can be treated as if it were for cylindrical pressure vessels. This particular case results in the existence of normal stress, σ_x (notation for

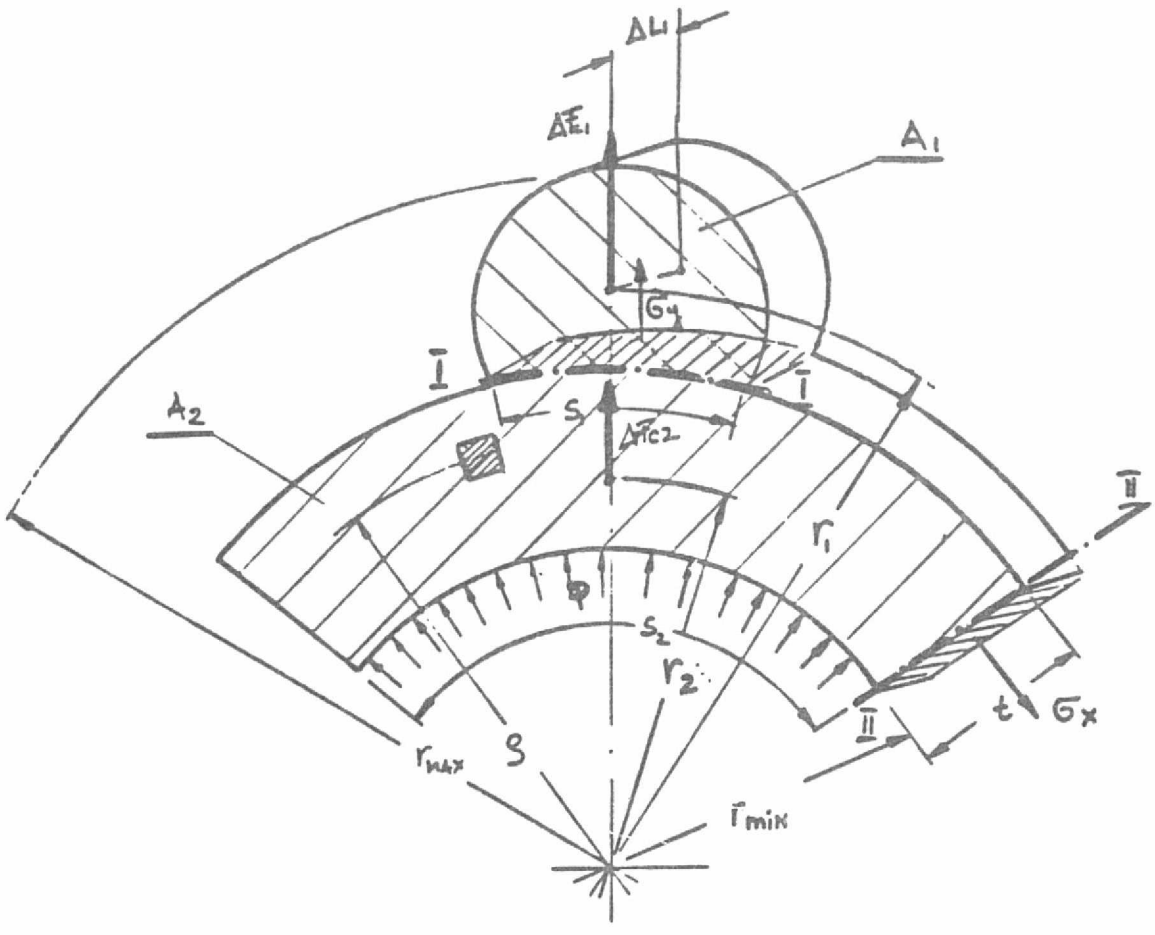

Figure 18. CENTRIFUGAL LOAD REPRESENTATION FOR ROTOR QUARTER

normal and shear stress is included in Figure 18), located in axial Section II of the shell described by equation:

$$\sigma_x = \frac{p\,\zeta}{t} \tag{52}$$

where:

p = Pressure exerted on internal surface of cylinder

ζ = Radius of internal surface of cylinder

t = Thickness of cylinder wall.

To adapt the centrifugal stress for the stress distribution model, a substitute pressure has to be defined. We assume that this pressure is exerted on the free internal cylindrical surface of the ceramic shell located at r_{min}, which can be found from:

$$p(r_{min}) = \frac{2F_c}{\pi\, r_{min}\, L} \tag{53}$$

From Equations 52 and 53:

$$\sigma_x = \frac{2F_c}{\pi t L} \tag{54}$$

Calculations based on the described stress distribution model were conducted for the following selected design dimensions and additional assumptions:

- Centrifugal stresses are calculated for the male rotor due to its higher rpm
- Asymmetric profile is replaced by a symmetric profile to simplify calculations
- Following dimensions are used for calculations (see Figure 19).

  Addendum radius of rotor: $R_{max} = 8.0$ cm

  Dedendum radius of rotor: $R_o = 4.8$ cm

  Lobe radius: $r_L = 3.0$ cm

  Lobe area centroid radius: $r_2 = 6.0$ cm

  Thin wall area centroid radius: $r_1' = 3.9$ cm

  Thick wall area centroid radius: $r_1'' = 2.9$ cm

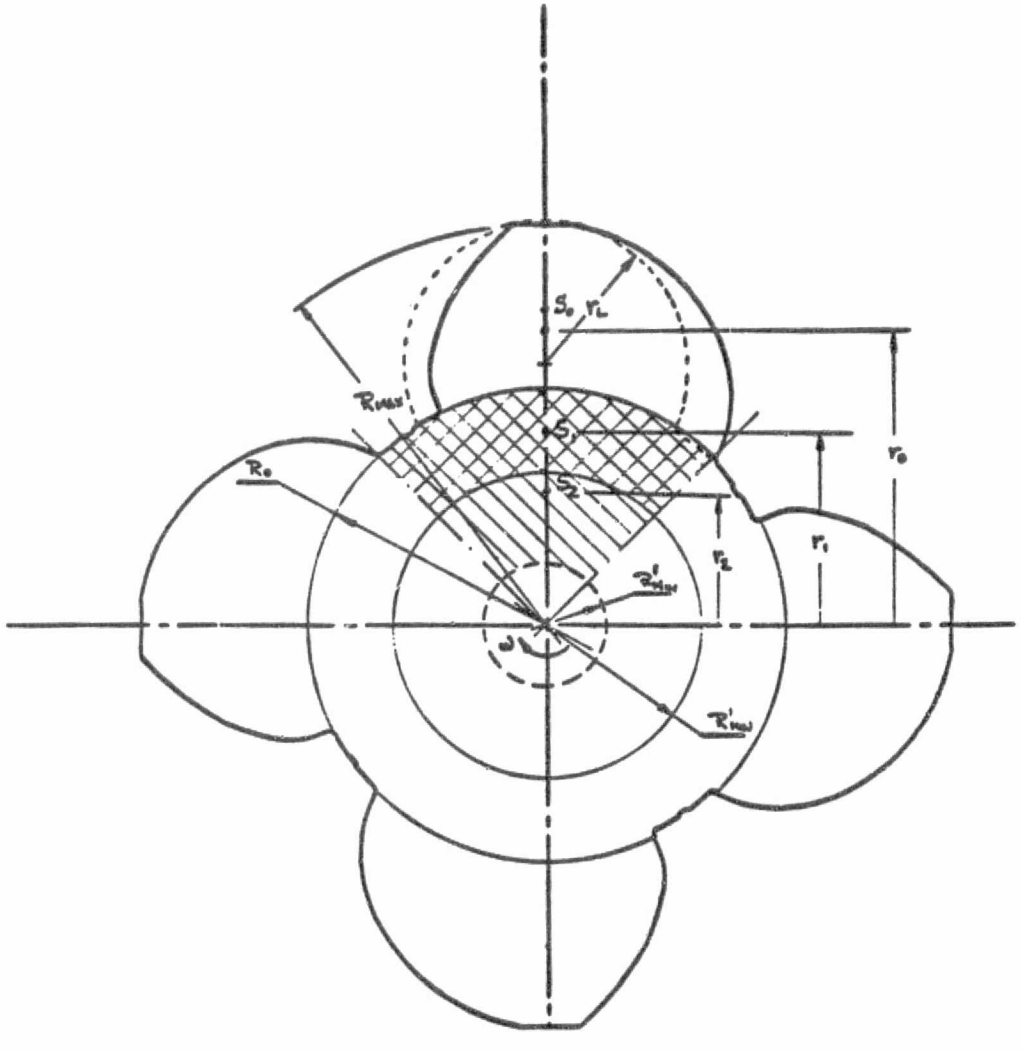

Figure 19. DIMENSIONS OF MALE ROTOR
USED IN STRESS ANALYSIS

Thin wall area ID: $R_{min}' = 3.0$ cm

Thick wall area ID: $R_{min}'' = 1.5$ cm

Ceramic density: 3.2 g/cm^3

Speed: 20,000 rpm.

Calculations of σ_x for the thin and thick wall section of the ceramic shell resulted in:

$$\sigma_x' = 1008 \text{ kg/cm}^2 \text{ (thin wall)}; \quad \sigma_x'' = 566 \text{ kg/cm}^2 \text{ (thick wall)}$$

For better characterization of the centrifugal stress for the ceramic shell, it was considered necessary to determine the approximate value of centrifugal stress normal to Section II (Figure 18) at the base of the lobe. This was found to be approximately 396 kg/cm^2.

Determination of Bending Stresses

According to the theories of bending of composite members (composed of two materials having different moduli of elasticity), its transformed cross section has to first be found before bending stresses in a given section can be determined. Another simplifying assumption that is made in determining the bending stress distribution (which will be used for torsion, shear and compression stresses as well) is that the working cross section of the rotor is restricted to the dedendum circle only. This eliminates the influence of the cross-sectional areas of the lobes which increases the strength of a loaded cross section. We know that the transformed area of the composite cross section is described by:

$$A' = A\, E_2/E_1 \tag{55}$$

where:

A = Area of the part of composite total area to be replaced by transformed area

E_2 = Young's modulus of ceramic material, replaced by equivalent steel

E_1 = Young's modulus of steel, substituting for ceramic material

and that the section of composite total area to be replaced is of annular shape, shown in Figure 20. The transformed section will be represented by a circle having:

$$R_o' = \sqrt{R_o^2\, n + R_{min}^2\, (1 - n)} \tag{56}$$

where:

n = E_2/E_1

R_o = Addendum diameter

R_{min} = Actual radius of ceramic shell.

The value of R_o' for our design is 5.1 cm.

After determining the transformed section, the maximum bending stresses in the rotor can be found for the rotor cross section located under the maximum of bending moment (Figure 16) from:

$$\sigma_{2r} = \frac{4\, M_{max}}{\pi\, R_o'^3} \tag{57}$$

For our design dimensions, $\sigma_{2r} = 147$ kg/cm^2. Bending stresses in the shaft at the ball bearing are $\sigma_{2s} = 303$ kg/cm^2.

Determination of Torsion Stresses

Torque is generated at the perimeter of the male rotor and it is distributed along the rotor at a rate which is a function of the pressure distribution. The torsion stress in the ceramic shell should be considered along its circumferential support with the concentric steel core. To minimize the torsion of the ceramic shell, a spline joint between it and the steel core is provided along the full length where torque transmission could occur. In general, the torsion-induced stresses that have to be determined are: shearing of spline, compression on spline surface, and shearing torsional stress in the steel core.

From the spline cross section shown in Figure 21, the following relationships are:

Spline loading tangent resultant:

$$P = \frac{T}{r} \tag{58}$$

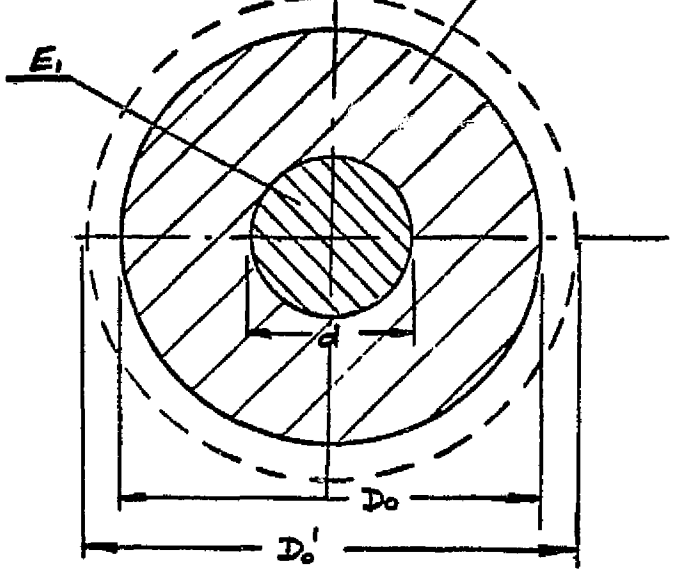

Figure 20. REPRESENTATION OF ROTOR CROSS-SECTION FOR DETERMINATION OF BENDING STRESSES

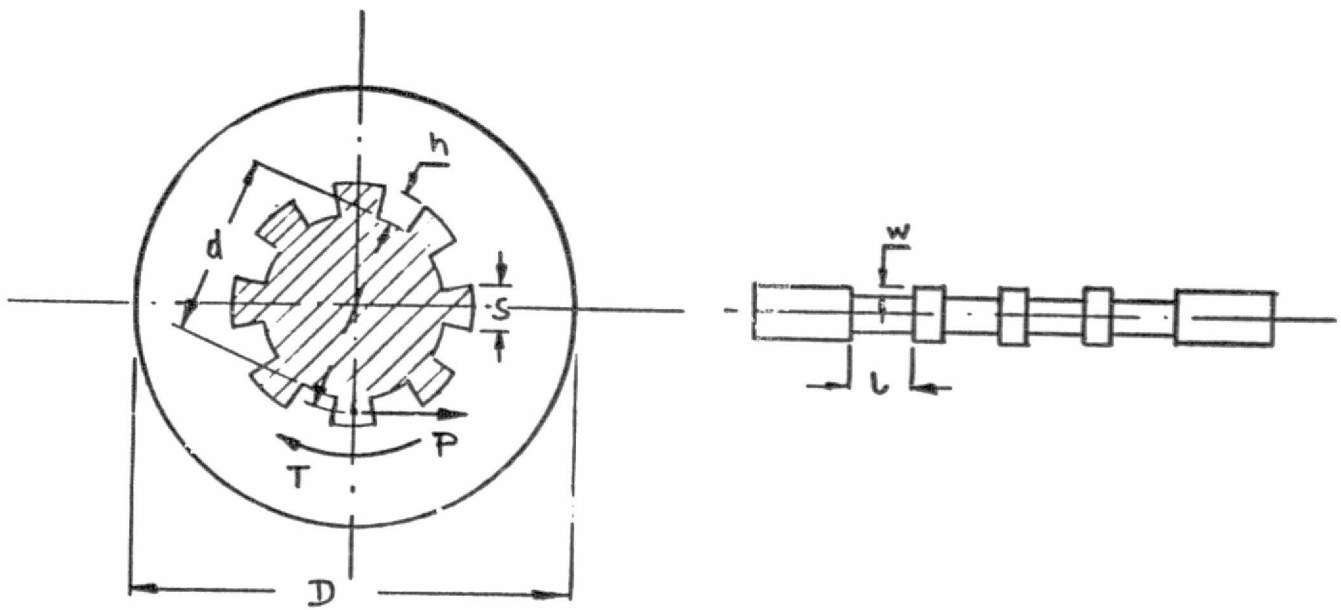

Figure 21. CROSS SECTION AND SIDE VIEW OF CERAMIC AND STEEL SPLINE CONNECTIONS

Ceramic spline shearing stress:

$$\tau_{yx}(c) = \frac{P}{S\ (iL + wj)\ n} \tag{59}$$

where:

S,L,w,h = Dimensions from Figure 21

i,j = Number of portions of the above dimensions

n = Number of splines

Ceramic and steel spline compression stress:

$$\sigma_x\ (c,s) = \frac{P}{h\ (i\ L + wj)\ n} \tag{60}$$

Maximum torsion shear stress in steel core:

$$\tau_{zx}(s) = \frac{2T}{\pi\ r^3} \tag{61}$$

Values of these stresses have been calculated for the following data: T = 7.5 kg (assuming that total torque is generated on the male rotor); r = 1 cm; L = 4 cm; w = 1.5 cm; i = 4; j = 7; h = 8; n = 0.3 cm; D = 6 cm.

For design conditions:

$\tau_{yx}(c)$ = 7.0 kg/cm^2

$\sigma_x(c,s)$ = 12.0 kg/cm^2

$\tau_{zx}(s)$ = 477.4 kg/cm^2

Thrust Compression

The ceramic shell is subjected to axial pressure load which must be absorbed by the steel core and then by the axial bearings. Thrust compression developed on the core thrust surfaces will contribute to the total stress in the rotor's ceramic shell.

Compression stress at ceramic thrust surface can be determined from equation:

$$\sigma_z = \frac{4\ F_{ax}}{m\ (D^2 - d^2)\ \pi} \tag{62}$$

where:

F_{ax} = Axial load

m = Number of thrust surfaces

For given design conditions σ_z = 9 kg/cm^3.

Transverse Shearing

The shearing stresses induced by transverse forces are not taken into account in this analysis due to their negligible values.

Summary of Stress Analysis

Our stress analysis revealed that the stresses of concern in the expander design (excluding bearings) are those in the ceramic portion of the rotors. The results of this analysis are summarized in Table 1. The table contains stress point locations, inducing load and corresponding stress value, principle stress value, maximum shearing stress, and estimated safety factor at the point. Mechanical properties of a candidate ceramic, silicon nitride (Si_3N_4), were used. Flexural strength for hot pressed Si_3N_4 is listed as 12,000 kg/cm^2, and for sintered Si_3N_4 as 8,500 kg/cm^2. A reliable shear strength was identified by the properties of brittle materials, in which it should be similar to the flexural strength.

The theoretical overall safety factor for the more heavily loaded male rotor is about 8. In spite of this acceptable value which was arrived at by our conservative approach, we believe that a more reliable estimate must be based on a detailed study of ceramic properties.

Our conclusions based on the stress analysis are:

- Ceramics potentially can be applied as structural material for screw expander rotors
- Fabric-reinforced ceramics should be considered due to the high centrifugal stress on the rotors.

Design Description

A characteristic feature of the screw expander design is its composite structure using both metallic and ceramic components. The design of the expander is shown in Figure 22, which is referenced in the detailed description below. A complete set of detailed drawing is appended.

Table 1. SUMMARY OF STRESS DISTRIBUTION DETERMINATION WITHIN THE CERAMIC SHELL OF MALE ROTOR

Stress Location Point	Stress Designation	Inducing Load	Stress Value	Principal Stress Value	Ultimate Strength	Safety Factor	Illustration of Components of Stress
			kG/cm^2	kG/cm^2	kG/cm^2		
Dedendum Diameter	G_z	Bending	147.0				
Central Point of Rotor Void	G_{xmax}	Centrif.	1008.0	1008	8500	~8.5	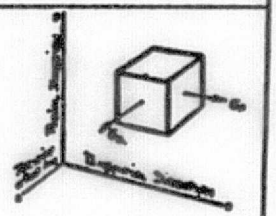
Maximum Bending Cross-Section	G_{xmin}	Stressing	566.0				
Dedendum Diameter	G_z	Bending	147.0				
Central Point of Rotor Lobe	G_x	Centrif.	566	566.0	8500	~15.0	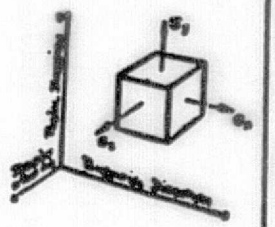
Maximum Bending Cross-Section	G_y	Stressing	396				
Spline Diameter of Shell Internal Bore	G_z	Bending	30.0				
	G_x	Centrif. Stressing	566.0	566.0	8500	~15.0	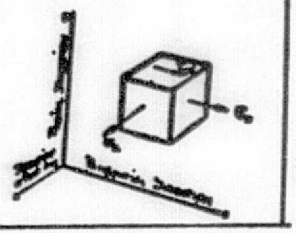
Maximum Bending Cross-Section	τ_{yx}	Spline Shearing	7.0				

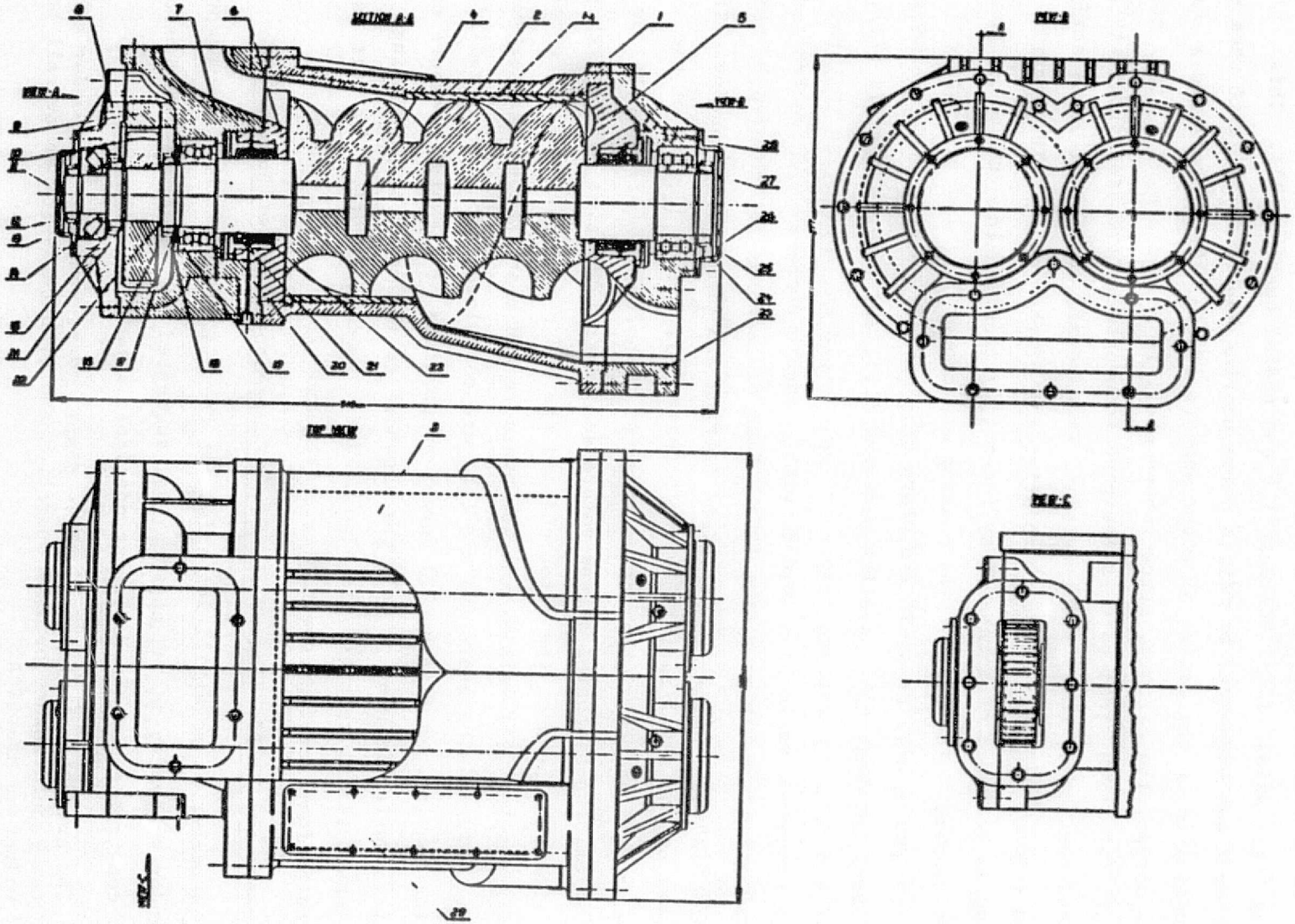

Figure 22. SCREW EXPANDER DESIGN

Two rotors, the male rotor (2) and the female rotor (3), are enclosed inside rotor housing (1) and are supported by three bearings each, the axial bearing (14), axial/radial bearing (19) and radial bearing (27). This arrangement was suggested by SKF, a Swiss bearing manufacturer, with whom we have consulted on the design of rotor support system. The rotors are a composite design; the ceramic, screw lobbed shell is molded around a steel core or shaft (4). The steel core is designed to provide structural integrity to the rotor assembly, carry the torsional, transverse, and thrust loads acting on the rotors, and contribute to the rigidity of the rotors. The rotor housing is composed of a ceramic cylinder (14) inserted into the metal casting of the housing. The ends of the housing are closed by a low pressure end plate (5) and a high pressure end plate (6), made of ceramic and incorporating shaft seal housings (20), sealing packages (21), and labyrinth seals (22). Intake and outlet ports are formed in the end plates, located so that the design expansion ratio is provided, with pressure overexpansion controlled by the expansion modulation system (29). Ease of assembly is achieved by using a split design of the high pressure end bearing and timing gear housing. This consists of the axial/radial bearing housing (7), intake ducting of the expander, and the axial bearing housing (8). Shaft nuts (12) and (16) permit precise axial positioning of the rotors and control the size of the high pressure clearance between the rotor end and the end plate. The one-piece radial bearing housing (23) retains the low pressure end plate and has the exhaust ducting. The timing gears (9) and (10) are contained in the axial/radial bearing housing. A flange (32) formed as portions of the high pressure end bearing housing is used to bolt the expander to the power train housing. The male shaft timing gear (10) is also used for power take-off. The unit is closed by four bearing covers, i.e., (11) and (26).

Placement and Manifolding of the Screw Compressor-Expander Subsystem

A number of possibilities exist for the placement of the screw compressor-expander subsystem on the engine. Our suggested placement described below has been constrained by the following considerations:

- The arrangement of the positive displacement compressor-expander subsystem should assure optimal operation and produce as low an overall box volume as practical

- Installation of the subsystem should permit power transfer in a manner similar to that used on the TCD-450 turbocompound system, in order to keep the numbers of unique parts to a minimum
- Installation of the subsystem should require a minimum number of changes to the existing engine assembly arrangement.

The suggested conceptual arrangement is shown in Figures 23, 24, and 25. The arrangement consists of the expander (1) and compressor (2) integrated in one assembly which is mounted on the right side of the engine block (as in the TCD-450). Location and general arrangement of the power train is basically the same as the turbocompound system's. For this arrangement, a new exhaust manifold (3) must be designed. During the initial development stages this can be of the steady-flow type.

The exhaust gases feed into the expander through an intake duct and exit the expander through an outlet duct located between the expander and the engine block. The space between the compressor and engine block would be used for ducting intake air to the compressor. The pressurized air exits the compressor through a duct similar to the one used with the turbocompressor.

The suggested arrangement of the positive displacement compound subsystem fits into the overall layout of the NTC-400 reasonably well. The primary area not addressed is that of the power train; however, the power train linking the screw expander and engine should be smaller than the one for the turbocompound system because of the lower gear ratio required.

Cost and Production Engineering Considerations

One of the most significant concerns in our assessment of the potential of screw machines has been the cost of the components, mainly the rotors. This is dictated by the inherent features of more bulk material compared to turbomachinery, and by the time-consuming production techniques. We refer to rotors of about 100 mm size, since this is the size for which we have obtained some reference data. Scaling the result linearly to the 160 mm range should not introduce significant error. The current production cost for a bare 102 mm, flooded compressor (material and labor) is about $1000 (1982). This is for an assembled machine that weighs about 110 pounds, with an approximate production run of 20/day. To achieve better surface quality and higher productivity, rotors for these machines are now being hobbed rather than milled on Holroyd special milling machines. This new technology has been developed by two

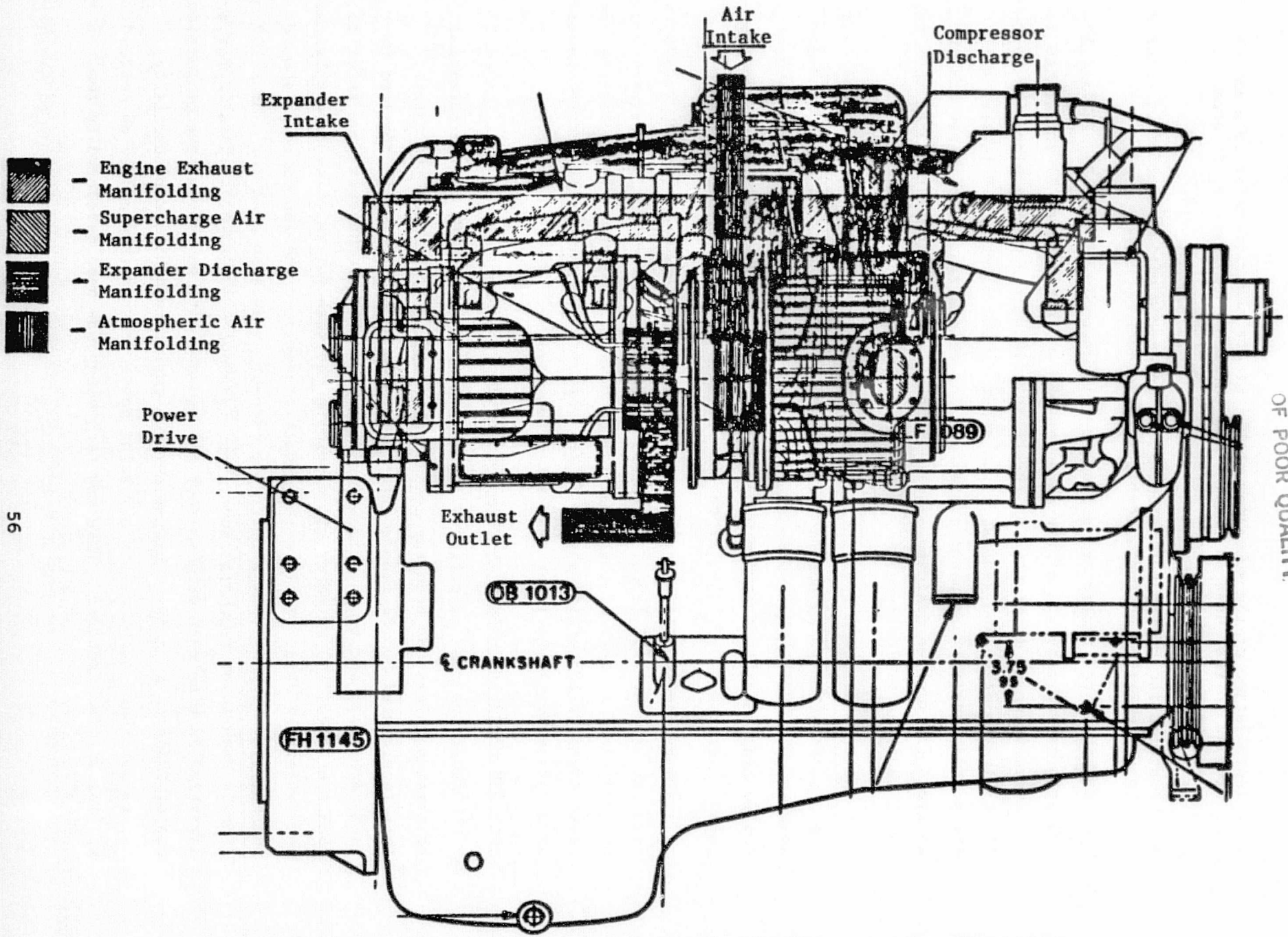

Figure 23. SIDE VIEW OF SCREW COMPRESSOR AND EXPANDER MOUNTING ARRANGEMENT

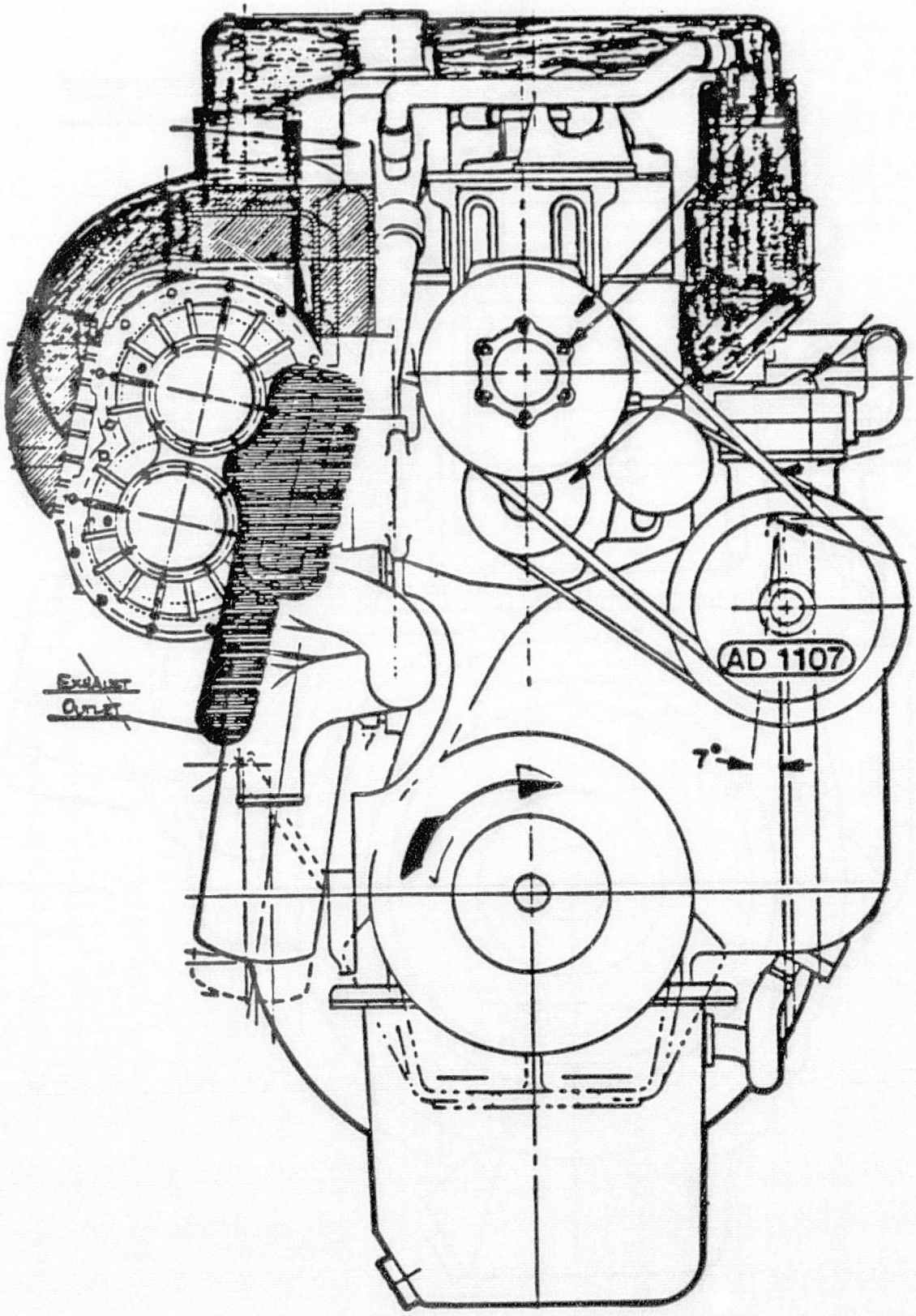

Figure 24. VIEW OF SCREW COMPRESSOR AND EXPANDER MOUNTING ARRANGEMENT

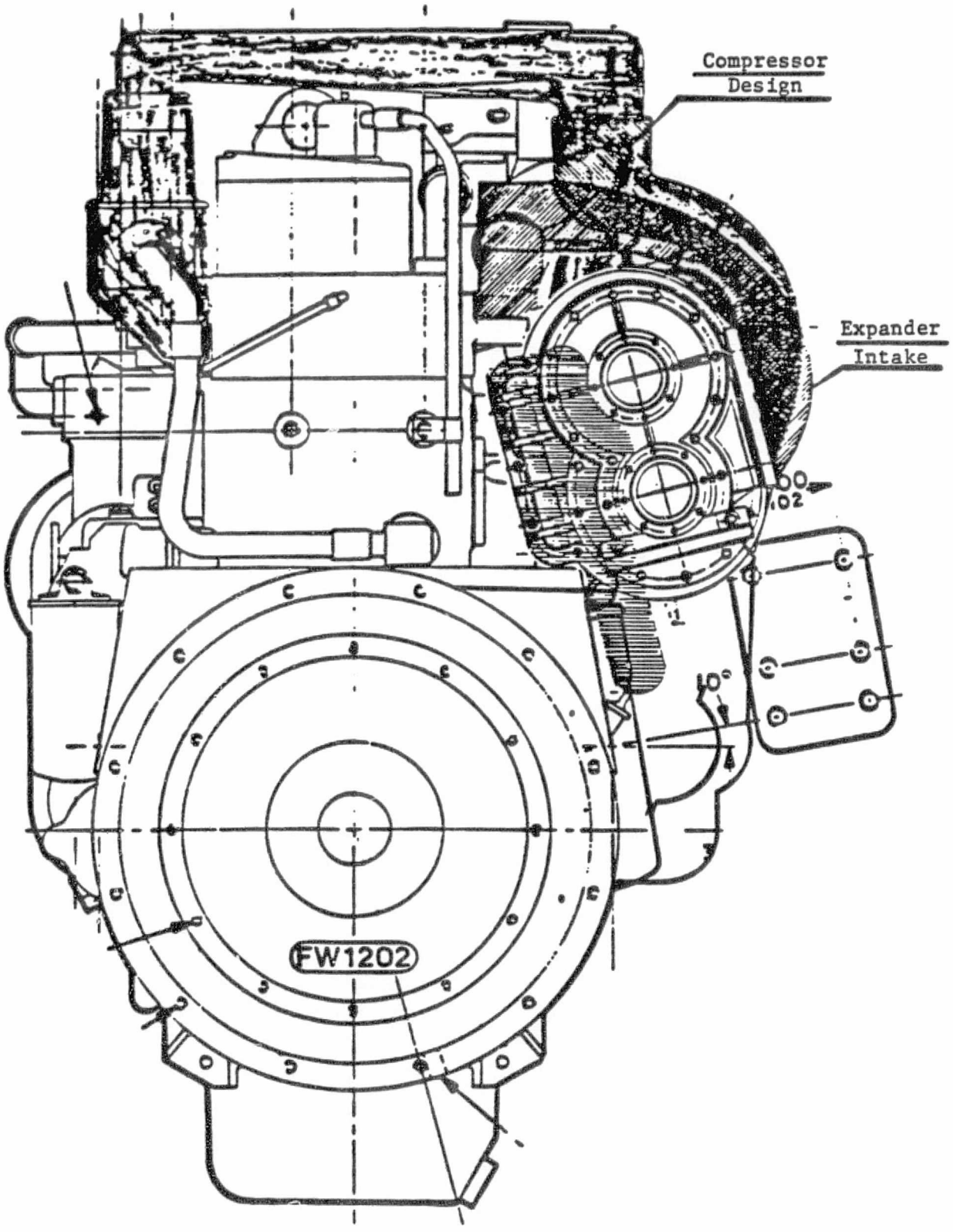

Figure 25. VIEW OF SCREW COMPRESSOR AND EXPANDER MOUNTING ARRANGEMENT

German companies, Pfauter and Lieb. However, implementing this manufacturing process has not resulted in the price reduction required for the application under study, and it is doubtful that any technique requiring final machining can achieve the necessary price reduction.

However, recent developments in ceramic technology show promise in rotor production applications. Recent work at Lawrence Livermore Labs (LLL) has demonstrated that silicon nitride rotors of this size may be cast using the advanced, experimental technique of reaction-bonding. This has been the work of five companies (3 in Europe and 2 in the U.S.) and has supposedly resulted in techniques in which the rotors can be manufactured to the required tolerances, with no further need of machining.

Any attempt to estimate the potential manufacturing cost of a composite material (ceramic/metal) version of a 100 mm machine would be difficult at this time. However, using the above information and an estimate of LLL that the ceramic segment of the rotor would be $15, we believe that a 50% reduction in manufacturing cost is feasible if the following assumptions are used:

a. Cost of a normal set of rotors is 45% to 50% of the total, $450

b. The steel portion of the new rotors would be equivalent to the rotor costs minus profile generation costs; this would be about 33%, $150

c. The cost of the ceramic portion of the rotors is $30 for both

d. Total cost of the rotors would be $180

e. The housing, bearings, gears, etc., cost $550

f. Reduction in size and complexity would account for a 40% reduction in cost, producing a new cost of $330

g. Then, the total cost for a new composite ceramic/metal expander would be $510.

It is possible that further cost reductions can be made by applying new process technology and mass production factors. However, we are not certain what their effect would be.

Testing Considerations

In general, supercharging and power recovery machines serving adiabatic diesels will have to sustain operation under very severe operating conditions and requirements. These conditions and requirements cannot be considered

common for any existing and marketed machine (positive displacement or dynamic). Screw machinery is not an exception since very little is known about their performance as dry expanders, about manufacturing them in composite metal/ceramic structures, and about making them much less expensive than commonly produced compressors. In this preliminary design and evaluation program we have considered all of the special conditions and requirements. Consequently, we have produced a design with many unique elements that will require the experimental expander to be first tested separately from the engine (reciprocator) with which it may eventually be compounded. A detailed work plan for an experimental phase encompassing such testing would include:

1. Materials and production techniques for rotors of composite structure. Particularly important are:
   - Cost of rotors
   - Practicality of tolerance field
   - Surface quality
   - Dimensional stability under temperature, pressure stress
   - Material uniformity and structure
   - Tolerance to mechanical contact.
2. Stress analysis of composite structure rotors. In this area problems appear to be solvable but a more detailed investigation is needed in:
   - Assessing the centrifugal stress in ceramic shells of rotors
   - Stress concentration in boundary zone of ceramic shell (next to steel core)
   - Dynamic deflection of rotor axis and possible interference with field of tolerance.
3. Design specifics of dry radial ball (needle) and axial roller bearings in terms of selecting size, type, and precision category with regard to:
   - Stressing of both rolling elements and bearing races caused by high centrifugal forces involved
   - High-frequency, low amplitude dynamic character of the load
   - Large temperature swings.

4. Design specifics of dry-operated timing gears (in case that such a design option would be selected) as to the selection of type, precision category, and type of coating, with respect to:

   - Assembly and adjustments
   - Noise
   - Mechanical loss.

5. Design specifics of discharge and filling manifolds and connecting pipes between the engine and the components; and compressor suction, expander discharge manifolds with respect to:

   - Pressure wave propagation, ram and blow-by effects
   - Exhaust and suction noise.

6. Design point and part-load performance. Selection of design operating point is of extreme importance for optimizing the size, operating speed range, and built-in volume ratio of the machines. The main parameters of size, speed, and absolute clearances will have to be analyzed as to their influence on the overall system performance over the range of engine operating conditions. Significance of this influence must be established in order to determine the design point conditions and design specifications of:

   - Tolerable clearances
   - Built-in volume ratio and need for its control
   - Preferred speed range.

In order to carry out this experimental phase the presented design of the expander would have to be changed nominally. It would include an extension of the male rotor shaft to directly engage (through a coupling) with a driving motor (for compression, mechanical, and stress testing) and/or a power output (torque) metering brake. Another essential element for testing would be the inlet and discharge absorption type silencers. The design of these elements has not been carried out as part of this project since it represents applying straight-forward engineering practices.

SUMMARY OF RESULTS AND CONCLUSIONS

In this project, we have evaluated the potential performance of a screw expander for operation in a positive displacement-compound diesel system. Through our evaluation of the potential performance of the expander based on compressor data, we have projected a maximum overall adiabatic efficiency of 95% and evaluated performance over an extended range of operating pressure ratios, up to 5. This has allowed us to project the potential overall system brake specific fuel consumption when using screw machinery in comparison with the current turbocompound system. Based on this evaluation, we have found that the positive displacement system has the potential of performing 7% better than the turbocompound system in brake mean effective pressure and 5% in brake specific fuel consumption at rated conditions. In addition, part load and lower speed operation has the potential of even better relative performance than the turbocompound system. These results would be further increased if the system were applied to an adiabatic diesel system.

We have accomplished the preliminary design of the screw expander and have evaluated the charging and expansion volumes. These results were used to adjust the initial dimensions of the machine and to establish preliminary port timing. We have also decided on the probable location of the positive displacement compound subsystem on the engine and the manifolding required. In doing so, we considered the current turbocompound system and used that as a guideline so that changes in incorporating the positive displacement subsystem may be kept at a minimum.

We have also evaluated the stresses on the designed expander, and have found that the design has a minimum safety factor of 8, assuming the use of a composite steel/ceramic rotor with silicon nitride of uniform quality. However, it is not known whether this value is acceptable.

In addition, we have included a concept which would eliminate the potential of overexpansion which may occur in a machine with a higher design pressure ratio than would be required under some operating conditions.

Finally, we have considered the testing requirements for a screw expander given that this design reaches the experimental stage.

As a result of our study of screw machinery applied as auxiliary equipment to a diesel engine, we have concluded that there is a definite potential

for these machines in this new type of service. We have shown that the potential performance of a compound diesel system using a screw expander is better than the baseline turbocompound diesel system at rated conditions and at part load, based on brake specific fuel consumption and brake mean effective pressure. Based on our stress analysis, we have concluded that the use of a composite steel/ceramic rotor is possible, allowing the rotors to operate in the high temperatures of the exhaust. We have also concluded that the positive displacement subsystem (of screw compressor and expander) can be interconnected with the engine requiring a minimum of changes to the method employed with the current turbocompound system. We have finally concluded that the concept of screw positive displacement compound diesel systems represents a significant technology that should be further pursued.

RECOMMENDATIONS

This preliminary assessment has indicated further work necessary before proceeding to experimental development of the screw expander. Specifically, we recommend:

- Further analytical work to verify the projected efficiency levels using a more rigorous approach to its assessment
- Detailed evaluation of the operating volume and port timing to include the effects of pressurized intake and rotor profiles
- Evaluation of the effects of overexpansion on the operation of the expander, to determine whether a modulation concept such as that presented in this report would significantly improve the part load performance of the expander
- Detailed assessment to more accurately determine the estimated stresses on the rotors of a composite steel/ceramic expander, specifically whether advanced, fabric-reinforced ceramics should be considered.

REFERENCES

Chlumsky, V., Reciprocating and Rotary Compressors. Prague, Czechoslovakia: SNTL-Publishers of Technical Literature, 1965.

Schibbey, H., "Present Status of the Screw Compressor and Its Noise Problems." Gas Warme International, 22 (11), 431-4 (1973) Nov.

Wichert, K. E., "Characteristics of Helical, Rotary, Positive Displacement Compressors." Paper No. 61-HYD-18 presented at the joint ASME-EIC Hydraulic Conference, Montreal, May 7-10, 1961.

EXPANDER DETAILED DRAWINGS

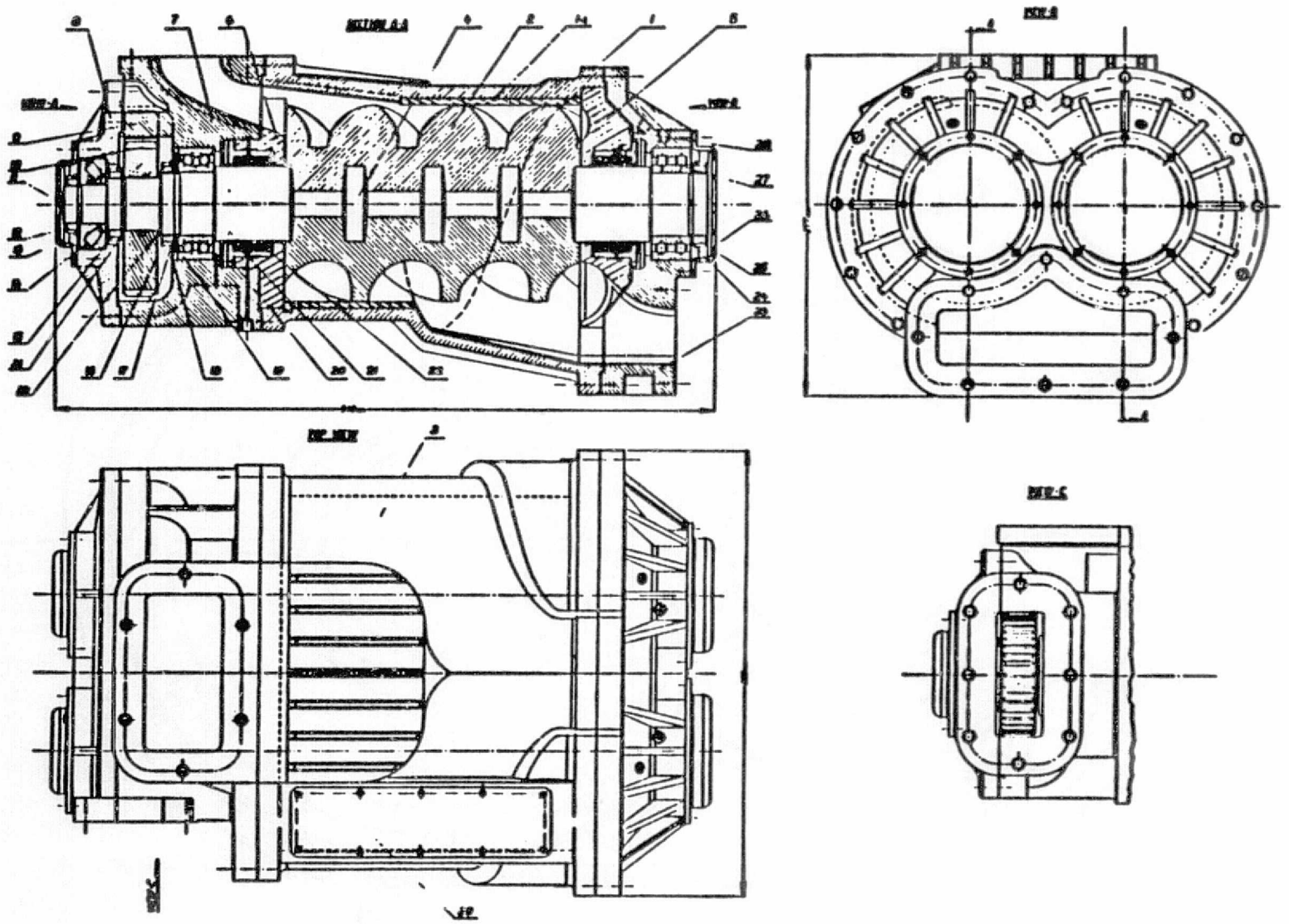

Figure A-1. SCREW EXPANDER DESIGN

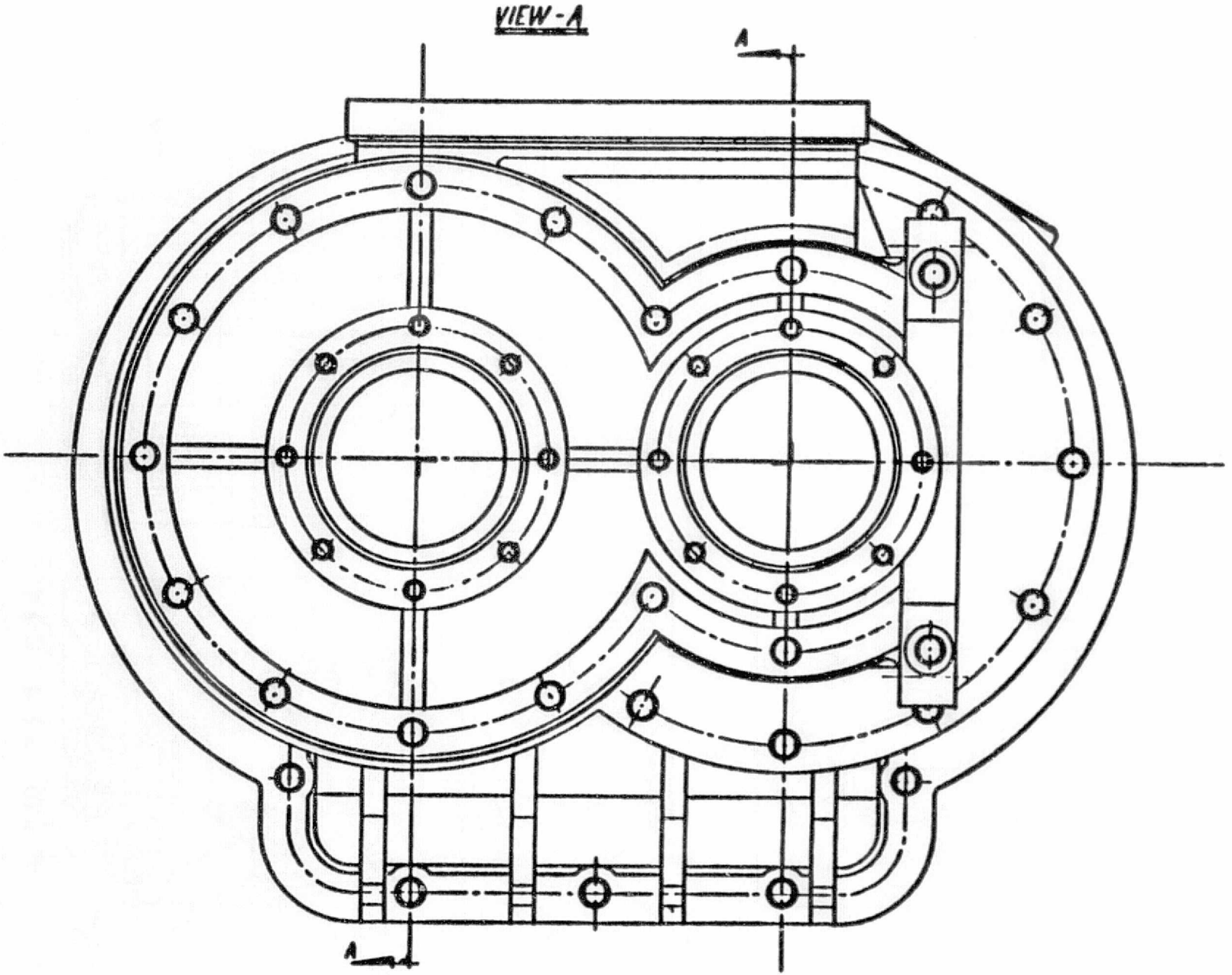

Figure A-2. TIMING GEAR END OF HOUSING (View A of Figure A-1)

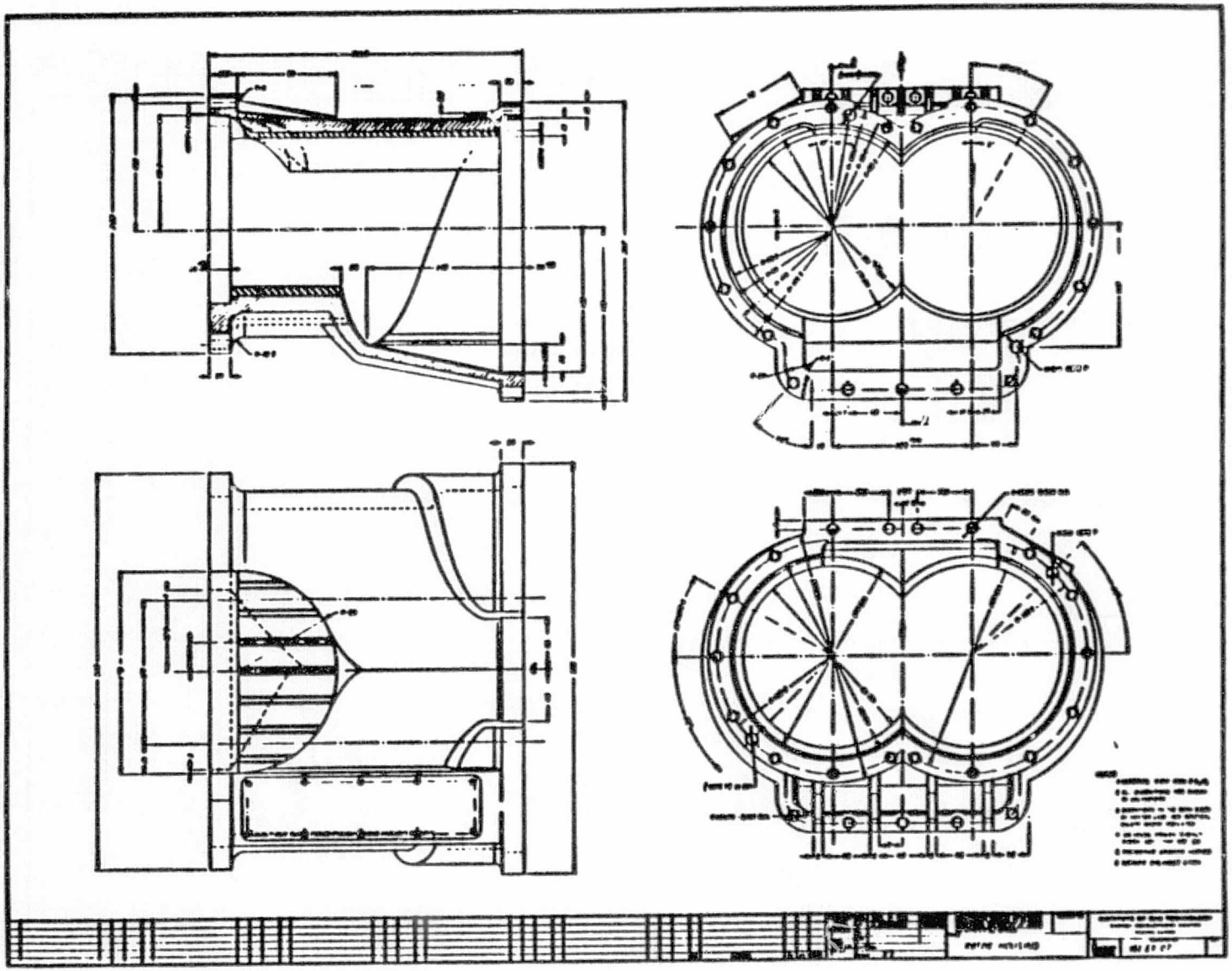

Figure A-3. ROTOR HOUSING

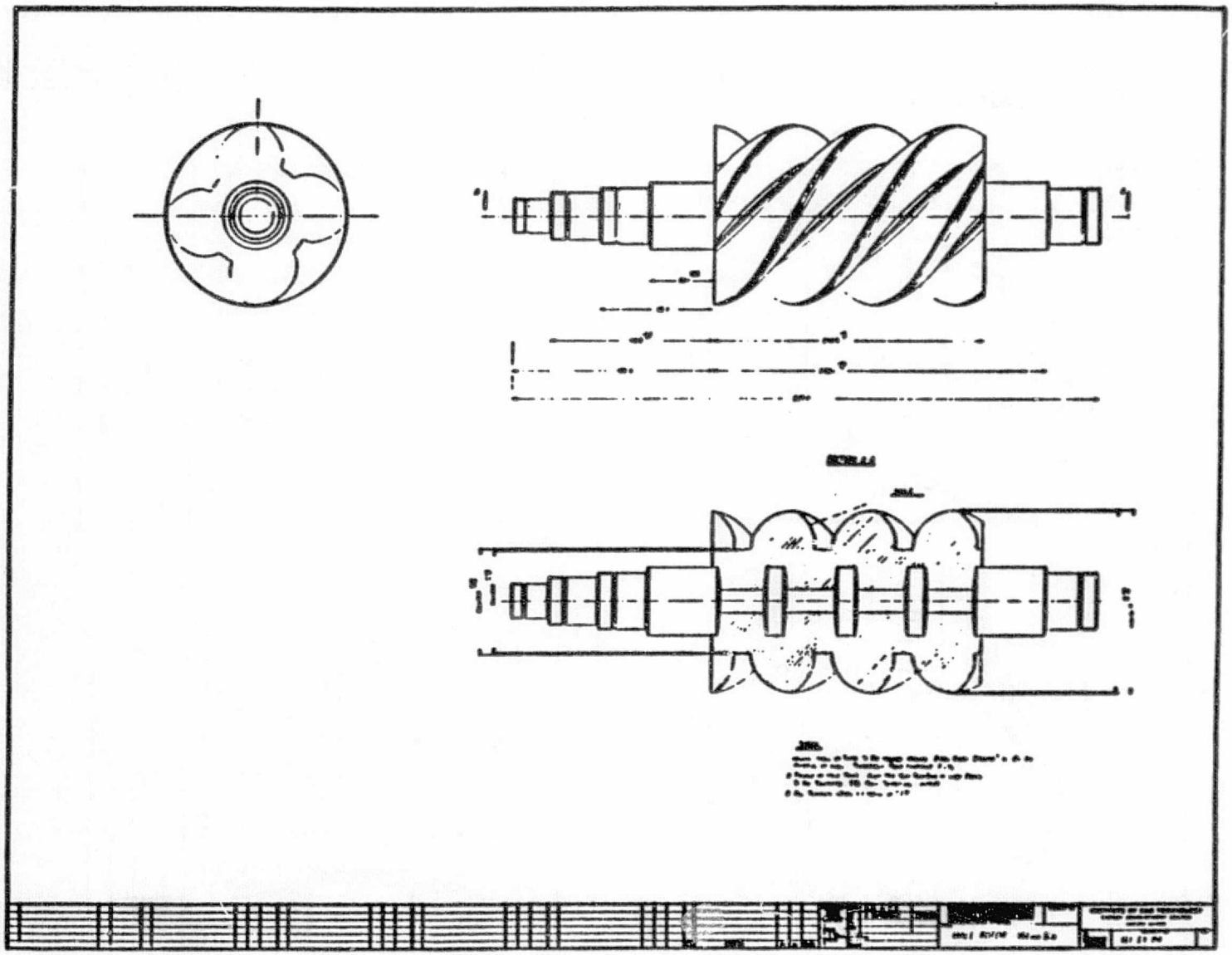

Figure A-4. EXPANDER MALE ROTOR

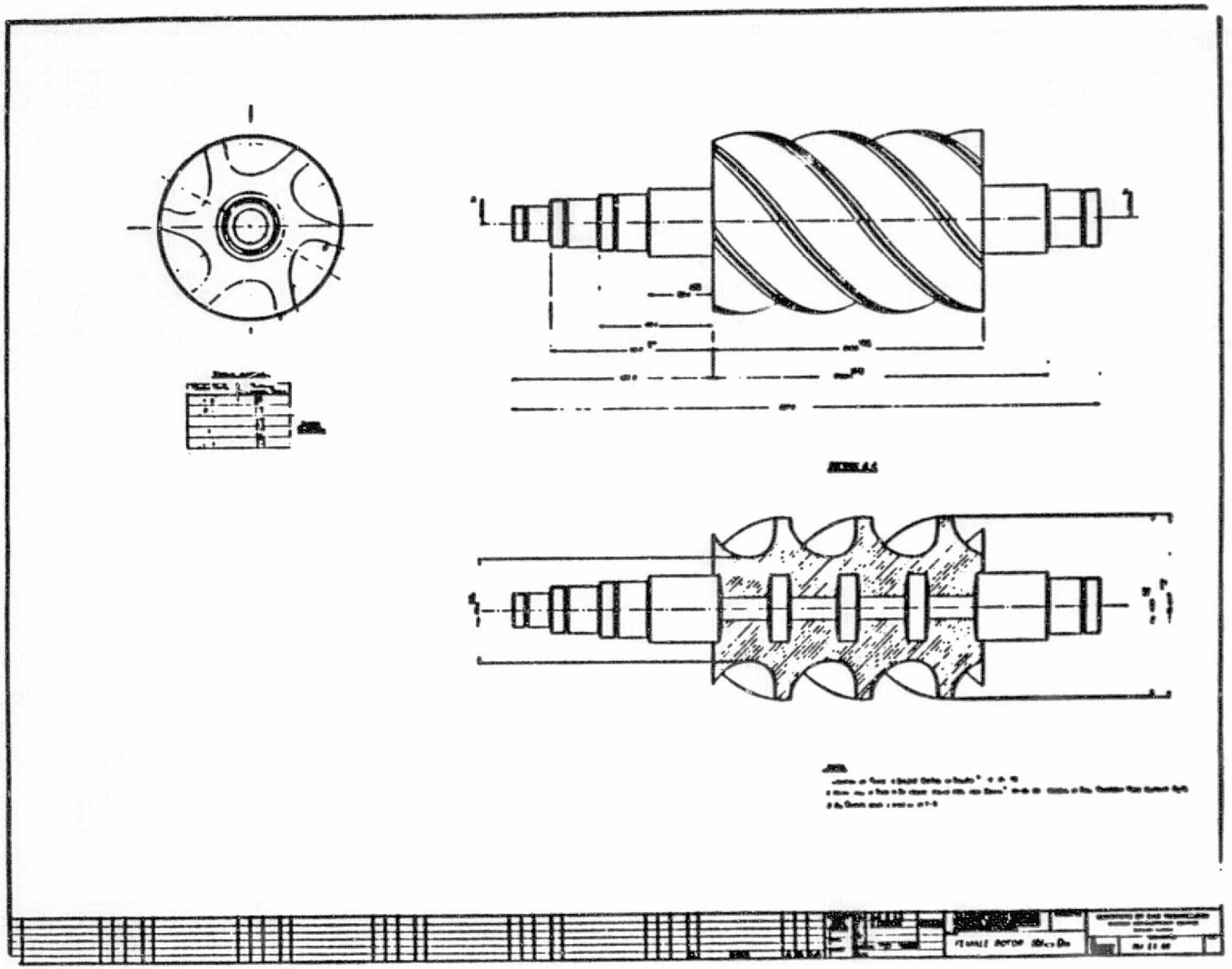

Figure A-5. EXPANDER FEMALE ROTOR

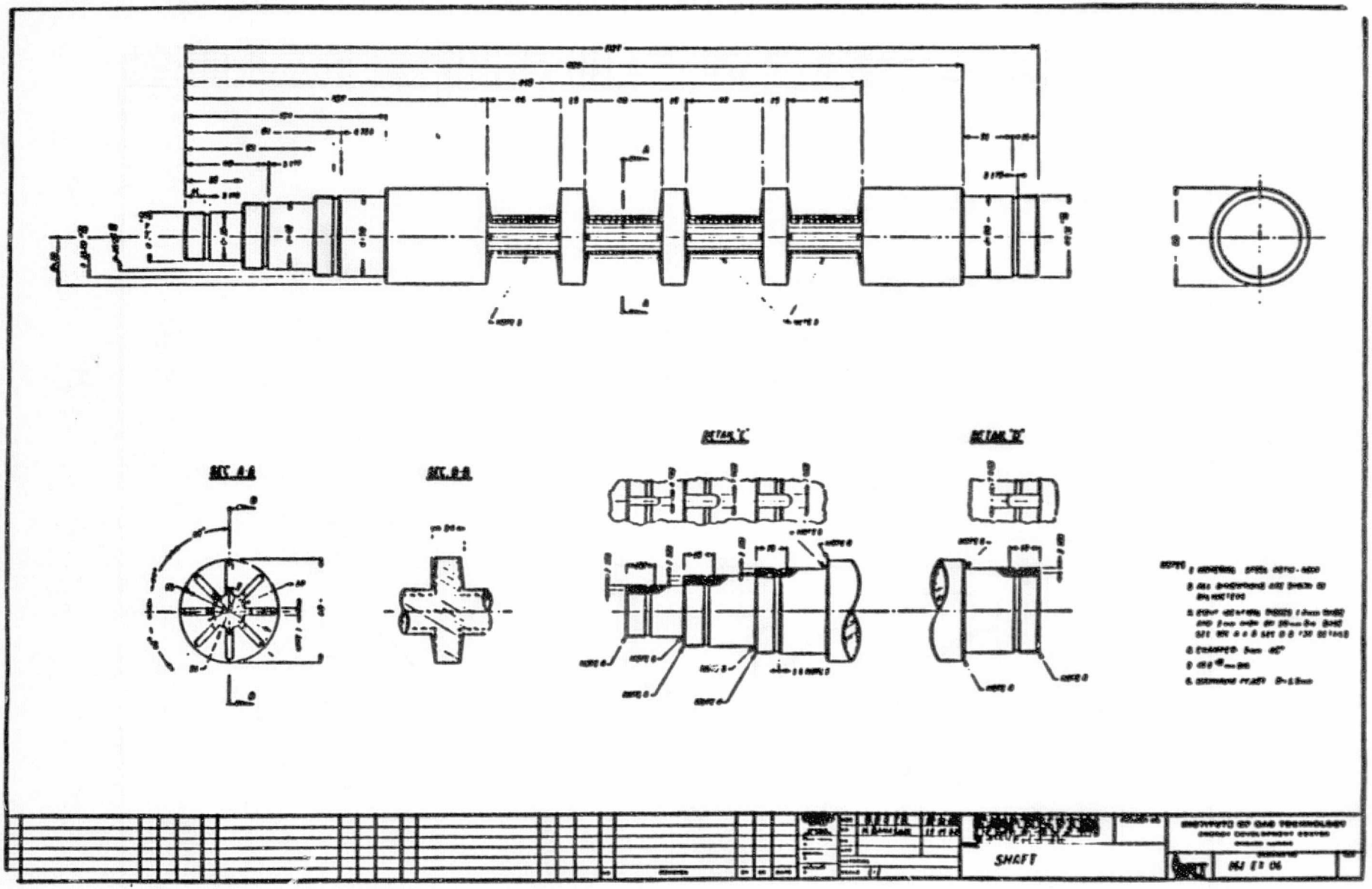

Figure A-6. EXPANDER ROTOR SHAFT

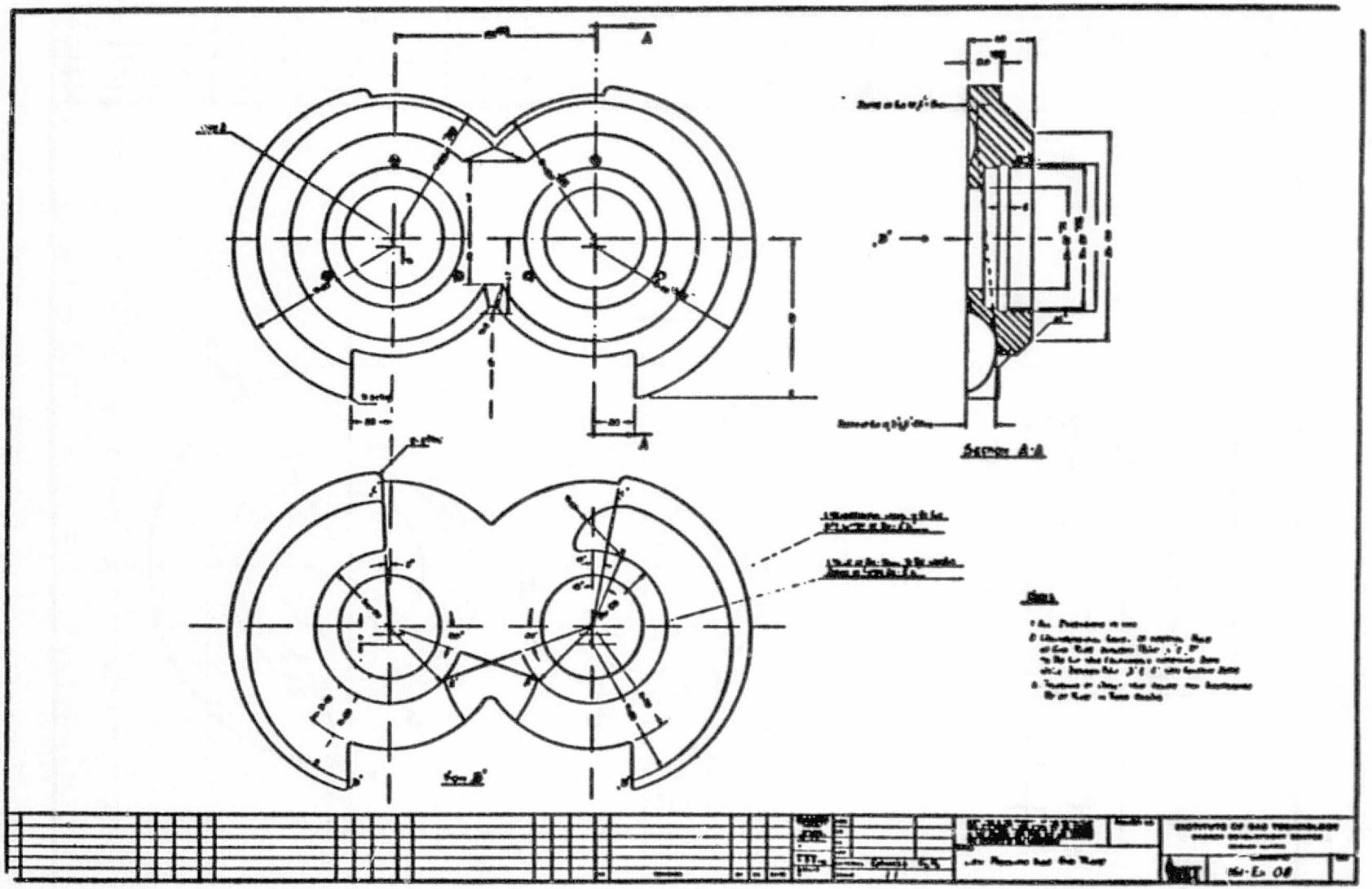

Figure A-7. LOW PRESSURE END PLATE

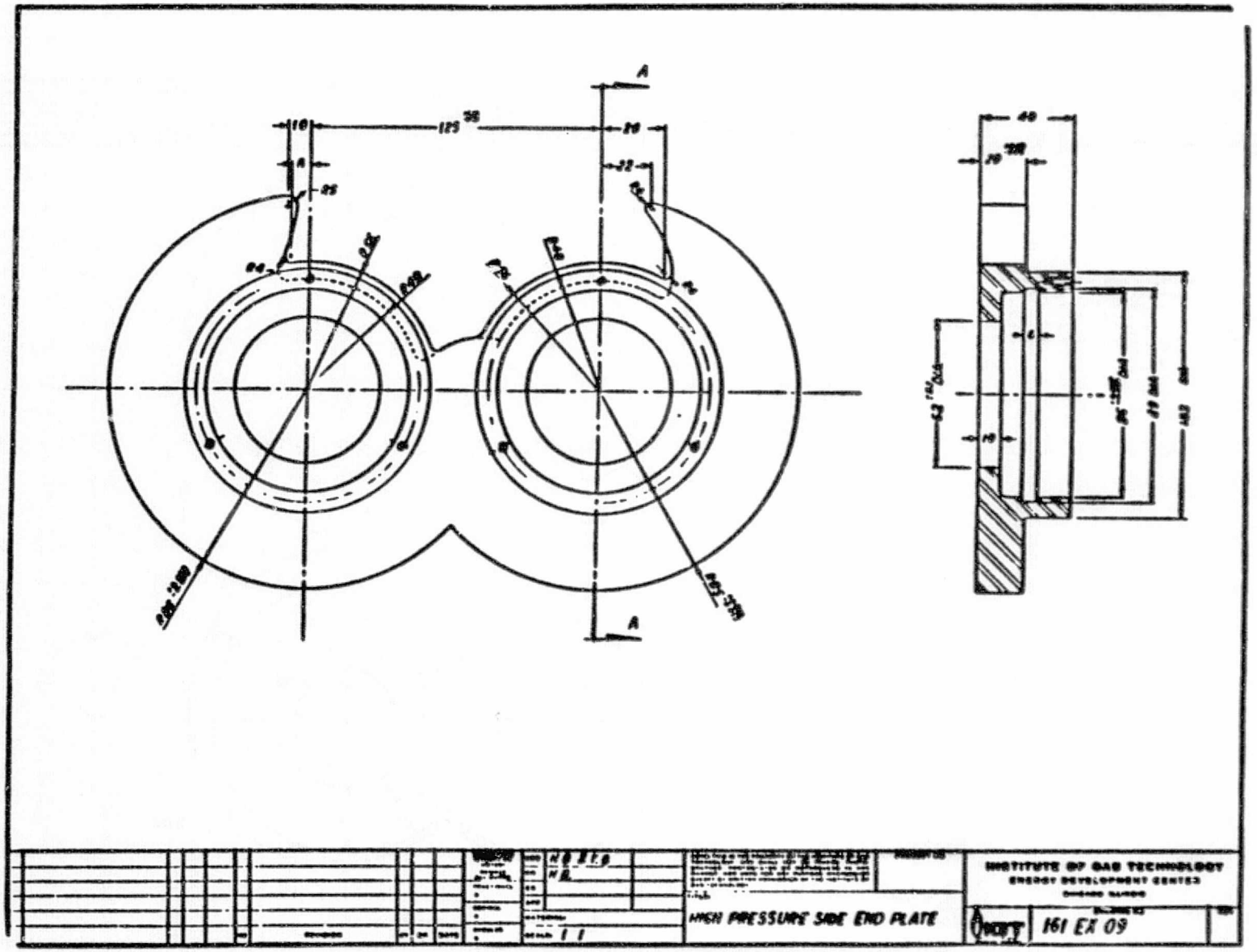

Figure A-8. HIGH PRESSURE END PLATE

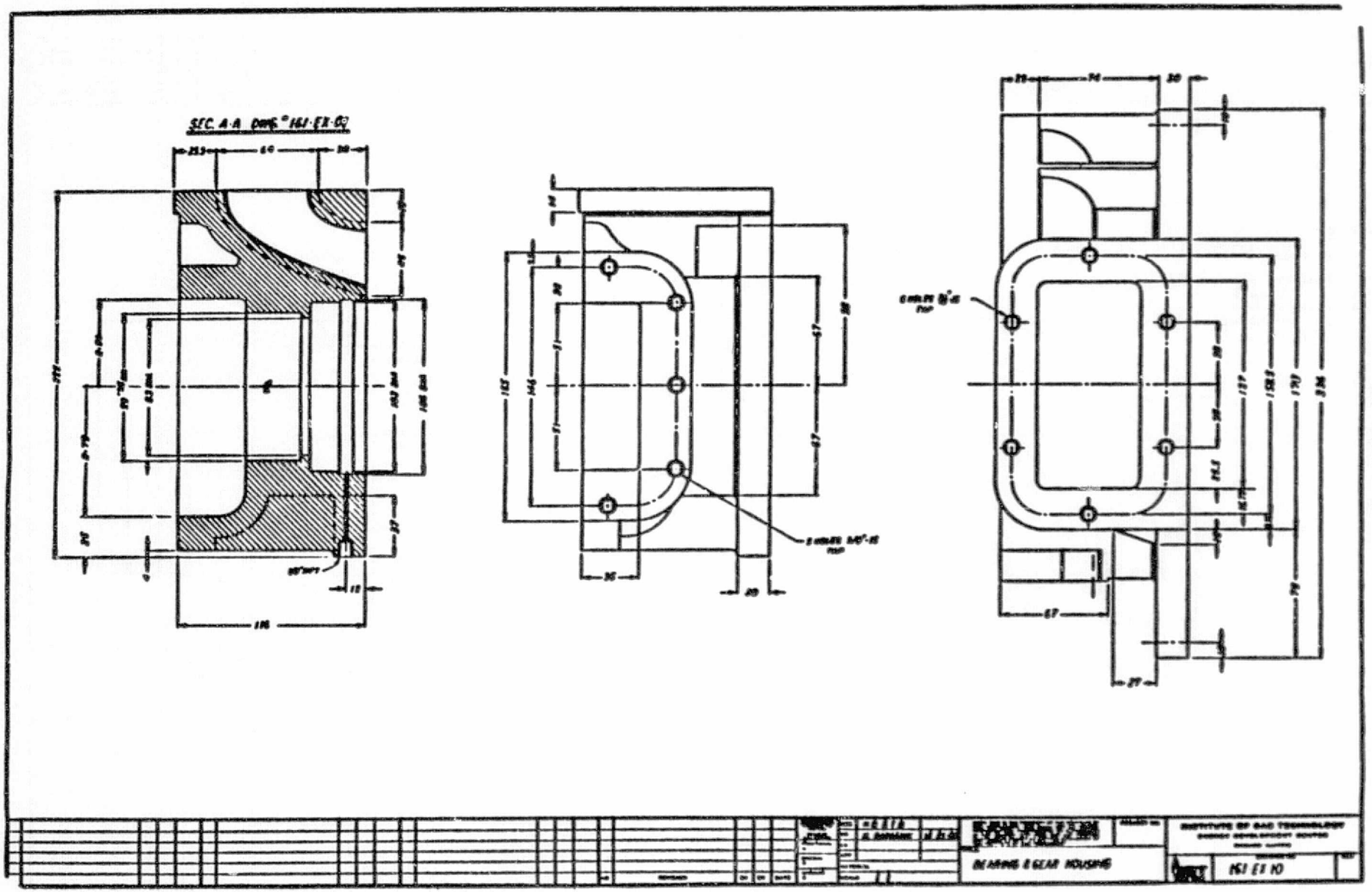

Figure A-9. BEARING AND GEAR HOUSING

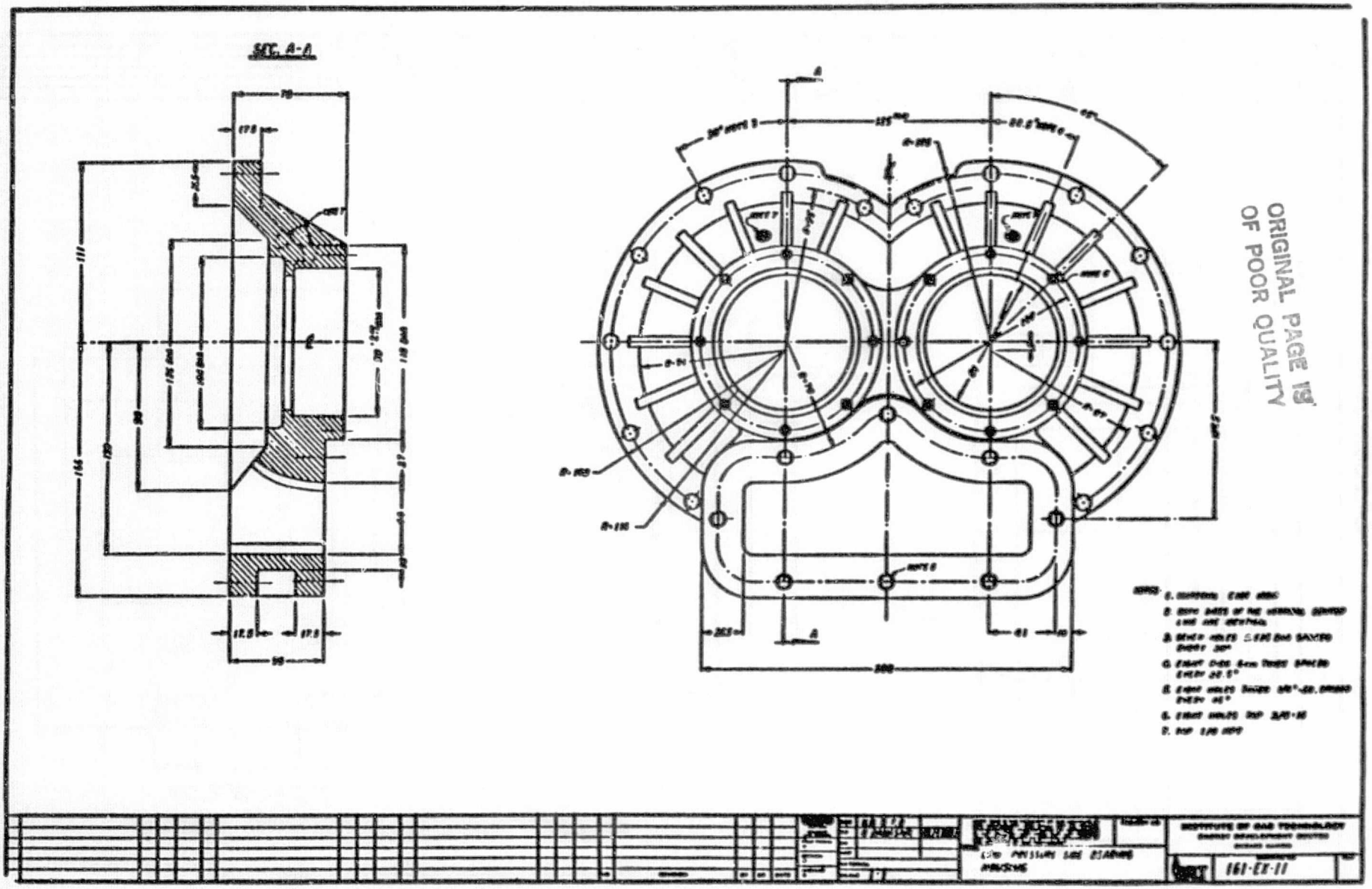

Figure A-10. LOW PRESSURE BEARING HOUSING

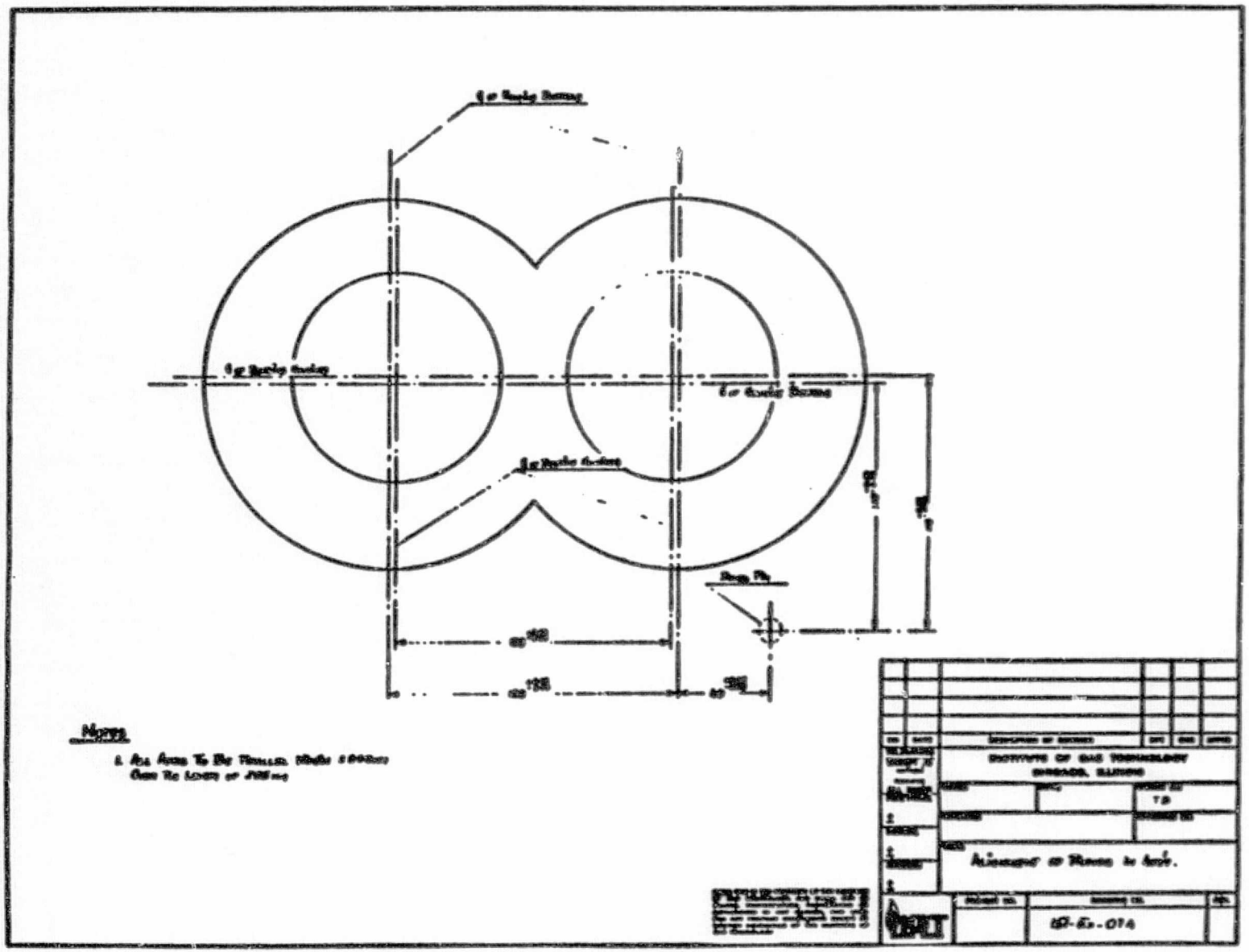

Figure A-11. ALIGNMENT OF ROTORS IN ASSEMBLY

APPENDIX 2

Evaluation of the Positive Displacement Compressor/Expander Subsystem for the Turbocompound Engine

by

M. M. Kamel
Cummins Engine Company, Inc.

DISCUSSION

An investigation by the Institute of Gas Technology (IGT) suggested that high component efficiencies could be expected from positive displacement compressors and expanders. Table 1 is a summary of their predicted efficiencies for a positive displacement compressor and expander system which was designed to replace the turbocharger and power turbine of the turbocompound 450 HP NH engine.

To predict the potential engine performance improvements using the positive displacement machines the cycle analysis program TRANSENG was used. The program had been previously used to predict the turbocompound engine performance and gave satisfactory results when compared to measured data. It was, therefore, decided to use it for this task. Since the positive displacement expander was designed to replace both the turbocharger turbine and the power turbine, it was convenient to model its performance by simply running the simulation program with current turbine and power turbine flow characteristics but with similar efficiency values. These characteristics were obtained from the turbocompound engine test data.

Table 2 shows some test data for the 450 HP turbocompound engine. Discrepancies have been detected in the (IGT) data in Table 1, when compared to engine test data. For the expander, the BMEP values quoted are not consistent; the 1600 rpm values are for the "Reciprocator" while the rest are for the "Turbocompound" engine. Also, all pressure ratio values for the expander are higher than the overall expansion ratios from the test data. This could be a design characteristic for the positive displacement expander (i.e. higher pressure ratio for the same mass flow) and could have implications on the engine performance. In the present investigation only the effect of the increased efficiencies was considered.

Since the main attractions of the positive displacement equipment are the predicted high efficiencies, it was decided to concentrate our prediction efforts on the effect of the increased efficiencies on overall engine system efficiency.

This was accomplished by using the cycle simulation program to predict the increase in engine power when the component efficiencies are increased while holding the fuel consumption (lb/hr) constant at the same speed.

Three engine speeds were considered: 1900, 1600, and 1300 rpm, at full load conditions only. For every engine speed, the engine power was predicted for three component efficiencies, 70, 80, and 90%. All components; namely, compressor, turbine, and power turbine, were assumed to be equal. The predicted data were normalized using predicted engine power for the 70% components efficiency case and is shown in Figure 1. The figure shows the total engine system power and the contribution of the power turbine.

From the figure, it is seen that an increase of component efficiencies from 70 to 90% is expected to render improvements in engine efficiency at 1900 and 1300 rpm of 9 and 12.5%, respectively. The corresponding increases of the power turbine contributions to the total engine power are 7 and 4%, respectively. The increase in the power turbine contribution amplifies the total efficiency gains as expected since the power turbine is directly connected to the engine crankshaft and any efficiency improvement for it would be reflected as an increased engine power. Figure 1 was used to predict potential engine efficiency improvements when using a positive displacement compressor/expander system. Examining Table 1, it was concluded that at full engine load, an average compressor and expander efficiency of 87.5% could be expected. The corresponding value for current turbomachine was considered to be 80%. Examining the test data in Table 2, it is known that some of the turbine efficiency values reported are too high due to our test measurement technique. More specifically, this is due to the fact that we do not accurately measure the integrated average state from which the efficiency is calculated.

It is concluded that for components efficiency improvements from 80% to 87.5%, the expected engine efficiency gains are 3.3 and 4.7% at 1900 and 1300 rpm, respectively.

Figure 1

PREDICTED PERFORMANCE

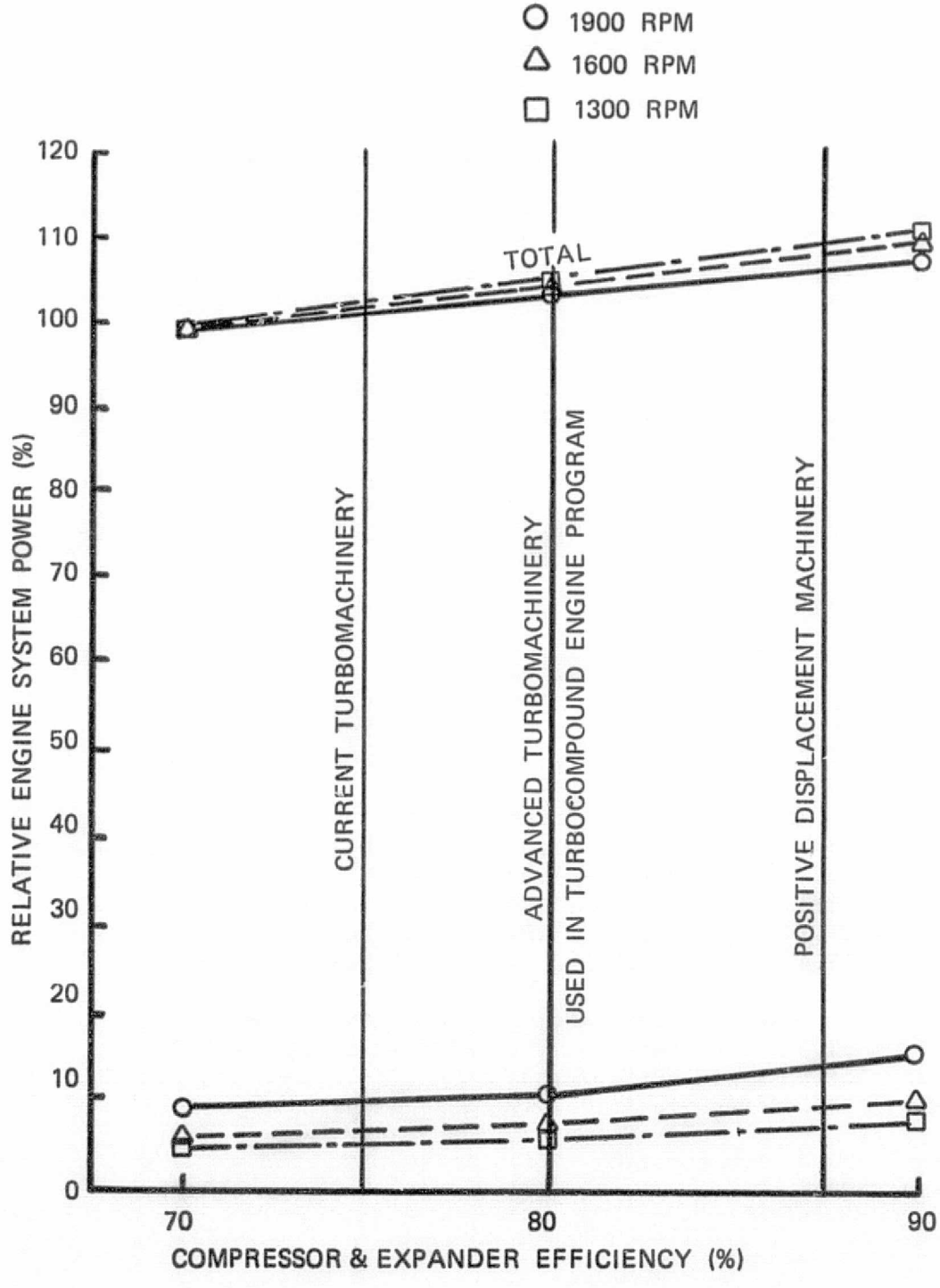

TABLE 1

PREDICTED EFFICIENCIES

CLEARANCE exp: 0.0050 engine speed: 1300.0 rpm
BMEP: 136.4 Press ratio: 2.36 EFFICIENCY exp = 0.866
BMEP: 202.8 Press ratio: 3.00 EFFICIENCY exp = 0.904
BMEP: 231.2 Press ratio: 3.23 EFFICIENCY exp = 0.909

CLEARANCE exp: 0.0050 engine speed: 1600.0 rpm
BMEP: 43.9 Press ratio: 1.56 EFFICIENCY exp = 0.535
BMEP: 88.2 Press ratio: 2.03 EFFICIENCY exp = 0.790
BMEP: 115.2 Press ratio: 2.28 EFFICIENCY exp = 0.844
BMEP: 141.0 Press ratio: 2.53 EFFICIENCY exp = 0.875
BMEP: 176.4 Press ratio: 2.85 EFFICIENCY exp = 0.900

CLEARANCE exp: 0.0050 engine speed: 1900.0 rpm
BMEP: 80.3 Press ratio: 2.18 EFFICIENCY exp = 0.807
BMEP: 104.1 Press ratio: 2.45 EFFICIENCY exp = 0.857
BMEP: 128.2 Press ratio: 2.86 EFFICIENCY exp = 0.899
BMEP: 159.6 Press ratio: 3.02 EFFICIENCY exp = 0.909
BMEP: 190.8 Press ratio: 3.32 EFFICIENCY exp = 0.922
BMEP: 198.5 Press ratio: 3.34 EFFICIENCY exp = 0.923

CLEARANCE comp: 0.0050 engine speed: 1300.0 rpm
BMEP: 136.4 Press ratio: 1.67 EFFICIENCY comp = 0.822
BMEP: 202.8 Press ratio: 2.07 EFFICIENCY comp = 0.856
BMEP: 231.2 Press ratio: 2.24 EFFICIENCY comp = 0.855

CLEARANCE comp: 0.0050 engine speed: 1600.0 rpm
BMEP: 43.9 Press ratio: 1.31 EFFICIENCY comp = 0.605
BMEP: 88.2 Press ratio: 1.57 EFFICIENCY comp = 0.751
BMEP: 115.2 Press ratio: 1.74 EFFICIENCY comp = 0.792
BMEP: 141.0 Press ratio: 1.91 EFFICIENCY comp = 0.813
BMEP: 176.4 Press ratio 2.14 EFFICIENCY comp = 0.822

CLEARANCE comp: 0.0050 engine speed: 1900.0 rpm
BMEP: 80.3 Press ratio: 1.74 EFFICIENCY comp = 0.745
BMEP: 104.1 Press ratio: 1.93 EFFICIENCY comp = 0.770
BMEP: 128.2 Press ratio: 2.12 EFFICIENCY comp = 0.781
BMEP: 159.6 Press ratio: 2.36 EFFICIENCY comp = 0.784
BMEP: 190.8 Press ratio: 2.61 EFFICIENCY comp = 0.778
BMEP: 198.5 Press ratio 2.64 EFFICIENCY comp = 0.777

Table 2

Engine Test Data

Cummins NTC-450 Turbocompound Engine

	TORQUE PEAK		RATED
ENGINE RPM	1300.5	1600.0	1901.2
FUEL RATE, LB/HR	103.0	94.0	141.1
RCP, TORQUE, FT. LB	1311.	936.	1125.
PT. TORQUE, FT. LB	60.	64.	125.
CPD. TORQUE, FT. LB	1371.	1000.	1250.
RCP. BHP	324.6	285.0	407.4
PT. BHP	14.9	19.6	45.1
CPD. BHP	339.5	304.6	452.5
RCP, BMEP, PSI	231.2	165.0	198.5
PT. BMEP, PSI	10.6	11.4	22.0
CPD. BMEP, PSI	241.8	176.4	220.5
RCP, BSFC, LB/HP/HR	.317	.330	.346
CPD. BSFC, LB/HP/HR	.304	.309	.312
FUEL/AIR RATIO	.0383	.0302	.0327
AIR/FUEL RATIO	26.1	33.1	30.6
VOLUMETRIC EFF. - AMBIENT	192.4	182.7	211.8
VOLUMETRIC EFF. - MANIFOLD	90.9	91.7	90.2
ACTUAL ENGINE AIRFLOW, LB/MIN	44.8	51.9	71.9
SMOKE READING	.00	.00	.00
PRESSURE DATA			
COMPRESSOR INLET (TOTAL ABS), IN-HG	29.03	28.64	28.21
COMPRESSOR DISCHRG (TOTAL ABS), IN-HG	65.16	61.46	74.51
MANIFOLD INTAKE (ABS), IN-HG	64.53	60.50	73.11
MANIFOLD EXHAUST (ABS), IN-HG	59.13	65.90	85.91
MANIFOLD INTAKE (GAGE)	34.90	31.10	43.60
MANIFOLD EXHAUST (GAGE)	29.50	36.50	56.40
TURBINE INLET (TOTAL ABS), IN-HG	61.19	68.14	89.57
TURBINE EXHAUST (ABS), IN-HG	37.23	39.20	46.61
P. TURBINE INLET (TOTAL ABS), IN-HG	37.33	39.33	47.00
P. TURBINE EXHAUST (ABS), IN-HG	30.53	30.40	31.41
P. TURBINE INLET (GAGE)	7.50	9.70	17.10
P. TURBINE EXHAUST (GAGE)	.90	1.00	1.90
DELTA P ENGINE, IN-HG	5.40	-5.40	-12.80
TEMPERATURE DATA			
COMPRESSOR INLET, DEGREES F	84.00	85.00	84.00
COMPRESSOR DISCHARGE, DEGREES F	259.	248.	312.
MANIFOLD INTAKE, DEGREES F	99.	101.	112.
MANIFOLD EXHAUST DEGREES F	960.	875.	1030.
TURBINE INLET, DEGREES F	1050.	925.	1070.
TURBINE OUTLET, DEGREES F	917.	780.	875.
TURBOCHARGER DATA			
COMPRESSOR MAP FLOW (545,29.38), LB/MIN	45.4	53.4	75.3
COMPRESSOR MAP FLOW (545,29.38), CFM	635.	748.	1054.
COMPRESSOR MAP FLOW (545,28.4), LB/MIN	43.9	51.6	72.8
COMPRESSOR MAP FLOW (545,28.4), CFM	635.	747.	1054.
TURBINE MAP FLOW, LB/MIN	22.0	21.8	24.4
COMPRESSOR WHEEL SPEED (545)	54170.	54000.	64499.
TURBINE WHEEL SPEED 91660)	56744.	59118.	67122.
COMPRESSOR PRESS RATIO	2.244	2.146	2.641
AD. EFF.	.806	.814	.760

	TORQUE PEAK		RATED
TURBINE PRESS RATIO	1.644	1.738	1.922
AD. EFF.	.923	.850	.898
COMBINED EFFICIENCY	.674	.631	.638
POWER TURBINE DATA			
TURBINE PRESS. RATIO	1.223	1.294	1.496
TURBINE MAP FLOW (1660,29.38), LB/MIN	33.5	34.8	42.0
TURBINE EFF. (ASSUMED)	.81	.81	.81
AD. TURBINE POWER	20.4	26.8	61.6